

J A E R I - M
86-181

MAGNETIC CHARACTERISTICS OF FERROMAGNETIC
STAINLESS STEELS,
SUS 403, SUS 410J1, TAF AND SUS 405

December 1986

Katsuyuki ARA, Masaharu YAMADA, Tsunemi KAKUTA
and Hideshi YAMAGISHI

日本原子力研究所
Japan Atomic Energy Research Institute

JAERI-Mレポートは、日本原子力研究所が不定期に公刊している研究報告書です。

入手の問合せは、日本原子力研究所技術情報部情報資料課（〒319-11 茨城県那珂郡東海村）あて、お申しこしください。なお、このほかに財団法人原子力弘済会資料センター（〒319-11 茨城県那珂郡東海村日本原子力研究所内）で複写による実費領布をおこなっております。

JAERI-M reports are issued irregularly.

Inquiries about availability of the reports should be addressed to Information Division Department of Technical Information, Japan Atomic Energy Research Institute, Tokaimura, Naka-gun, Ibaraki-ken 319-11, Japan.

© Japan Atomic Energy Research Institute, 1986

編集兼発行 日本原子力研究所
印 刷 日青工業株式会社

Magnetic Characteristics of Ferromagnetic Stainless Steels,
SUS 403, SUS 410J1, TAF and SUS 405

Katsuyuki ARA, Masaharu YAMADA, Tsunemi KAKUTA
and Hideshi YAMAGISHI

Department of Reactor Engineering,
Tokai Research Establishment,
Japan Atomic Energy Research Institute
Tokai-mura, Naka-gun, Ibaraki-ken

(Received November 21, 1986)

Ferromagnetic stainless steels have been used in magnetic and electro-magnetic devices which are exposed to severe environments such as an incore of nuclear reactor. Wide use of these materials is naturally due to their ferromagnetism, and also due to their excellent properties in corrosion, radiation and heat resistances. Easy machining process at a low cost and good availability in the market are counted for them as another advantage. However, their magnetic properties are not well established in a standard form as referred in handbooks, because they are originally developed as a structure material. This situation, the lack of sufficient data, leads us to study the magnetic properties of the martensitic stainless steels, SUS 403, SUS 410J1 and TAF, and the ferritic stainless steel, SUS 405, in connection with the development of incore instruments.

The magnetic properties were measured for many specimens after various heat treatments such as quenching and tempering, low temperature annealing and full annealing. Temperature dependence of magnetic properties was measured with an electric furnace. Magnetic properties measured in this study were of initial magnetization, dc hysteresis, ac permeability and inverse magnetostriction, and Curie point as well.

The martensitic stainless steels show somewhat semi-hard characteristics (H_c ; 5 - 15 oersteds) and the ferritic stainless steel is rather soft (H_c ; 2 - 5 oersteds). The Curie points range from 720 to 750 °C. The saturation magnetization is about 15000 gausses. The large inverse magnetostriction is observed in SUS 403 and SUS 405, and this may be utilized

in acoustic and sonic application as well as in force and pressure measurements. Because the magnetic properties depend on the heat treatments, the optimum condition of heat treatment may be chosen so as to satisfy requirements to the magnetic characteristics.

The data in this report would be useful also for design and development of big magnetic machines in other field such as nuclear fusion, magnetic levitation and so on.

Keywords: Stainless Steel, SUS403, SUS410J1, TAF, SUS405, Magnetic Characteristic, Magnetization Curve, Permeability, Curie Point, Inverse Magnetostriction.

強磁性ステンレス鋼,
SUS 403, SUS 410J1, TAF および SUS 405 の磁気特性

日本原子力研究所東海研究所原子炉工学部
荒 克之・山田 政治・角田 恒巳・山岸 秀志

(1986 年 11 月 21 日受理)

原子炉あるいは原子炉周辺の比較的環境の厳しい場所で使用される磁気応用計測制御機器では、しばしば磁性材料として強磁性を示すマルテンサイト系のステンレス鋼が使われる。その理由は、これらの材料が強磁性を示すことの他に、耐食性、耐放射線性、耐熱性、加工性などを同時に満足することと、一般の構造材料として比較的容易に、しかも安価に入手できるからである。しかし、これらの材料はもともと構造材料として開発されたものであるために、応用的立場からの磁気的な特性はほとんど調べられていない。また、調べられていたにせよ、一般的ハンドブック等には十分なデータが公表されていない。そのため、炉内計測センサの開発に関連して、マルテンサイト系ステンレス鋼 SUS 403, SUS 410J1, TAF およびフェライト系ステンレス鋼 SUS 405 の磁気特性を調べた。

試料は各種の熱処理（焼入れ焼戻し、低温焼なまし、完全焼なまし）を施したのち、常温での磁気特性を測定するとともに、電気炉内に挿入して、温度による磁気特性の変化も調べた。測定した磁気特性は、初期磁化特性、ヒステリシス磁化特性、交流初期透磁率、逆磁歪特性、およびこれらの温度による変化とキューリ温度である。

マルテンサイト系ステンレス鋼は磁気的に半硬質な性質 ($H_c \approx 5 \sim 15$ エルステッド) を示し、フェライト系 (SUS 405) は比較的軟質 ($H_c = 2 \sim 5$ エルステッド) である。キューリ温度は材料によって異なるが $720 \sim 750^{\circ}\text{C}$ 程度である。飽和磁束密度は約 15000 ガウスである。SUS 403 および SUS 405 は逆磁歪も大きいので、音響・超音波分野および力・圧力計測への利用が考えられる。熱処理条件によって磁気特性も大きく変化するので、利用形態によって最適な熱処理を選ぶことができる。

本報告書のデータは核融合、磁気浮上などの他の分野の大型磁気装置の設計や開発にも役立つと考える。

CONTENTS

I. INTRODUCTION -----	1
II. PREPARATION OF TEST PIECES -----	1
1. Magnetic Properties of Fe-Cr Alloys and Selection of Materials -----	1
2. Toroidal Test Pieces and Heat Treatments -----	4
3. Rod Test Pieces and Heat Treatments -----	6
III. MEASURING METHODS -----	6
1. DC Magnetization Curves at Room Temperature -----	6
2. DC Magnetization Curves at Elevated Temperature -----	7
3. AC Permeability -----	7
4. Inverse Magnetostriiction -----	9
IV. RESULTS OF MEASUREMENTS: MAGNETIZATION CHARACTERISTICS -----	12
1. Magnetization Characteristics of SUS 403 -----	12
2. Magnetization Characteristics of SUS 410J1 -----	14
3. Magnetization Characteristics of TAF -----	14
4. Magnetization Characteristics of SUS 405 -----	15
5. Annexes -----	15
V. RESULTS OF MEASUREMENTS: INVERSE MAGNETOSTRICTION -----	42
1. Inverse Magnetostriiction of SUS 403 -----	42
2. Inverse Magnetostriiction of SUS 410J1 -----	42
3. Inverse Magnetostriiction of TAF -----	43
4. Inverse Magnetostriiction of SUS 405 -----	43
5. Annexes: Metallographical Observation -----	43
VI. SUMMARY -----	55
ACKNOWLEDGEMENT -----	56
REFERENCES -----	56
APPENDICES: INVERSE MAGNETOSTRICTION DATA OF FERROMAGNETIC STAINLESS STEELS -----	57
Appendix I Inverse Magnetostriiction Data, Measured with 400 Hz-excitation and at Room Temperature -----	60
Appendix II Inverse Magnetostriiction Data, measured with 400 Hz-excitation and at 300 °C -----	75

目 次

I. はじめに	1
II. 試験試料の製作	1
1. Fe-Cr合金の磁気的性質と材料の選定	1
2. トロイダル状試料と熱処理	4
3. 棒状試料と熱処理	6
III. 測定法	6
1. 室温における直流磁化曲線	6
2. 高温における直流磁化曲線	7
3. 交流透磁率	7
4. 透磁歪	9
IV. 測定結果：磁化特性	12
1. SUS 403 の磁化特性	12
2. SUS 410J1 の磁化特性	14
3. TAF の磁化特性	14
4. SUS 405 の磁化特性	15
5. 追加事項	15
V. 測定結果：逆磁歪	42
1. SUS 403 の逆磁歪	42
2. SUS 410J1 の逆磁歪	42
3. TAF の逆磁歪	43
4. SUS 405 の逆磁歪	43
5. 追加事項：金相観察	43
VI. まとめ	55
謝 辞	56
文 献	56
付録：強磁性ステンレス鋼の逆磁歪データ集	57
付録 I 室温・400Hzにおける逆磁歪	60
付録 II 300°C・400Hzにおける逆磁歪	75

LIST OF TABLES, FIGURES AND PHOTOGRAPHS

Table 2.1-1	Chemical compositions of selected materials for tests	3
Table 4.4-1	Magnetic characteristics of SUS-403 virgin-pieces	17
Table 4.5-1	Vickers hardnesses and coercive forces of heat-treated SUS 403's	39
Table 4.5-2	Variations of effective ac permeabilities of SUS 410J1's, TAF's and SUS 405 with heat cycle	39
Table 4.5-3	Variations of effective ac permeabilities of SUS 410J1's, TAF's and SUS 405's with heat cycles	39
Fig. 2.1-1	Phase diagram of Fe-Cr alloys	2
Fig. 2.1-2	Saturation induction of Fe-Cr alloys at 20 °C	3
Fig. 2.1-3	Magnetic induction of Fe-Cr alloys at various field strengths	3
Fig. 2.2-1	Machining of troidal test pieces	4
Fig. 2.2-2	Temperature record of quenching-and-tempering in Ar atmosphere	5
Fig. 2.2-3	Temperature record of low-temperature annealing in Ar atmosphere	5
Fig. 2.2-4	Temperature record of full (high-temperature) annealing in Ar atmosphere	5
Fig. 2.3-1	Rod test piece and its dimensions	6
Fig. 3.3-1	Instrument setup for ac permeability measurement	7
Fig. 3.4-1	Instrument setup for inverse magnetostriction measurement	8
Fig. 4.1-1	Representative of dc hysteresis magnetization curves of SUS-403 virgin-pieces	18
Fig. 4.1-2	Representative of dc initial magnetization curves of SUS-403 virgin-pieces	18
Fig. 4.1-3	Irregularity band of dc initial magnetization curves of SUS-403 virgin-pieces	19
Fig. 4.1-4	Changes of dc initial magnetization curve of SUS-403 virgin-piece with temperatures	19

Fig. 4.1-5	Saturation induction of SUS-403 virgin-piece and its variations with temperatures at excitation strength of 30 oersteds	-----	20
Fig. 4.1-6	AC initial permeability of SUS-403 virgin-piece for various excitation frequencies and its changes with temperatures	-----	20
Fig. 4.1-7	AC initial permeability of SUS-403 virgin-piece at various temperatures and its changes with excitation frequencies	-----	21
Fig. 4.1-8	Variations of dc hysteresis magnetization curve of SUS 403 with heat treatments	-----	22
Fig. 4.1-9	Variations of dc initial magnetization curve of SUS 403 with heat treatments	-----	22
Fig. 4.1-10	Effect of magnetic annealing on dc hysteresis magnetization curve of SUS 403	-----	23
Fig. 4.1-11	Effect of magnetic annealing on dc initial magnetization curve of SUS 403	-----	23
Fig. 4.1-12	Changes of dc initial magnetization curve of quenched-and-tempered SUS 403 with temperatures	---	24
Fig. 4.1-13	Changes of dc initial magnetization curve of full (high-temperature) annealed SUS 403 with temperatures	-----	24
Fig. 4.1-14	Changes of dc initial magnetization curve of low-temperature annealed SUS 403 with temperatures	-----	25
Fig. 4.1-15	Effective ac permeabilities of heat-treated SUS 403's and their changes with temperatures	-----	25
Fig. 4.1-16	Effective ac permeabilities of heat-treated SUS 403's and their changes with temperature cycles	---	26
Fig. 4.1-17	Effective ac permeabilities of heat-treated SUS 403's and their changes with temperature cycles	---	26
Fig. 4.1-18	Effective ac permeabilities of heat-treated SUS 403's and their changes with temperature cycles	---	27
Fig. 4.2-1	Variations of dc hysteresis magnetization curve of SUS 410J1 with heat treatments	-----	28
Fig. 4.2-2	Variations of dc initial magnetization curve of SUS 410J1 with heat treatments	-----	28
Fig. 4.2-3	Changes of dc initial magnetization curve of SUS-410J1 virgin-piece with temperatures	-----	29

Fig. 4.2-4	Changes of dc initial magnetization curve of quenched-and-tempered SUS 410J1 with temperatures	---	29
Fig. 4.2-5	Changes of dc initial magnetization curve of low-temperature annealed SUS 410J1 with temperatures	-----	30
Fig. 4.2-6	Changes of dc initial magnetization curve of full (high-temperature) annealed SUS 410J1 with temperatures	-----	30
Fig. 4.2-7	Effective ac permeabilities of heat-treated SUS 410J1's and their changes with temperatures	-----	31
Fig. 4.3-1	Variations of dc hysteresis magnetization curve of TAF with heat treatments	-----	32
Fig. 4.3-2	Variations of dc initial magnetization curve of TAF with heat treatments	-----	32
Fig. 4.3-3	Changes of dc initial magnetization curve of TAF virgin-piece with temperatures	-----	33
Fig. 4.3-4	Changes of dc initial magnetization curve of quenched-and-tempered TAF with temperatures	-----	33
Fig. 4.3-5	Changes of dc initial magnetization curve of low-temperature annealed TAF with temperatures	---	34
Fig. 4.3-6	Changes of dc initial magnetization curve of full (high-temperature) annealed TAF with temperatures	-----	34
Fig. 4.3-7	Effective ac permeabilities of heat-treated TAF's and their changes with temperatures	-----	35
Fig. 4.4-1	Variations of dc hysteresis magnetization curve of SUS 405 with heat treatments	-----	36
Fig. 4.4-2	Variations of dc initial magnetization curve of SUS 405 with heat treatments	-----	36
Fig. 4.4-3	Changes of dc initial magnetization curve of SUS-405 virgin-piece with temperatures	-----	37
Fig. 4.4-4	Changes of dc initial magnetization curve of low-temperature annealed SUS 405 with temperatures	--	37
Fig. 4.4-5	Changes of dc initial magnetization curve of full (high-temperature) annealed SUS 405 with temperatures	-----	38
Fig. 4.4-6	Effective ac permeabilities of heat-treated SUS 405's and their changes with temperatures	-----	38
Fig. 5.1-1	Inverse magnetostrictions of virgin and heat-treated SUS 403's at room temperature and 300 °C	---	44

Fig. 5.2-1	Inverse magnetostrictions of virgin and heat-treated SUS 410J1's at room temperature and 300 °C	--	45
Fig. 5.3-1	Inverse magnetostrictions of virgin and heat-treated TAF's at room temperature and 300 °C	-----	46
Fig. 5.4-1	Inverse magnetostrictions of virgin and full-annealed SUS 405's at room temperature and 300 °C	--	47
Photo. 4.5-1(1)	Microstructures of virgin and heat-treated SUS 403 test pieces (I)	-----	40
Photo. 4.5-1(2)	Microstructures of virgin and heat-treated SUS 403 test pieces (II)	-----	41
Photo. 5.5-1(1)	Microstructures of virgin and heat-treated SUS 403 pieces for inverse magnetostriction tests (I)	-----	48
Photo. 5.5-1(2)	Microstructures of virgin and heat-treated SUS 403 pieces for inverse magnetostriction tests (II)	-----	49
Photo. 5.5-2(1)	Microstructures of virgin and heat-treated SUS 410J1 pieces for inverse magnetostriction tests (I)	-----	50
Photo. 5.5-2(2)	Microstructures of virgin and heat-treated SUS 410J1 pieces for inverse magnetostriction tests (II)	-----	51
Photo. 5.5-3(1)	Microstructures of virgin and heat-treated TAF pieces for inverse magnetostriction tests (I)	-----	52
Photo. 5.5-3(2)	Microstructures of virgin and heat-treated TAF pieces for inverse magnetostriction tests (II)	-----	53
Photo. 5.5-4	Microstructures of virgin and full-annealed SUS 405 pieces for inverse magnetostriction tests	-----	54

I. INTRODUCTION

The magnetic and electro-magnetic devices are generally very reliable and durable so that many measuring instruments and control devices utilizing magnetic characteristics of the material have been used in many industrial fields. Also, such devices have been used in the system of reactor control and instrumentation in the nuclear field, where endurance against severe environments is strongly required to the devices. The examples are found in some incore instruments, control-rod drive mechanisms, control-rod position indicators, and so on. In these devices, the ferro-magnetic material is very essential for a good performance of their operational functions.

The magnetic material, which is used in the reactor core and in the vicinity of reactor vessel, must have large heat, corrosion and radiation resistivities in addition to good magnetic characteristics; and its machinability is required as well in most cases. By this reason, a ferromagnetic stainless steel has been often used as a magnetic material. However, magnetic characteristics of stainless steels have not been well established, though their mechanical properties have been investigated in very detail since stainless steels were originally developed as a structure material. This fact led us to an investigation of magnetic characteristics of ferro-magnetic stainless steels in connection with development of incore instruments. The materials treated in the investigation were the martensitic stainless steels, SUS 403, SUS 410J1 and TAF, and the ferritic stainless steel, SUS 405. The data obtained would be useful also for design and development of big magnetic machines in other fields such as nuclear fusion technology, magnetic levitation and so on.

II. PREPARATION OF TEST PIECES

1. Magnetic Properties of Fe-Cr Alloys and Selection of Materials

It is known that the magnetic properties can be divided into two groups; structure-sensitive and structure-insensitive groups⁽¹⁾. Permeability, coercive force and hysteresis loss belong to the former one and vary sensitively with chemical composition, internal strain, temperature, crystal structure, crystal orientation and so on. Saturation

I. INTRODUCTION

The magnetic and electro-magnetic devices are generally very reliable and durable so that many measuring instruments and control devices utilizing magnetic characteristics of the material have been used in many industrial fields. Also, such devices have been used in the system of reactor control and instrumentation in the nuclear field, where endurance against severe environments is strongly required to the devices. The examples are found in some incore instruments, control-rod drive mechanisms, control-rod position indicators, and so on. In these devices, the ferro-magnetic material is very essential for a good performance of their operational functions.

The magnetic material, which is used in the reactor core and in the vicinity of reactor vessel, must have large heat, corrosion and radiation resistivities in addition to good magnetic characteristics; and its machinability is required as well in most cases. By this reason, a ferromagnetic stainless steel has been often used as a magnetic material. However, magnetic characteristics of stainless steels have not been well established, though their mechanical properties have been investigated in very detail since stainless steels were originally developed as a structure material. This fact led us to an investigation of magnetic characteristics of ferro-magnetic stainless steels in connection with development of incore instruments. The materials treated in the investigation were the martensitic stainless steels, SUS 403, SUS 410J1 and TAF, and the ferritic stainless steel, SUS 405. The data obtained would be useful also for design and development of big magnetic machines in other fields such as nuclear fusion technology, magnetic levitation and so on.

II. PREPARATION OF TEST PIECES

1. Magnetic Properties of Fe-Cr Alloys and Selection of Materials

It is known that the magnetic properties can be divided into two groups; structure-sensitive and structure-insensitive groups⁽¹⁾. Permeability, coercive force and hysteresis loss belong to the former one and vary sensitively with chemical composition, internal strain, temperature, crystal structure, crystal orientation and so on. Saturation

magnetization, Curie point, saturation magnetostriction and crystal anisotropy constant are included in another group and are less sensitive to the structural factors. The structure-sensitive magnetic properties of ferro-magnetic stainless steels could, therefore, be surmized from those of alloys having about the same composition of main chemical elements; and the structure-sensitive properties must be understood with relation to their own histories of production process and heat treatments.

Ferro-magnetic stainless steels are basically Fe-Cr alloys which contain a little amount of Ni, Mn, C, Si and others, and have a martensitic or ferritic structure. Figure 2.1-1 represents the phase diagram of Fe-Cr binary alloys⁽²⁾. The Curie point increases slightly with an increase of Cr content until it reaches to about 5 %, and then decreases. It is above 700 °C in the range of Cr content less than 15 %. With an increase of Cr content over 20 %, it decreases largely and the intermetallic-compound sigma-phase appears. The saturation magnetization and induction magnetization decrease with an increase of Cr content as shown in Figs. 2.1-2 and 2.1-3⁽³⁾. The saturation magnetization is about 18000 gauss at a Cr-content of 10 %. It is said that the permeability decreases sharply with an increase of Cr in a region of Cr-content less than 10 % and magnetostriction becomes small at about 20 %⁽⁴⁾. The Fe-Cr alloys with a Cr-content of less than 6 % are well known as a material of old-type permanent magnets. The structure sensitive properties, such as permeability and coercive force, of these alloys greatly depend on heat treatments and doping of non-metallic elements: for example, the coercive force reaches 60 oersteds with an addition of C by 1 %⁽⁵⁾.

From the above, one can suspect that a stainless steel with a smaller content of Cr has a larger Curie point and a larger saturation magnetization, and a proper heat treatment may produce better

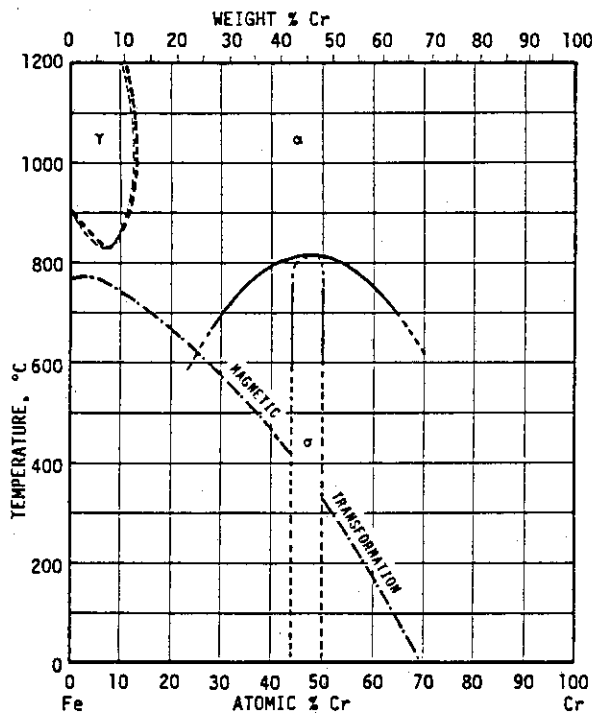


Fig. 2.1-1 Phase diagram of Fe-Cr alloys⁽²⁾.

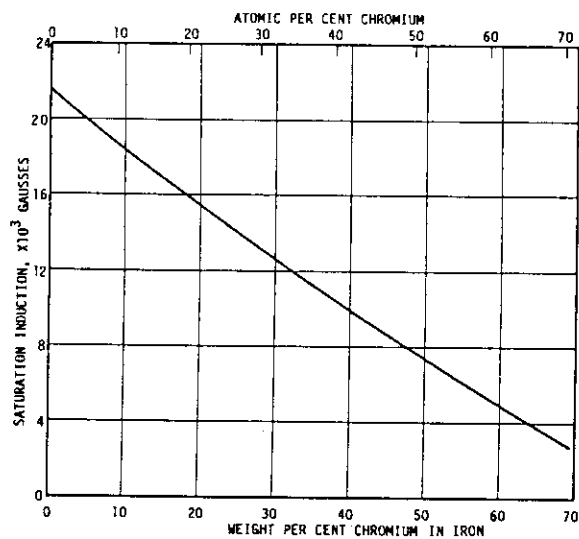


Fig. 2.1-2 Saturation induction of Fe-Cr alloys at 20 °C⁽³⁾.

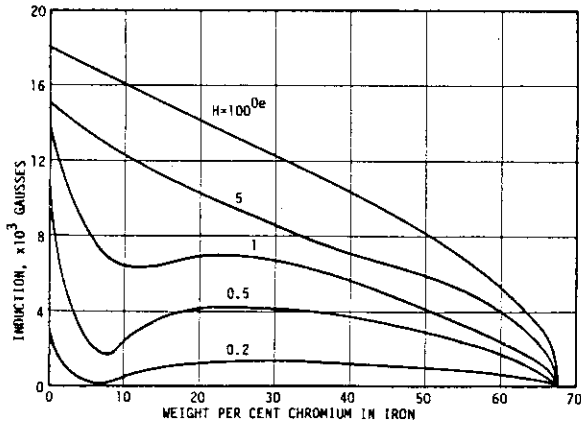


Fig. 2.1-3 Magnetic induction of Fe-Cr alloys at various field strengths⁽³⁾.

magnetization characteristics. Stainless steels, which contain Cr of about 12 - 13 %, are so-called martensitic stainless steels and ferritic ones: and those which contain a lower amount of C have softer magnetic characteristics. The representative steels of this sort are martensitic SUS 403 and ferritic SUS 405. SUS 403 and 405 are the equivalent of AISI 403 and 405, respectively. Also, one can select some from so-called super 12-Cr steels, which contains a small amount of Mo for application where a high grade of high-temperature mechanical-strength and corrosion resistivity are required. Interesting steels of this sort are SUS 410J1 and TAF. There are no equivalent of them in the U.S.A. standard, but they are about similar to AMS 5614 and MIL S 861A, Class 403. Chemical compositions of these selected materials are shown in table 2.1-1.

Table 2.1-1 Chemical compositions of selected materials for tests.

	C	Si	Mn	P	S	Ni	Cr	Mo	Al	Fe
SUS 403	0.13	0.29	0.37	0.27	0.17	0.12	11.76	-	-	bal.
SUS 410J1	0.11	0.32	0.51	0.025	0.005	-	11.55	0.42	-	bal.
TAF	0.15	0.60	0.72	0.015	0.003	-	11.30	0.69	-	bal.
SUS 405	0.05	0.33	0.55	0.25	0.99	0.16	13.12	-	0.16	bal.

in wt. %

2. Toroidal Test Pieces and Heat Treatments

The toroidal test pieces were machined out of bar materials, as shown in Fig. 2.2-1, for the measurements of magnetization curves and permeabilities. Fifty-seven pieces of SUS 403, and thirty pieces of each of others were produced. These pieces were divided into two groups; i.e., non-heat-treatment and heat-treatment groups. Also, the pieces of heat-treatment group were divided into three groups of (1st) quenching-and-tempering, (2nd) low-temperature annealing and (3rd) full annealing. Generally, raw material of steel is supplied as it has been heat-treated in a production process by a manufacturer. New treatments under newly-set conditions were, therefore, performed to erase different histories of past heat treatments from all the test pieces and to give the same heat-treated conditions. The pieces were placed in an electric furnace and heat-treated in an Ar atmosphere.

Figure 2.2-2 shows the temperature record of quenching-and-tempering treatment. The pieces of 1st group were heated up to 1000 °C from a room temperature by taking a time of 2.3 hours to obtain austenite states. Temperature fluctuations were caused in the process of heating-up because the temperature was controlled by a semi-automatic means. The austenite-start-temperatures of test-piece materials are about 750 - 800 °C, and the heating of test pieces up to 900 °C seems to be very sufficient. The temperature was, however, raised up to 1000 °C to prevent a possible happening of insufficient heating in some pieces by an unflat furnace-temperature distribution. The holding time of 1000 °C was about 25 min. This seems to be sufficient to obtain fully austenite states in the pieces. The quenching was performed by taking the pieces out of the furnace and cooling them by Ar-gas blowing. As seen in Fig. 2.2-2, it took about 15 min to reach the Ms point (the martensite-start-temperature, about 300 to 200 °C). This

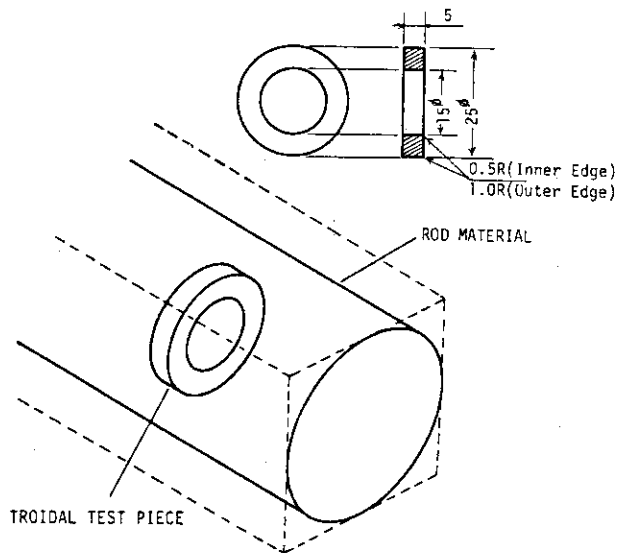


Fig. 2.2-1 Machining of toroidal test pieces.

condition seems to be very satisfactory for ordinary quenching. At the temperatures below the Ms point, Ar-blown was stopped and the pieces were naturally cooled. After several hours passed, the pieces were tempered. Tempering temperature of about 700 °C was adopted to prevent temper brittleness, and the pieces were cooled down with the same way as quenching.

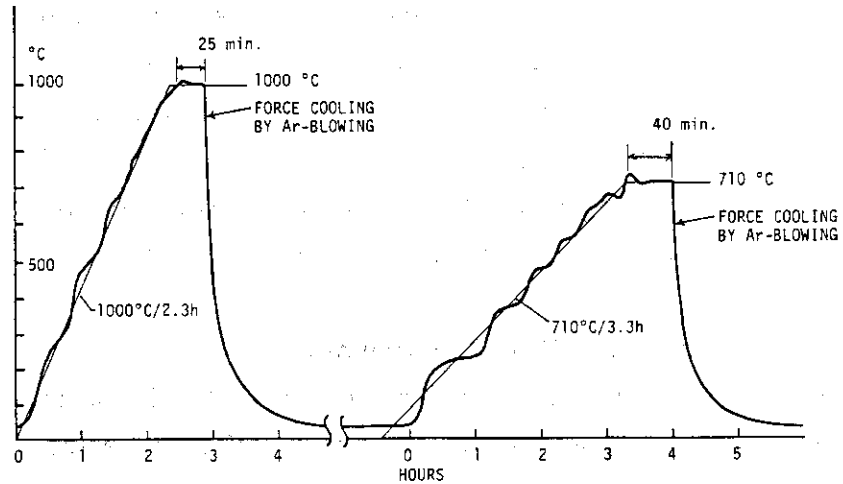


Fig. 2.2-2 Temperature record of quenching-and-tempering in Ar atmosphere.

Figure 2.2-3 shows the temperature record of low-temperature annealing. The purpose of this treatment was not for erasure of past heat-treated conditions but for relaxation of internal strains. The pieces of 2nd group were heated up to 700 °C by taking 3.7 hours and held at 700 °C for 1 hour, and then cooled down rapidly. Figure 2.2-4 shows the temperature record of full annealing. The pieces of 3rd group were heated up to 1000 °C by taking 1.5 hours, and they were cooled down very slowly to 600 °C for getting complete austenite phases,

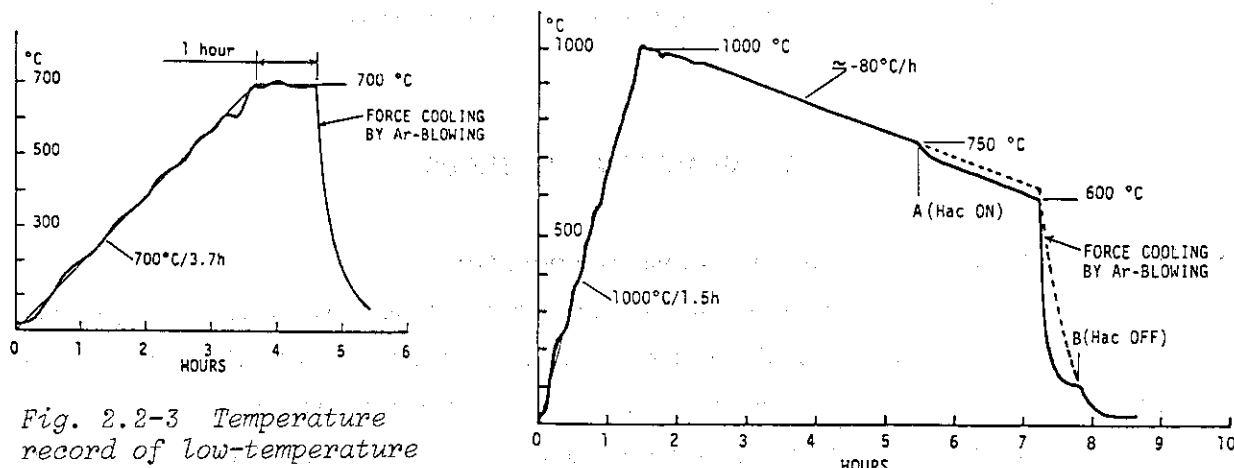


Fig. 2.2-3 Temperature record of low-temperature annealing in Ar atmosphere.

Fig. 2.2-4 Temperature record of full (high-temperature) annealing in Ar atmosphere.

and then cooled down rapidly. In this process, some of SUS 403 pieces were treated with magnetic annealing: a few pieces had been prepared with a coil of 20 turns, made of a metal-sheathed MgO-insulated wire, and were treated with magnetic annealing by an excitation of (0.6 A)/(50 Hz) through the coil. The magnetic annealing started at the temperature of 750 °C (i.e., just over the Curie point). Because the temperature control during the full annealing were made with reference to the temperature of the pieces for magnetic annealing, the temperature of non-magnetic annealing pieces (full line in Fig. 2.2-4) was a little lower than that of magnetic annealing ones (dotted line) by the effect of electric heating with excitation.

3. Rod Test Pieces and Heat Treatments

The rod test pieces, shown in Fig. 2.3-1, were prepared for the investigation of inverse magnetostriiction (Villari effect). In this case, the pieces were machined out of materials which were heat-treated in advance: the performed heat-treatments were the same as the toroidal pieces had.

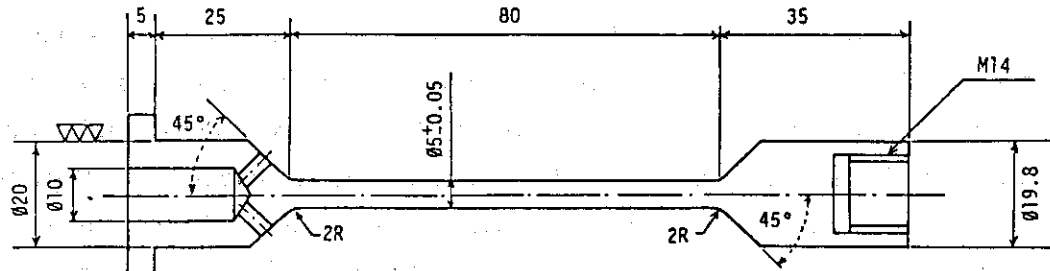


Fig. 2.3-1 Rod test piece and its dimensions.

III. MEASURING METHODS

1. DC Magnetization Curves at Room Temperature

An insulation tape was wound on each of all toroidal test pieces, and a primary coil of 200 turns and a secondary of 10 turns were wound on. Then, dc hysteresis and initial magnetization curves of all pieces were measured at room temperature with an automatic dc-magnetization-curve tracer. The hysteresis curves were measured with an excitation field of +/- 100 oersteds, and the initial magnetization curves

and then cooled down rapidly. In this process, some of SUS 403 pieces were treated with magnetic annealing: a few pieces had been prepared with a coil of 20 turns, made of a metal-sheathed MgO-insulated wire, and were treated with magnetic annealing by an excitation of (0.6 A)/(50 Hz) through the coil. The magnetic annealing started at the temperature of 750 °C (i.e., just over the Curie point). Because the temperature control during the full annealing were made with reference to the temperature of the pieces for magnetic annealing, the temperature of non-magnetic annealing pieces (full line in Fig. 2.2-4) was a little lower than that of magnetic annealing ones (dotted line) by the effect of electric heating with excitation.

3. Rod Test Pieces and Heat Treatments

The rod test pieces, shown in Fig. 2.3-1, were prepared for the investigation of inverse magnetostriiction (Villari effect). In this case, the pieces were machined out of materials which were heat-treated in advance: the performed heat-treatments were the same as the toroidal pieces had.

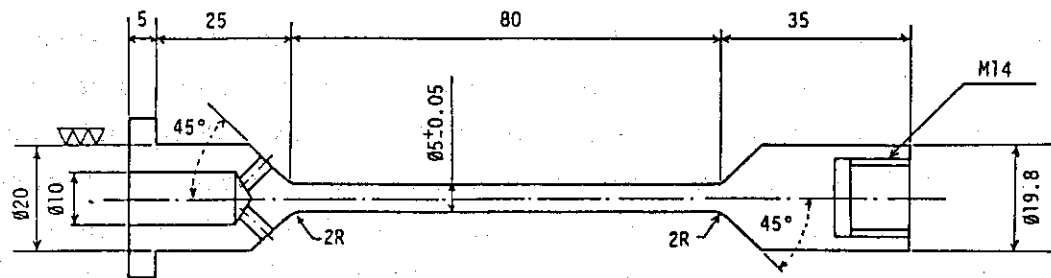


Fig. 2.3-1 Rod test piece and its dimensions.

III. MEASURING METHODS

1. DC Magnetization Curves at Room Temperature

An insulation tape was wound on each of all toroidal test pieces, and a primary coil of 200 turns and a secondary of 10 turns were wound on. Then, dc hysteresis and initial magnetization curves of all pieces were measured at room temperature with an automatic dc-magnetization-curve tracer. The hysteresis curves were measured with an excitation field of +/- 100 oersteds, and the initial magnetization curves

with 30 oersteds. In each measurement, the test piece was demagnetized with applying a maximum demagnetization current of (5 A,r.m.s)/(50 Hz) to the primary coil. This current caused a maximum demagnetizing field of 282 oersteds which could saturate the magnetic flux of the piece sufficiently for full demagnetization. After measurements, all pieces were unclothed and put into a waiting box for following tests at elevated temperatures.

2. DC Magnetization Curves at Elevated Temperature

Silica-wool insulators were wound on some of the toroidal test pieces, and heat-resisting wires (glass-wool-insulated wires or mineral-insulated wires) were wound on to provide primary coils of 100 turns and secondary of 10 turns. These pieces were installed in an electric furnace and heated up with measuring initial magnetization curves. The maximum excitation in each measurement was 30 oersteds, and the demagnetization was made with a maximum current of (3 A,r.m.s)/(50 Hz); i.e., 85 oersteds.

3. AC permeability

The effective ac permeabilities were measured in the temperature range from room temperature to about 800 °C to find out the Curie points. Figure 3.3-1 shows the measuring circuit. The toroidal pieces were excited with an ac current of (30 - 200 mA)/(100 Hz - 10 kHz) through heat-resisting primary coils, and the induced secondary voltages were measured. The number of turns of coils were 10 - 50 turns, depending on types of used coil-wires. The effective ac permeability μ_{ac} can be represented as; $\mu_{ac} = B_{ac}/H_{ac}$, in terms of specific

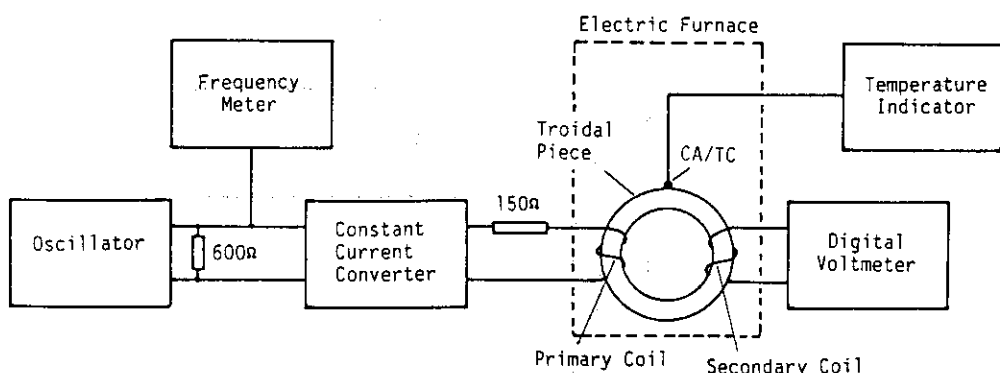


Fig. 3.3-1 Instrument setup for ac permeability measurement.

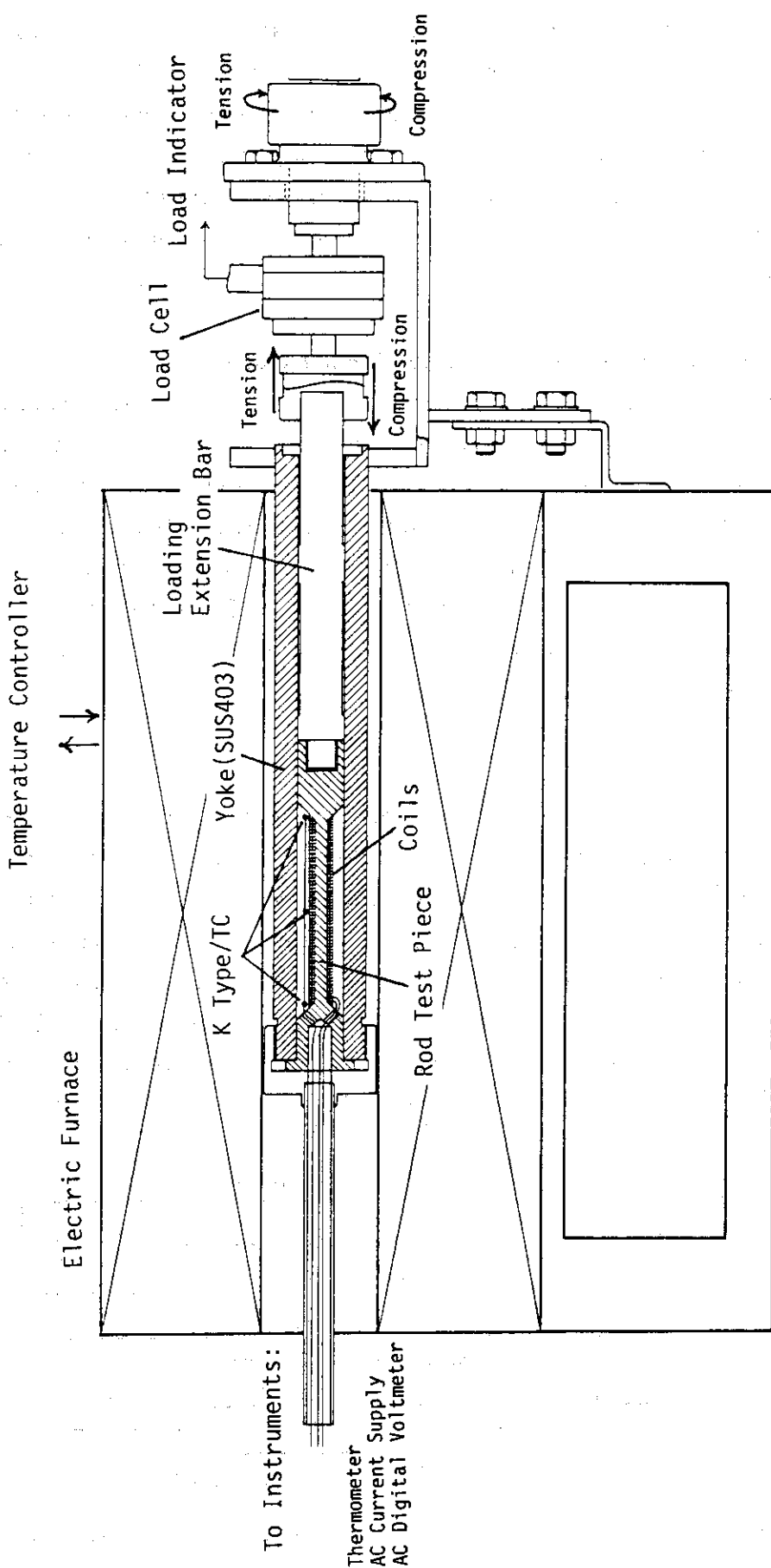


Fig. 3.4-1 Instrument setup for inverse magnetostriction measurement.

permeability where B_{ac} and H_{ac} are the peak values of magnetic induction and excitation. Here,

$$B_{ac} = 0.915 \times \frac{V_2}{N_2 f} \times 10^8 \text{ (gauss)}, \quad H_{ac} = 0.2828 \times N_1 I_1 \text{ (oersted)},$$

where I_1 is the r.m.s value of excitation current, V_2 the induced secondary voltage, f the excitation frequency, N_1 and N_2 the number of turns of the primary coil and the secondary coil.

Since the eddy current losses are included in the measured u_{ac} 's, the term "effective" ac permeability was adopted.

4. Inverse Magnetostriiction

Inverse magnetostrictions were measured to investigate their applicability to electro-mechanical sensors. Since the inverse magnetostriiction is reciprococal to the magnetostriction, the data could be referred in a structure design of big magnetic machine, in which a ferromagnetic stainless steel is used and a large stress appears internally. Figure 3.4-1 shows the setup of instruments used in the measurements. A glass-wool insulator was wound on the rod test piece, and the primary coil of 1000 turns and the secondary of 50 turns with mineral-insulated wires were wound on it. Chromel-alumel thermocouples (K type/TC's) were instrumented at the center and at the both ends of the piece to measure the temperature. The test piece was settled in the cylinder yoke made of SUS 403. The one end of the piece (left side in Fig. 3.4-1) was locked with the screw mechanism. A load (tension or compresion) was applied from the another end through the loading extension bar and the load cell by rotating the screw system.

The magnetic reluctance, R_g , of gaps at the surfaces where the test piece contacts with the cylinder yoke is expressed as;

$$R_g = \frac{g_1}{\mu_0 S_1} + \frac{g_2}{\mu_0 S_2},$$

where, μ_0 is the permeability of air, g_1 and g_2 are the gaps of left and right side contact-surfaces, S_1 and S_2 the contact-surface areas of gaps g_1 and g_2 , respectively.

Here, $g_1 = 0.05 \text{ mm}$, $g_2 = 0.2 \text{ mm}$, $S_1 = 3.14 \times 20 \times 18 \text{ mm}^2$

and $S_2 = 3.14 \times 19.8 \times 28 \text{ mm}^2$, and therefore;

$$R_g = 5 \times 10^{-1} / (3.14\mu_0) \quad (\text{AT/Wb})$$

On the other hand, the magnetic reluctance, R_r , of the part to be stressed; i.e., the thinner part of test piece with a diameter of 5 mm and a length 80 mm, is;

$$R_r = 12.8 \times 10^3 / (3.14\mu) \quad (\text{AT/Wb})$$

Thus,

$$R_g/R_r = 0.39 \times 10^{-4} \times (\mu/\mu_0),$$

where (μ/μ_0) is the specific permeability of the material. By estimating the maximum of (μ/μ_0) as 1000, one obtains, $(R_g/R_r)=0.04$. This may permit neglect of counting the magnetic reluctance of gaps. Further, the magnetic reluctance of cylinder yoke is very small as compared with that of the thinner part of test piece. In the result, one can consider that the applied magnetomotive force through the primary coil is all applied to the thinner part of the test piece.

The maximum excitation magnetic field, H_p (peak value), is

$$H_p = \sqrt{2} I_1 N_1 / L ,$$

where N_1 is the number of turns of primary coil, I_1 the r.m.s. value of excitation current, L the length of effective magnetic circuit. Here, $L = 80 \text{ mm}$ and $N_1 = 1000$, so that

$$H_p = 17.7 \times 10^3 \times I_1 \quad (\text{AT/m}), \text{ or}$$

$$H_p = 0.222 \times 10^3 \times I_1 \quad (\text{oersteds})$$

The induced magnetic flux density in peak value, B_p , is

$$B_p = \frac{\sqrt{2} V_2}{2 \times 3.14 \times f N_2 S}$$

where f is the excitation frequency, N_2 the number of turns of secondary coil, V_2 the induced secondary voltage (r.m.s.), S the cross sectional area of thinner part of test piece.

Here, $N_2 = 50$, $S = 3.14 \times 2.5^2 \times 10^{-6}$ (m^2), so that

$$B_p = 0.229 \times 10^3 \times (V_2/f) \quad (\text{Wb}/\text{m}^2), \text{ or}$$

$$B_p = 2.29 \times 10^6 \times (V_2/f) \quad (\text{gauss})$$

Therefore, the effective ac permeability, μ_{ac} , in terms of specific permeability is,

$$\mu_{ac} = (B_p \text{ in gausses}) / (H_p \text{ in oersteds})$$

$$= 10.3 \times \frac{V_2 \times 10^3}{f \times 10^{-3}} \times \frac{1}{I_1 \times 10^3}$$

When the measuring units, (mV) for V_2 , (kHz) for f and (mA) for I_1 , are applied;

$$\mu_{ac} = 10.3 \times \frac{V_2}{f \times I_1}$$

On the other hand, the expression of applied stress, s , is

$$s = W / (3.14 \times 2.5^2) = 0.051 \times W \quad (\text{kg}/\text{mm}^2),$$

where W is the applied weight in kg; i.e., the reading of load cell.

The measurements of inverse magnetostrictions were performed as follows: (1) by applying a few cycles of loading of $+/- (80 - 90)$ kg, the test piece was stabilized so that the secondary induced voltages at zero load became stably constant; then, (2) the loading to the test piece for

measurements started as, 0 to +80 kg to 0 to -80 kg to 0, with measuring the secondary voltages. The measurements were carried out at room temperature and 300 °C for the excitation of (10, 20, 30, 50, 70, and 100 mA) of 400 Hz.

IV. RESULTS OF MEASUREMENTS: MAGNETIZATION CHARACTERISTICS

1. Magnetization Characteristics of SUS 403

1) DC magnetization characteristics of virgin pieces at room temperature

DC hysteresis and initial magnetization curves were measured at room temperature for twenty-seven virgin pieces (sample #1 to #27). Table 4.1-1 shows the results, where B_m is the maximum induction at the maximum excitation of 100 oersteds, B_r the residual induction, H_c the coercive force, μ_0 the initial permeability and μ_m the maximum permeability. The mean values \bar{X} , the standard deviations σ , the deviation values S.S., and the grades of deviation from the mean value by sign (-2 to +2), are shown in the table, as well. Figures 4.1-1 and -2 show the magnetization curves of sample #19 which has the most "standard-like" characteristics among the tested samples. Figure 4.1-3 shows the irregularity band of initial magnetization curves, in which largely deviated ones from the mean characteristics are excluded.

2) Changes of initial magnetization curve with temperatures

The changes of the initial magnetization curve of a virgin piece with temperatures were measured at various temperatures up to 700 °C. The results are shown in Fig. 4.1-4. The inductions for the excitation of 30 oersteds are plotted in Fig. 4.1-5 with reference to the temperatures: one can extrapolate the Curie point of about 715 °C in the figure.

3) Temperature and frequency characteristics of ac permeability

AC permeabilities of a virgin piece were measured at temperatures up to 750 °C with the excitations of (0.42 oersted in peak)/(100 Hz to 10 kHz). The results are shown in Figs. 4.1-6 and -7. One can find out the Curie point of 730 °C in Fig. 4.1-6. This is a little higher than the previous value: the difference may be resulted from an inaccuracy of temperature measurement. The decrease of ac permeability with the

measurements started as, 0 to +80 kg to 0 to -80 kg to 0, with measuring the secondary voltages. The measurements were carried out at room temperature and 300 °C for the excitation of (10, 20, 30, 50, 70, and 100 mA) of 400 Hz.

IV. RESULTS OF MEASUREMENTS: MAGNETIZATION CHARACTERISTICS

1. Magnetization Characteristics of SUS 403

1) DC magnetization characteristics of virgin pieces at room temperature

DC hysteresis and initial magnetization curves were measured at room temperature for twenty-seven virgin pieces (sample #1 to #27). Table 4.1-1 shows the results, where B_m is the maximum induction at the maximum excitation of 100 oersteds, B_r the residual induction, H_c the coercive force, μ_0 the initial permeability and μ_m the maximum permeability. The mean values \bar{X} , the standard deviations σ , the deviation values S.S., and the grades of deviation from the mean value by sign (-2 to +2), are shown in the table, as well. Figures 4.1-1 and -2 show the magnetization curves of sample #19 which has the most "standard-like" characteristics among the tested samples. Figure 4.1-3 shows the irregularity band of initial magnetization curves, in which largely deviated ones from the mean characteristics are excluded.

2) Changes of initial magnetization curve with temperatures

The changes of the initial magnetization curve of a virgin piece with temperatures were measured at various temperatures up to 700 °C. The results are shown in Fig. 4.1-4. The inductions for the excitation of 30 oersteds are plotted in Fig. 4.1-5 with reference to the temperatures: one can extrapolate the Curie point of about 715 °C in the figure.

3) Temperature and frequency characteristics of ac permeability

AC permeabilities of a virgin piece were measured at temperatures up to 750 °C with the excitations of (0.42 oersted in peak)/(100 Hz to 10 kHz). The results are shown in Figs. 4.1-6 and -7. One can find out the Curie point of 730 °C in Fig. 4.1-6. This is a little higher than the previous value: the difference may be resulted from an inaccuracy of temperature measurement. The decrease of ac permeability with the

increase of excitation frequency is caused from the increase of eddy current loss.

4) Heat treatments and dc magnetization curves

Variations of dc hysteresis and initial magnetization characteristics due to heat treatments are shown in Figs. 4.1-8 and -9. The rectangularity and the coercive force of quenched-and-tempered (Q-&T) piece are larger than those of the virgin one; namely the Q-&T treatment makes the magnetic characteristics hard. This is caused by a martensite formation on quenching. The increase of the coercive force leads to the change of the initial magnetization curve with decreasing the permeability.

Low-temperature annealing (L.T.A.) increases the rectangularity slightly: consequently, the initial magnetization curve becomes steep with increasing the permeability.

Full annealing (high-temperature annealing, H.T.A.) does not change the rectangularity and the coercive force, but makes the saturation induction smaller than that of the virgin one. According to the decrease of saturation induction, the initial magnetization characteristic becomes "gentle-sloping" with decreasing the initial permeability. The cause of these decreases may come from the precipitation of iron- and chromium-carbides by the formation of ferrite phase during annealing.

Figures 4.1-10 and -11 show the effect of magnetic annealing in the process of full annealing by ac magnetic excitation (H_{ac}). It is shown that the magnetic annealing increases the rectangularity and the permeability.

5) Temperature effect on initial magnetization curves of heat-treated pieces

Figures 4.1-12 to -14 show changes of the initial magnetization curves of heat-treated pieces with temperatures up to 350 °C. The trend of changes with temperatures is similar to that of the virgin one (ref. Fig. 4.1-4).

6) Temperature effect on ac permeabilities of heat treated pieces

The effective permeabilities of heat-treated pieces were measured with an excitation of 1.2 oersteds (peak) in the temperature range up to 800 °C. The results are shown in Fig. 4.1-15. The quenched-and-tempered piece shows its Curie point of about 730 °C and the

full-annealed one 750 °C. This high value of full-annealed one may be caused by the precipitation of carbides during annealing.

Variations of the permeability with temperature cycles were investigated, as well. The results are shown in Figs. 4.1-16 to -18. The performed temperature cycles were; from/to room temperature to/from 350 °C, 450 °C and 600 °C. One can observe the variation of a few percent between 1st and 2nd cycle, but after 2nd cycle the permeabilities were stabilized. This suggests the effectiveness of aging with temperature cyclings.

2. Magnetization Characteristics of SUS 410J1

1) DC magnetization characteristics

Figures 4.2-1 and -2 show the dc hysteresis and initial magnetization curves and their changes with heat treatments. The quenched-and-tempered piece and the low-temperature annealed one have slightly harder and rectangularer characteristics than that of the virgin one. On the contrary to expectations, however, the full annealed piece showed a large coercive force with a small saturation induction. This may be caused from a large structural change formed during annealing.

2) Changes of initial magnetization curves with temperatures

Changes of the initial magnetization curves with temperatures up to 350 °C are shown in Figs. 4.2-3 to -6.

3) Changes of effective ac permeabilities with temperatures

Figure 4.2-7 shows changes of the effective ac permeabilities with temperatures. The Curie points are about 720 °C with a deviation band of +/- 10 °C depending on heat treatments.

3. Magnetization Characteristics of TAF

1) DC magnetization characteristics

Figures 4.3-1 and -2 show the dc hysteresis and initial magnetization curves and their changes with heat treatments. The virgin, quenched-and-tempered and low-temperature-annealed pieces have almost the same characteristics. The coercive forces are about 15 oersteds. The full annealed piece are magnetically soft, as expected, as compared with the others.

2) Changes of initial magnetization curves with temperatures

Changes of the initial magnetization curves with temperatures up to 350 °C are shown in Figs. 4.3-3 to -6.

3) Changes of effective ac permeabilities with temperatures

Figure 4.3-7 shows changes of the effective ac permeabilities with temperatures. The Curie points of martensitic pieces are about 730 °C, but that of the ferritic (full-annealed) piece decreases to 700 °C. This decrease may be caused from the precipitation of iron- and chromium-carbides with resulting in the change (decrease) of Fe/Cr composition ratio.

4. Magnetization Characteristics of SUS 4051) DC magnetization characteristics

Figures 4.4-1 and -2 show the dc hysteresis and initial magnetization curves and their changes with temperatures. Since SUS 405 is ferritic material, its magnetic characteristics are softer than those of the martensitic ones. The full annealed piece has a coercive force of 2 oersteds.

2) Changes of initial magnetization curves with temperatures

Figures 4.4-3 to -5 show changes of the initial magnetization curves with temperatures up to 350 °C.

3) Changes of effective ac permeabilities with temperatures

Figure 4.4-6 shows changes of the effective ac permeabilities with temperatures. The Curie point is about 730 °C and decreases with temperature annealing to about 710 °C.

5. Annexes1) Mechanical hardnesses and microstructures of SUS 403's

Vickers hardnesses of test pieces were measured and referred to the coercive forces (ref. Figs. 4.1-8 and -10) as shown in Table 4.5-1. It is confirmed that there exists a clear proportion between the coercive forces and the hardnesses. The hardness and the coercive force of quenched-and-tempered piece are about twice larger than those of others. This is an explanation of that the martensite, formed by

quenching, was not softened fully by tempering. This can be confirmed by the observation of microstructures as shown in Photo. 4.5-1, as well. The virgin piece shows an annealed structure; i.e., (master phase of ferrite) + (precipitated carbides). On the other hand, quenched-and-tempered piece shows a high-temperature tempered martensite structure. Other interesting evidence is that the magnetic annealing seems to restrain the precipitation of carbides.

2) Changes of ac permeabilities of SUS 410J1, TAF and SUS 405 with temperatures

To investigate stabilities of the permeabilities for temperature cycles, the test pieces were heated up to 750 °C and cooled down to room temperature. The permeabilities before and after heating were measured at room temperature and compared with one another. The results are shown in Table 4.5-2. Since this temperature cycle was similar to the annealing process, the permeabilities increased slightly. Also, the temperature cycles were tried out as that the temperature-increase started from room temperature (R.T) to 350 °C and cooled down to R.T at 1st cycle, and R.T to 450 °C to R.T at 2nd cycle, and then R.T to 600 °C to R.T at final cycle; and the permeabilities and their changes were measured at room temperature. The results are shown in Table 4.5-3. The permeability tends to increase with proceeding of cycle. Also, the increases due to the after effect were observed after cooled down to R.T from 450 °C. Specially this after effect is remarkable in the case of full-annealed SUS 410J1. It seems that the degraded magnetic characteristics of SUS 410J1 by full annealing were recovered by this after effect. On the other hand, the full annealed TAF kept comparatively stable values. On the contrary, the permeabilities of heat-treated (L.T.A. and H.T.A.) SUS 405's were decreased, although that of the virgin one was finally increased. The aging by a relatively low temperature seems to stabilize the magnetic characteristics of SUS 405.

Table 4.4-1 Magnetic characteristics of SUS-403 virgin-pieces.

SAMPLE #	Bm, Gauss;(S.S.)	Br,Gauss;(S.S.)	Hc,0E;(S.S.)	μ_0 ;(S.S.)	μ_{H} ;(S.S.)	Br/Bm
1	15300 (51.4) 0	9100 (45.3) +0	5.5 (42.5) -1	193 (62.7) +2	762 (45.3) -0	0.5948 (44.1) -1
2	15240 (42.0) -1	9700 (59.2) +1	5.6 (48.3) 0	168 (47.2) -0	813 (55.1) +1	0.6365 (60.7) +2
3	15240 (42.0) -1	9000 (43.0) -1	5.8 (60.0) +1	167 (46.6) -0	744 (41.8) -1	0.5906 (42.4) -1
4	15340 (57.6) +1	9530 (55.3) +1	5.6 (48.3) 0	180 (54.6) +0	798 (52.2) +1	0.6213 (54.6) +0
5	15280 (48.3) 0	8940 (41.6) -1	5.3 (31.0) -2	170 (48.4) 0	736 (40.3) -1	0.5851 (40.2) -1
6	15420 (70.0) +2	9460 (53.7) +0	5.4 (36.8) -2	180 (54.6) +0	830 (58.3) +1	0.6135 (51.5) 0
7	15200 (35.8) -2	8600 (33.8) -2	5.6 (48.3) 0	161 (42.8) -1	691 (31.6) -2	0.5658 (32.5) -2
8	15350 (59.2) +1	9760 (60.6) +2	5.6 (48.3) 0	172 (49.7) 0	827 (57.8) +1	0.6358 (60.4) +2
9	15320 (54.5) +0	9260 (49.0) 0	5.6 (48.3) 0	177 (52.8) +0	773 (47.4) -0	0.6044 (47.9) -0
10	15260 (45.2) -0	9940 (64.8) +2	5.4 (36.8) -2	183 (56.5) +1	878 (67.6) +2	0.6514 (66.6) +2
11	15240 (42.0) -1	9550 (55.8) +1	5.6 (48.3) 0	168 (47.2) -0	776 (48.0) 0	0.6266 (56.7) +1
12	15280 (48.3) 0	9400 (52.3) +0	5.6 (48.3) 0	163 (44.1) -1	798 (52.2) +0	0.6152 (52.2) +0
13	15260 (45.2) -0	9460 (53.7) +0	5.7 (54.0) +0	173 (50.3) 0	766 (46.0) -0	0.6199 (54.1) +0
14	15220 (38.9) -2	8300 (26.8) -3	6.0 (71.3) +3	136 (27.4) -3	693 (32.0) -2	0.5453 (24.3) -3
15	15380 (63.8) +2	10060 (67.6) +2	5.5 (42.5) -1	173 (50.3) 0	869 (65.8) +2	0.6541 (67.7) +2
16	15240 (42.0) -1	8900 (40.7) -1	5.9 (65.5) +2	164 (44.7) -1	760 (44.9) -1	0.5840 (39.7) -2
17	15300 (51.4) 0	9280 (49.5) 0	5.7 (54.0) +0	189 (60.2) +2	816 (55.7) +1	0.6065 (48.7) 0
18	15400 (67.0) +2	10040 (67.1) +2	5.4 (36.8) -2	207 (71.3) +3	911 (73.9) +3	0.6519 (66.8) +2
19	15260 (45.2) -0	9280 (49.5) 0	5.7 (54.0) +0	172 (49.7) 0	781 (48.9) 0	0.6081 (49.4) 0
20	15240 (42.0) -1	8960 (42.1) -1	5.4 (36.8) -2	207 (71.3) +3	782 (49.1) 0	0.5879 (41.3) -1
21	15320 (54.5) +0	9220 (48.1) 0	5.7 (54.0) +0	169 (47.8) -0	796 (51.8) 0	0.6018 (46.8) -0
22	15300 (51.4) 0	9520 (55.1) +1	5.9 (65.5) +2	139 (29.2) -3	770 (46.8) -0	0.6222 (55.0) +0
23	15360 (60.7) +2	9220 (48.1) 0	5.6 (48.3) 0	194 (63.3) +2	830 (58.3) +1	0.6003 (46.2) -0
24	15180 (32.7) -2	9180 (47.2) -0	5.7 (54.0) +0	157 (40.4) -1	758 (44.5) -1	0.6047 (48.0) 0
25	15420 (70.0) +2	8730 (36.8) -2	5.8 (60.0) +1	167 (46.6) -0	709 (35.1) -2	0.5661 (32.6) -2
26	15230 (40.5) -1	9880 (63.4) +2	5.5 (42.5) -1	170 (48.4) 0	828 (58.0) +1	0.6487 (65.5) +2
27	15280 (48.3) 0	8860 (39.8) -2	5.9 (65.5) +2	160 (42.2) -1	742 (41.4) -1	0.5798 (38.1) -2
\bar{x}	15291.1	9301.1	5.63	172.6	786.6	0.6097
σ	64.2	432.1	0.17	16.2	52.0	0.0251

σ	-2 σ	- σ	0	+ σ	+2 σ
S.S.	30	40	48	52	60
Sign	-2	-1	0	+0+1	+2
%			68.3		95.5

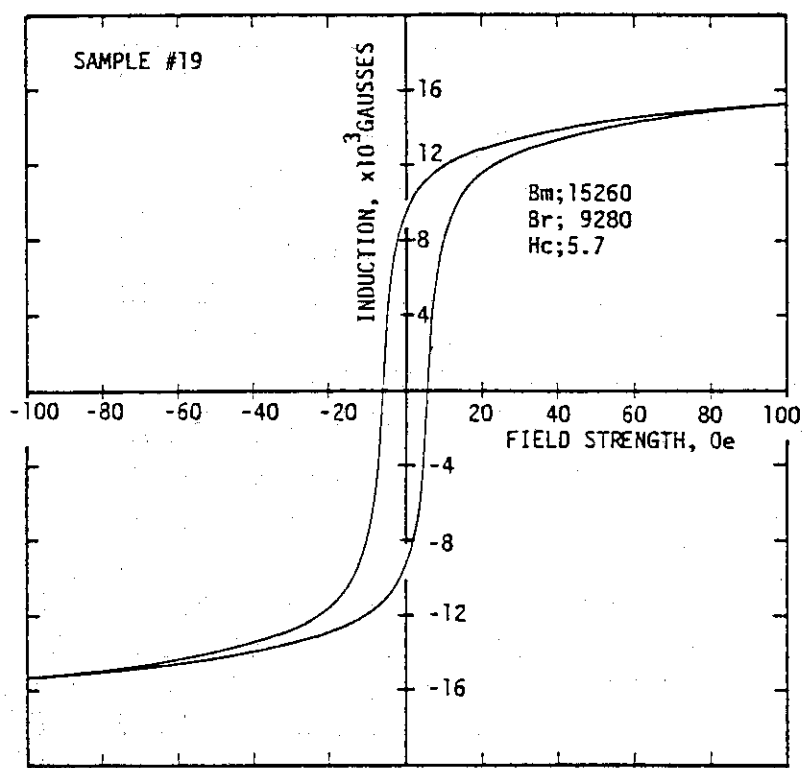


Fig. 4.1-1 Representative of dc hysteresis magnetization curves of SUS-403 virgin-pieces.

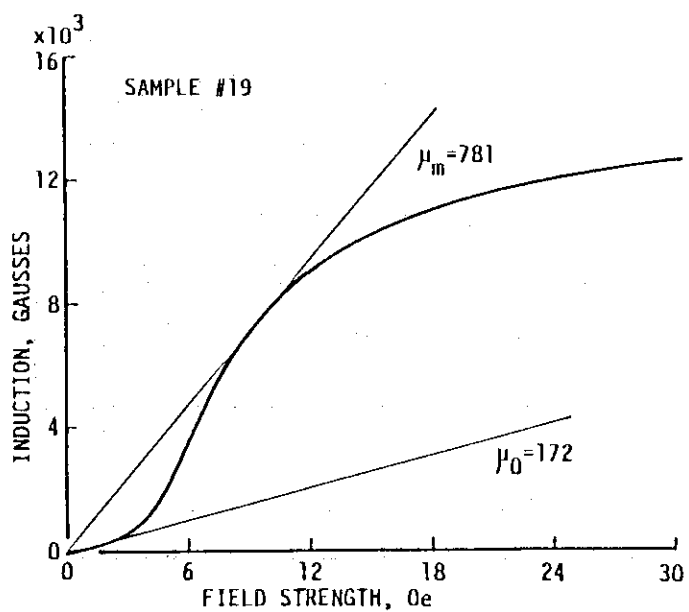


Fig. 4.1-2 Representative of dc initial magnetization curves of SUS-403 virgin-pieces.

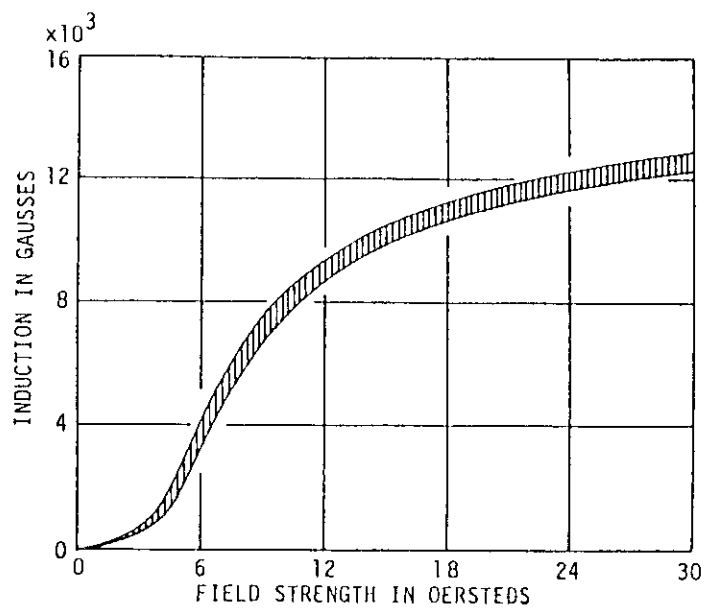


Fig. 4.1-3 Irregularity band of dc initial magnetization curves of SUS-403 virgin-pieces.

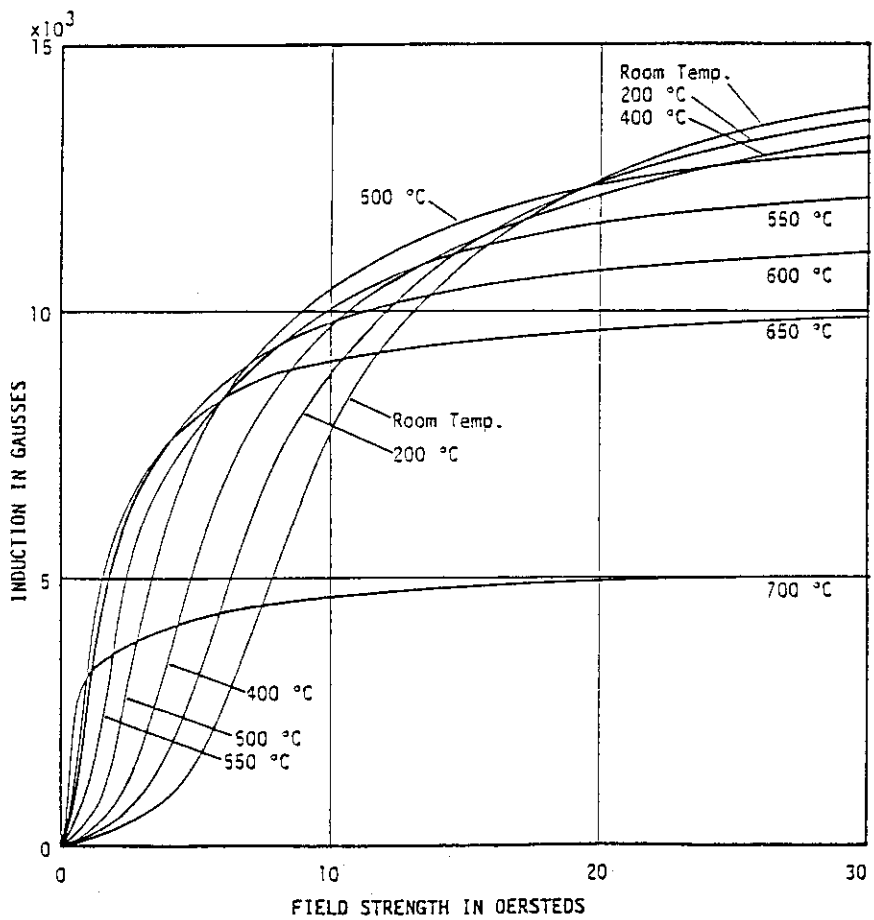


Fig. 4.1-4 Changes of dc initial magnetization curve of SUS-403 virgin-piece with temperatures.

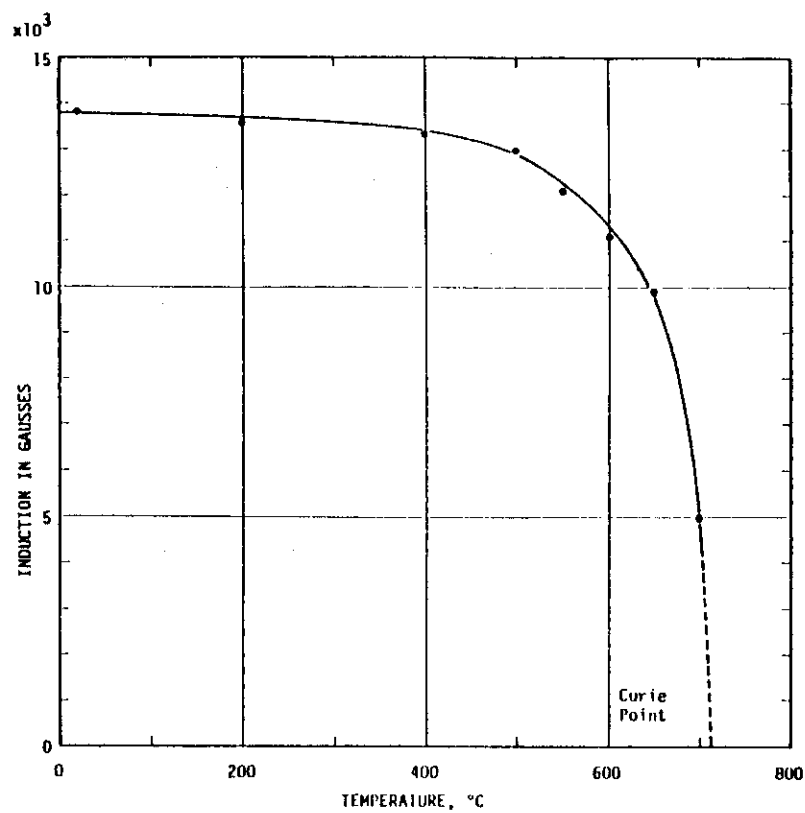


Fig. 4.1-5 Saturation induction of SUS-403 virgin-piece and its variations with temperatures at excitation strength of 30 oersteds.

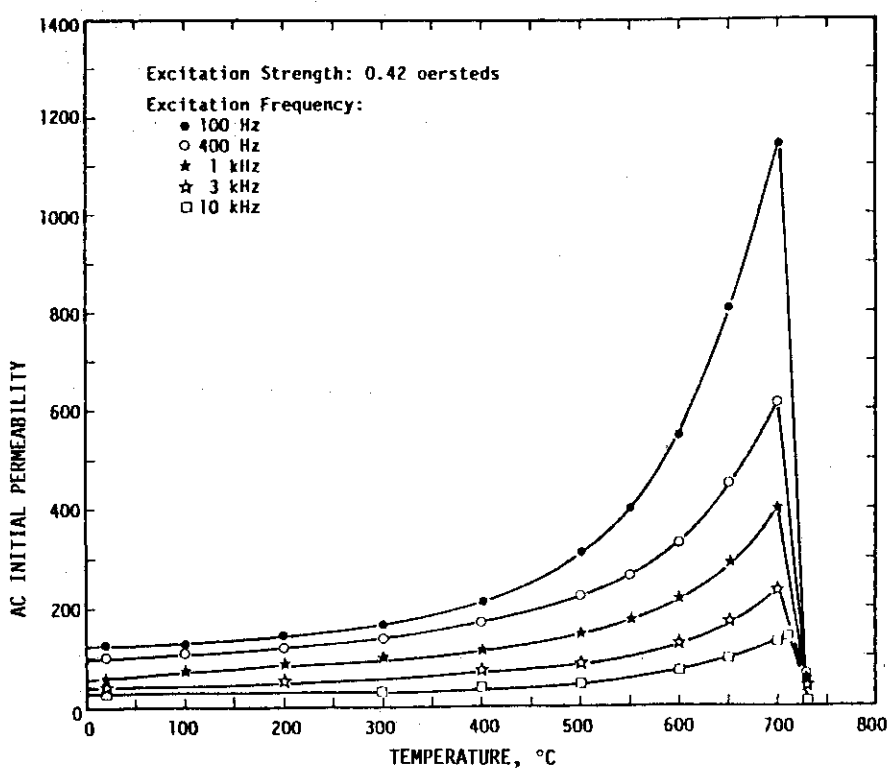


Fig. 4.1-6 AC initial permeability of SUS-403 virgin-piece for various excitation frequencies and its changes with temperatures.

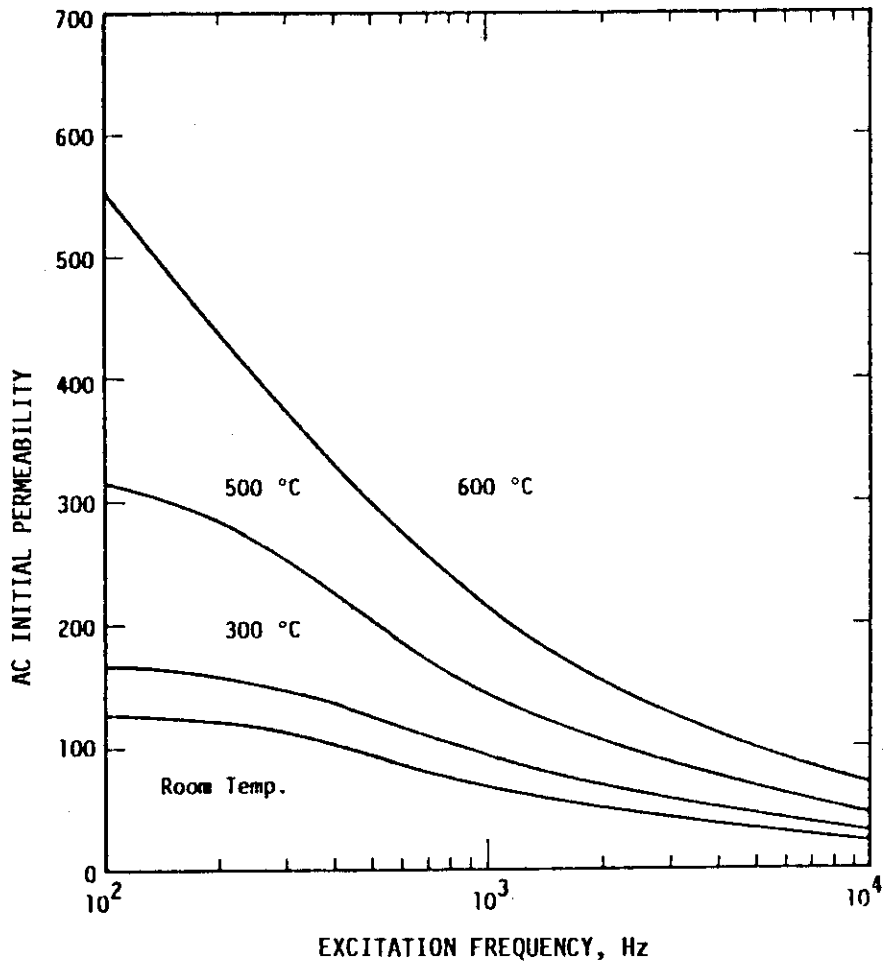


Fig. 4.1-7 AC initial permeability of SUS-403 virgin-piece at various temperatures and its changes with excitation frequencies.

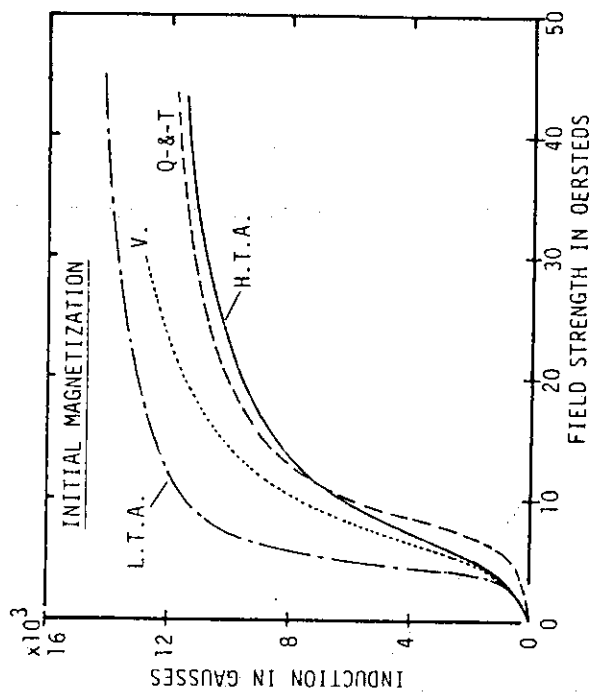
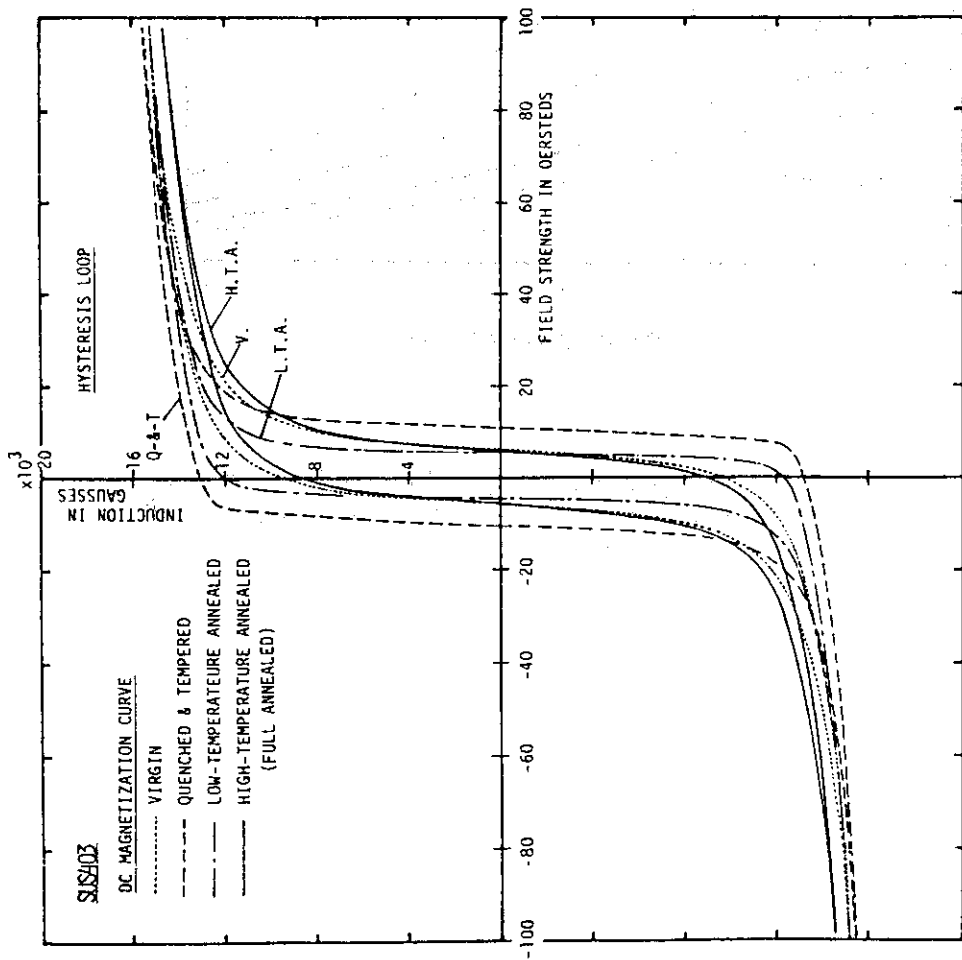


Fig. 4.1-8 Variations of dc hysteresis magnetization curve of SUS 403 with heat treatments.
Fig. 4.1-9 Variations of dc initial magnetization curve of SUS 403 with heat treatments.



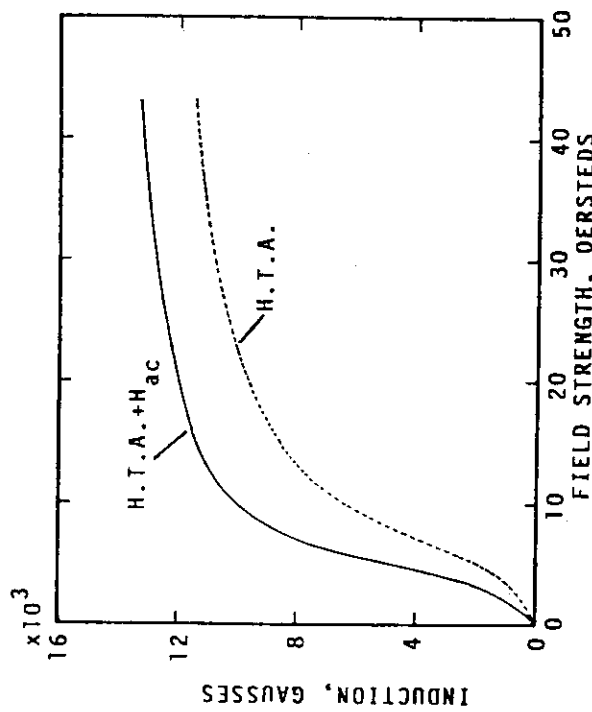


Fig. 4.1-11 Effect of magnetic annealing on dc initial magnetization curve of SUS 403.

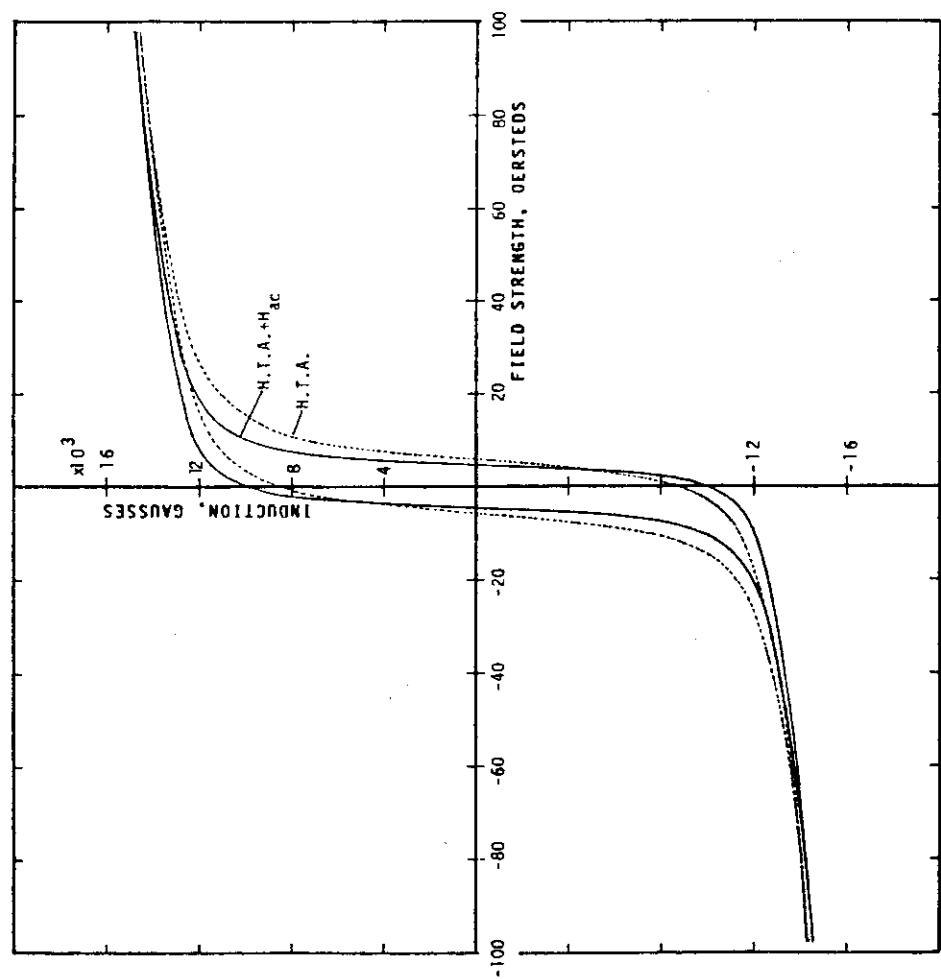


Fig. 4.1-10 Effect of magnetic annealing on dc hysteresis magnetization curve of SUS 403.

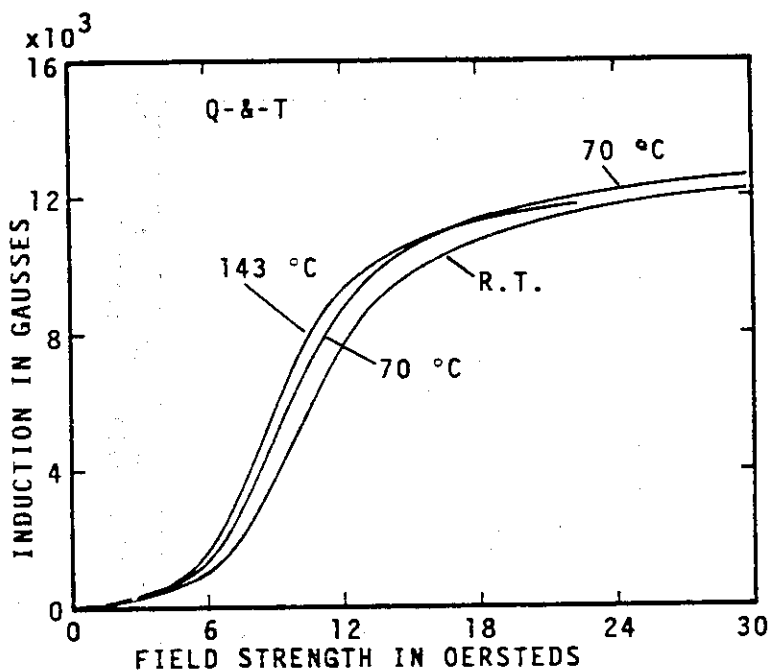


Fig. 4.1-12 Changes of dc initial magnetization curve of quenched-and-tempered SUS 403 with temperatures.

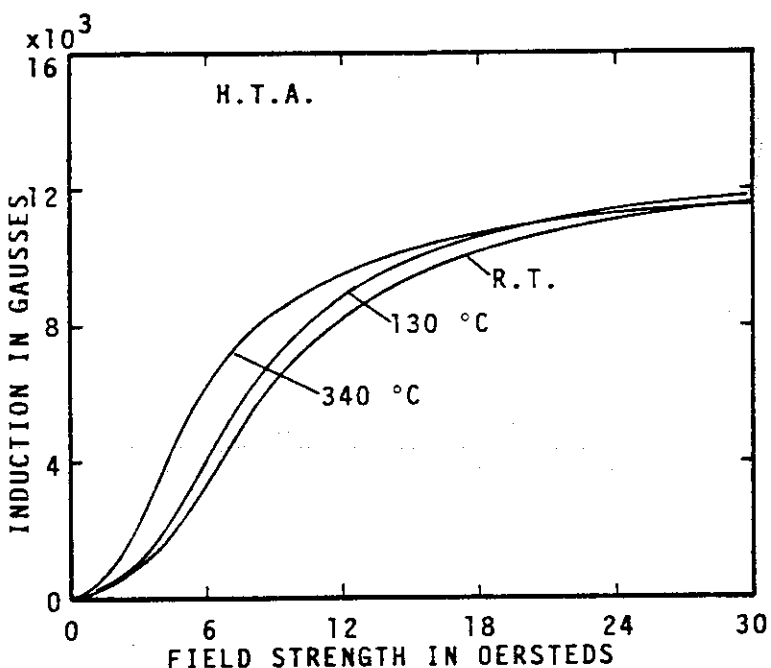


Fig. 4.1-13 Changes of dc initial magnetization curve of full (high-temperature) annealed SUS 403 with temperatures.

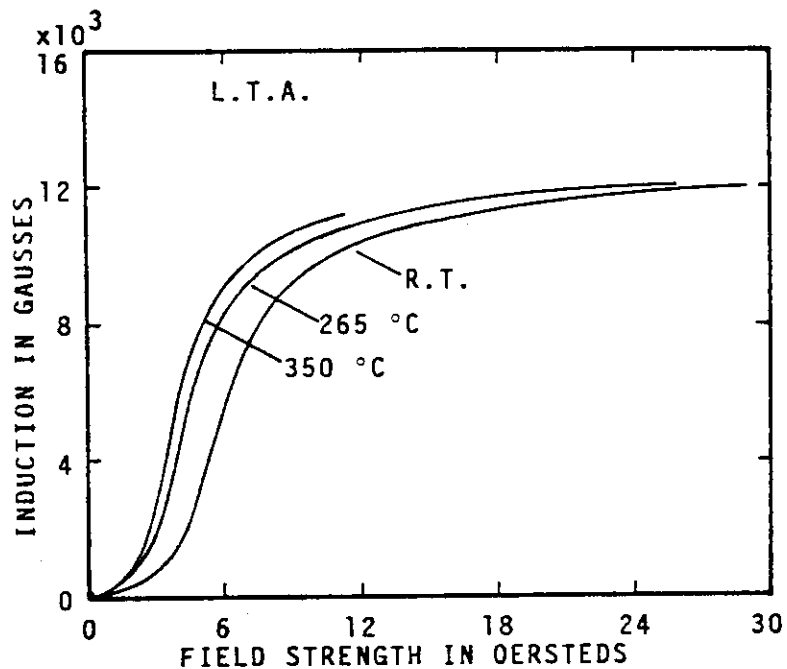


Fig. 4.1-14 Changes of dc initial magnetization curve of low-temperature annealed SUS 403 with temperatures.

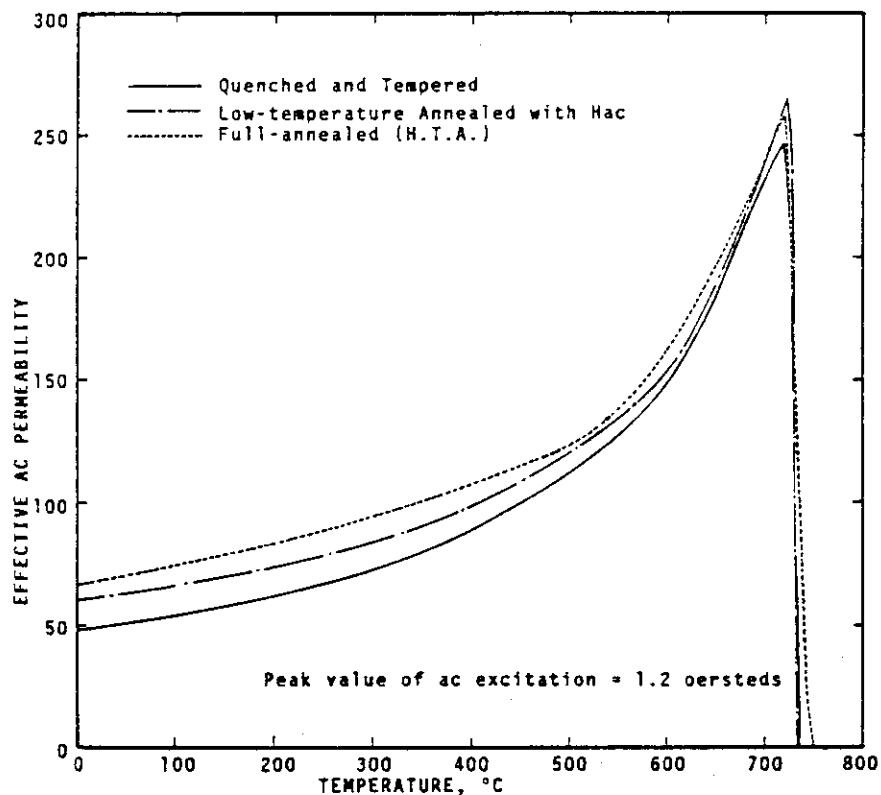


Fig. 4.1-15 Effective ac permeabilities of heat-treated SUS 403's and their changes with temperatures.

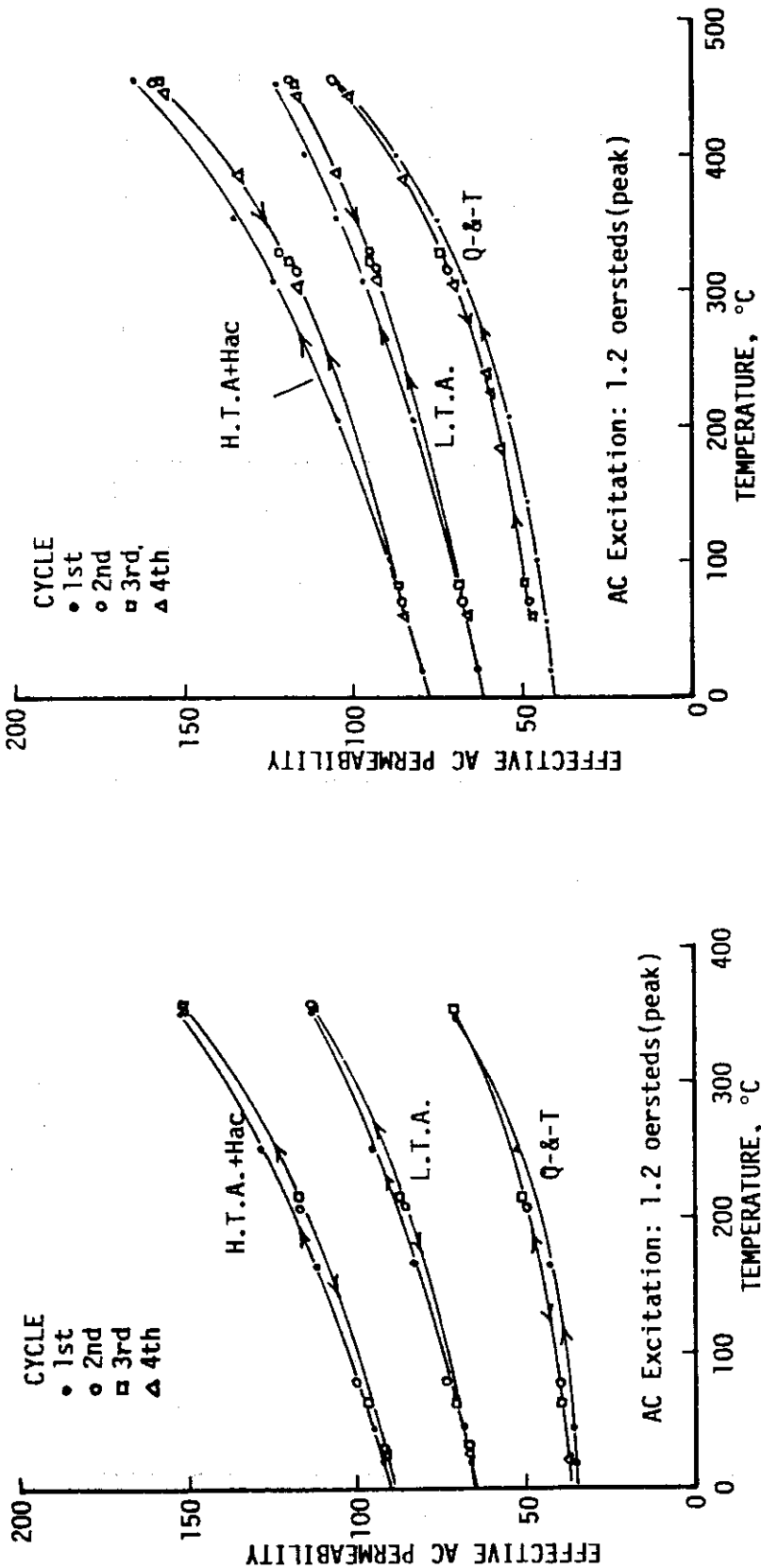


Fig. 4.1-16 Effective ac permeabilities of heat-treated SUS 403's and their changes with temperature cycles.

Fig. 4.1-17 Effective ac permeabilities of heat-treated SUS 403's and their changes with temperature cycles.

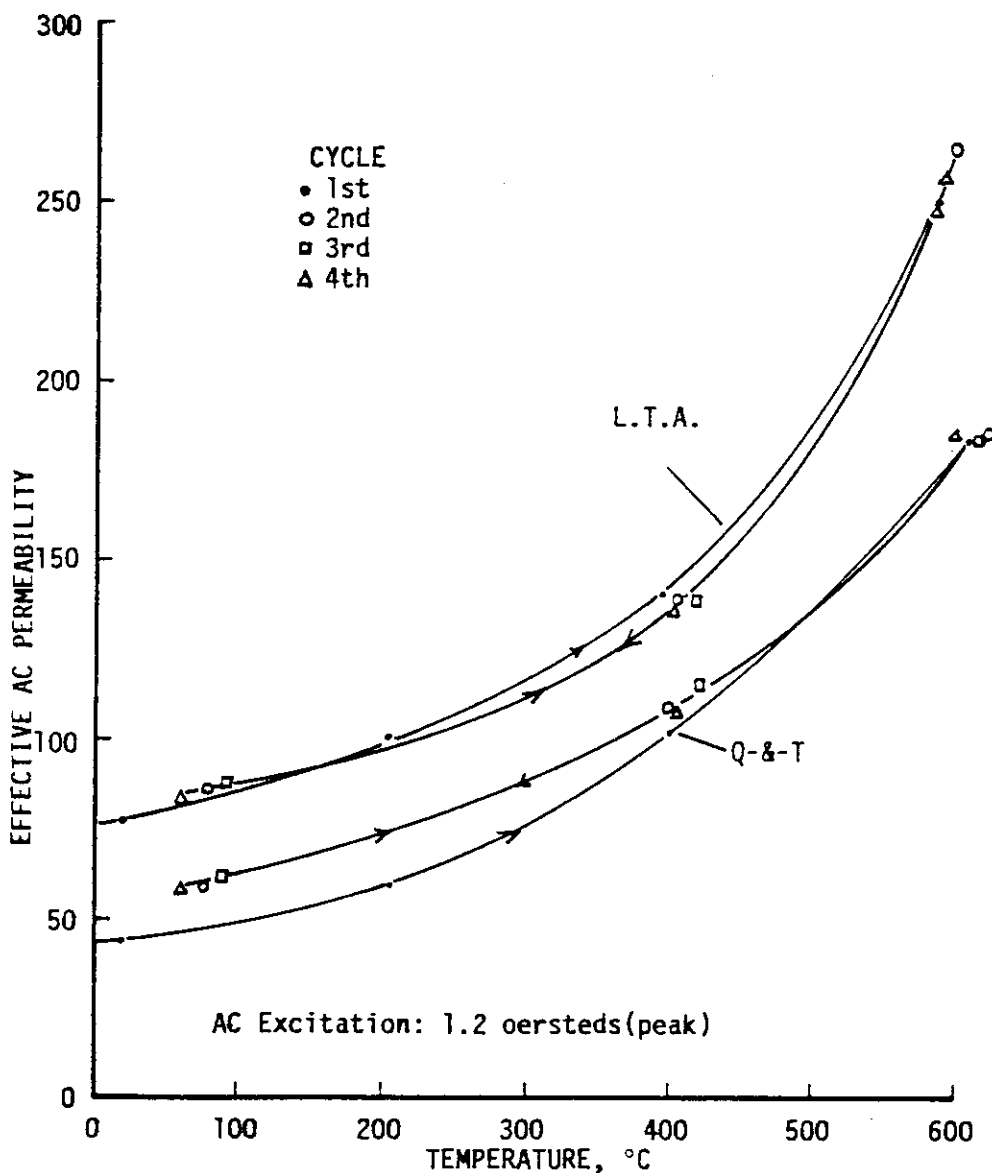


Fig. 4.1-18 Effective ac permeabilities of heat-treated SUS 403's and their changes with temperature cycles.

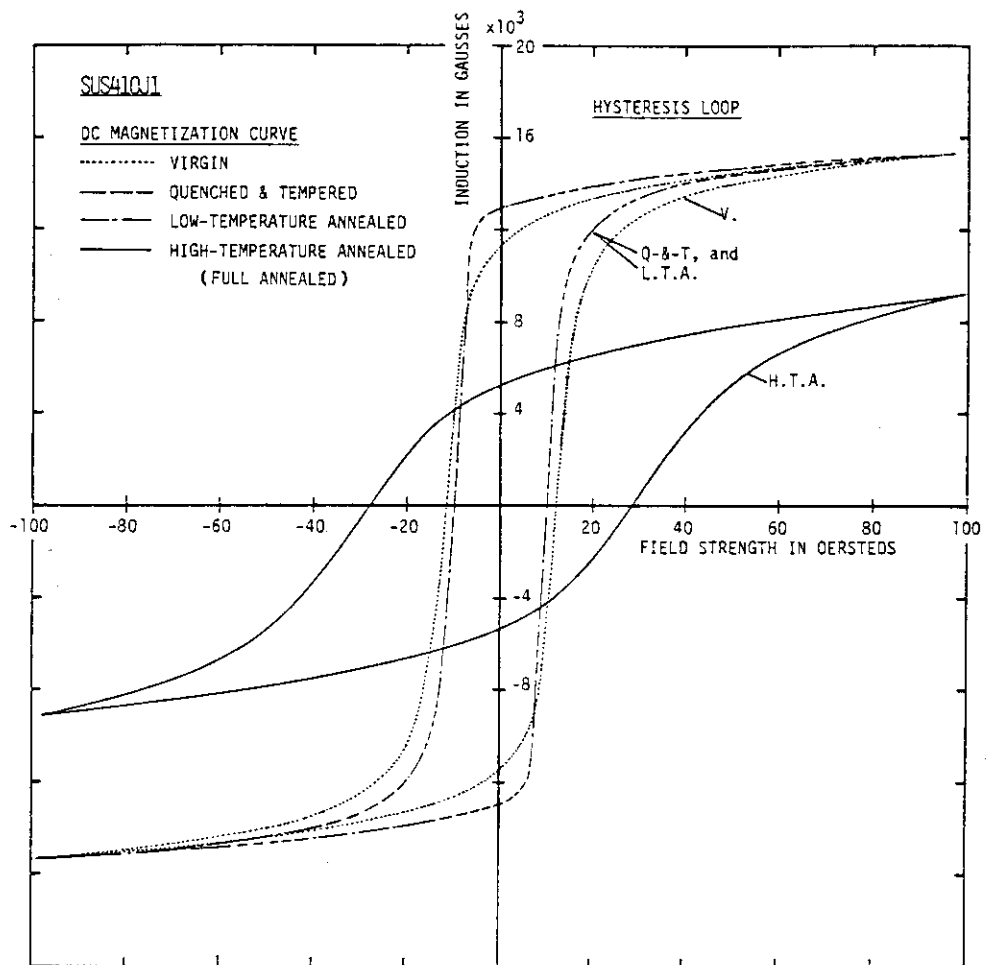


Fig. 4.2-1 Variations of dc hysteresis magnetization curve of SUS 410J1 with heat treatments.

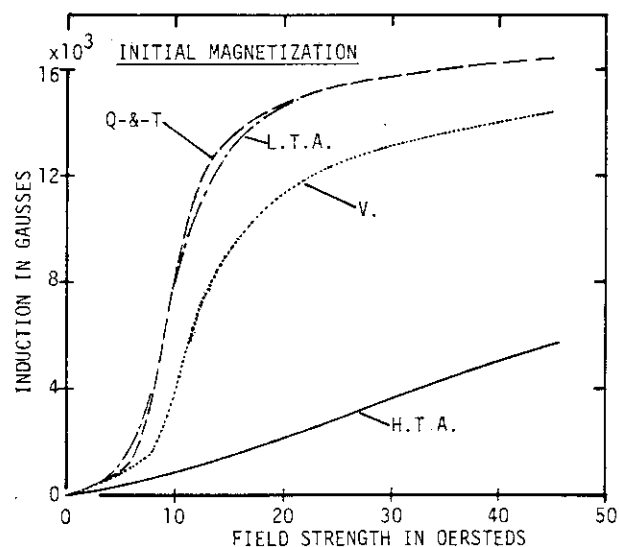


Fig. 4.2-2 Variations of dc initial magnetization curve of SUS 410J1 with heat treatments.

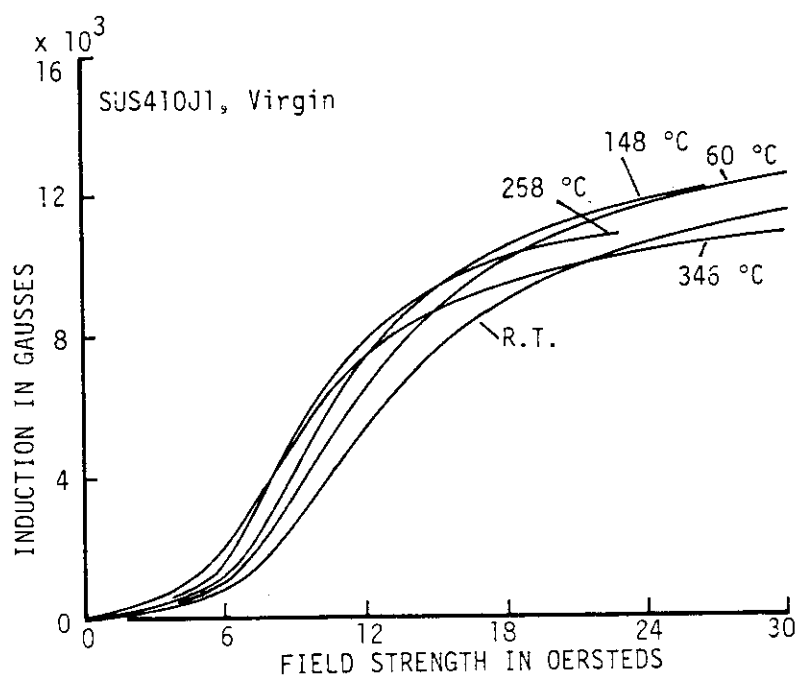


Fig. 4.2-3 Changes of dc initial magnetization curve of SUS-410J1 virgin-piece with temperatures.

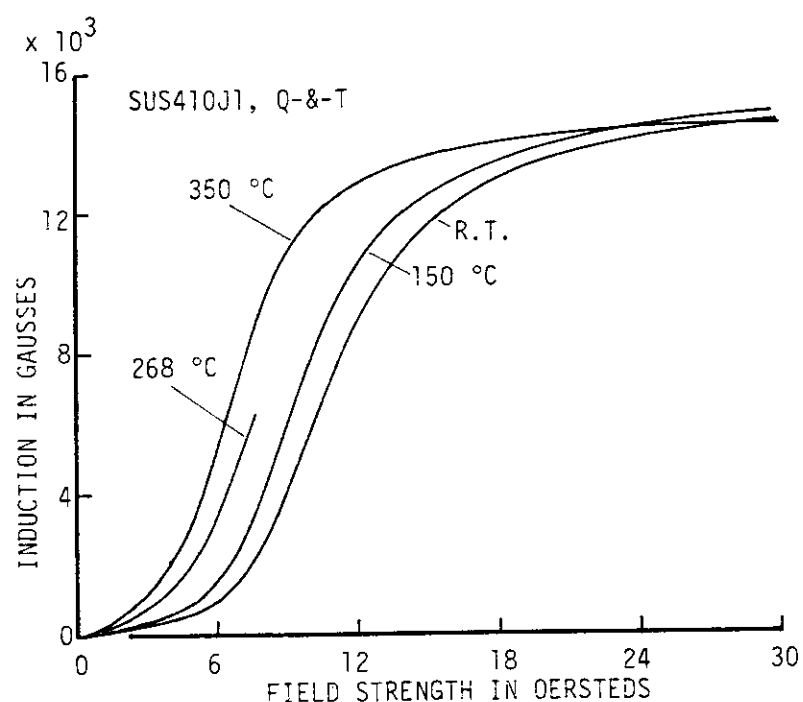


Fig. 4.2-4 Changes of dc initial magnetization curve of quenched-and-tempered SUS 410J1 with temperatures.

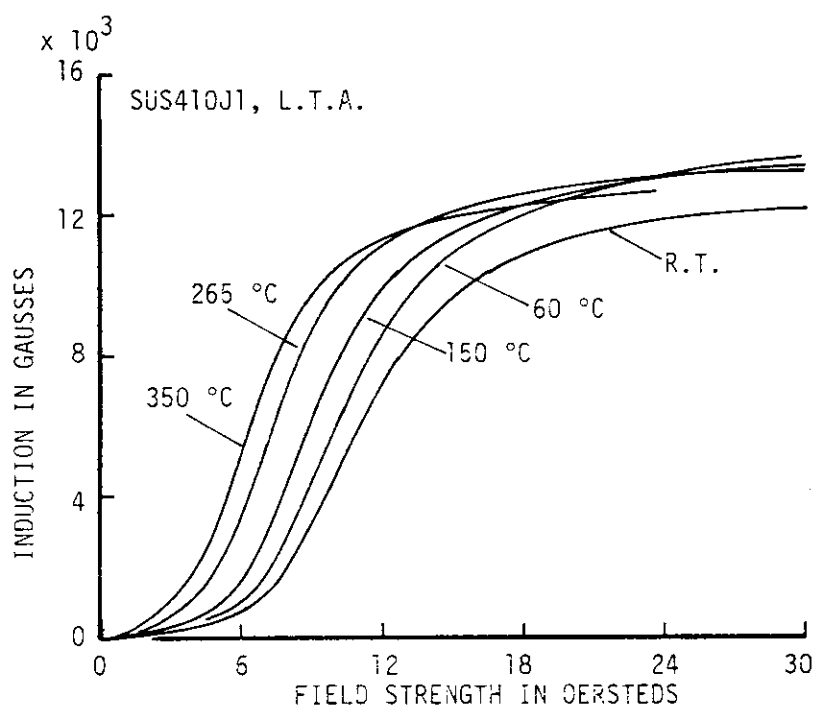


Fig. 4.2-5 Changes of dc initial magnetization curve of low-temperature annealed SUS 410J1 with temperatures.

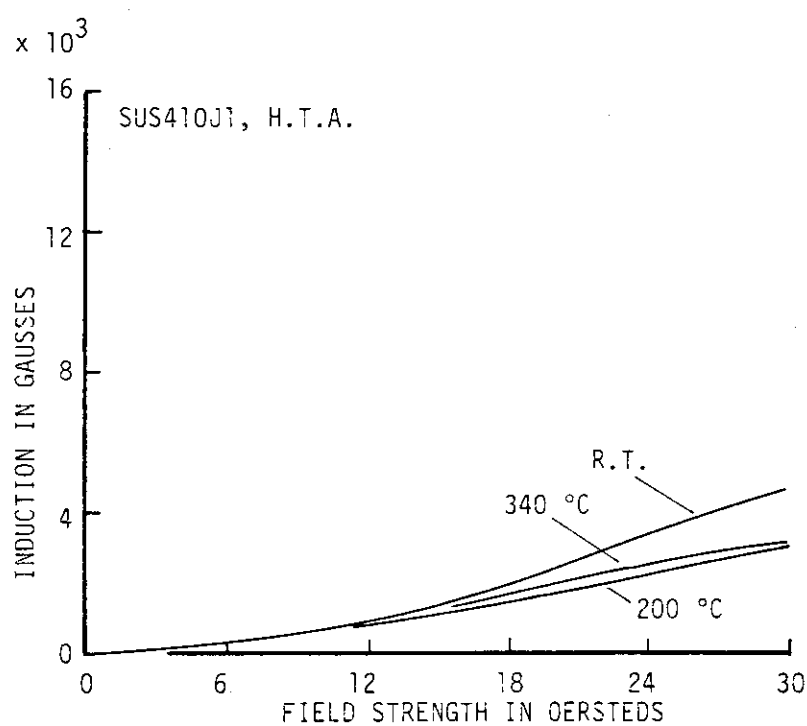


Fig. 4.2-6 Changes of dc initial magnetization curve of full (high-temperature) annealed SUS 410J1 with temperatures.

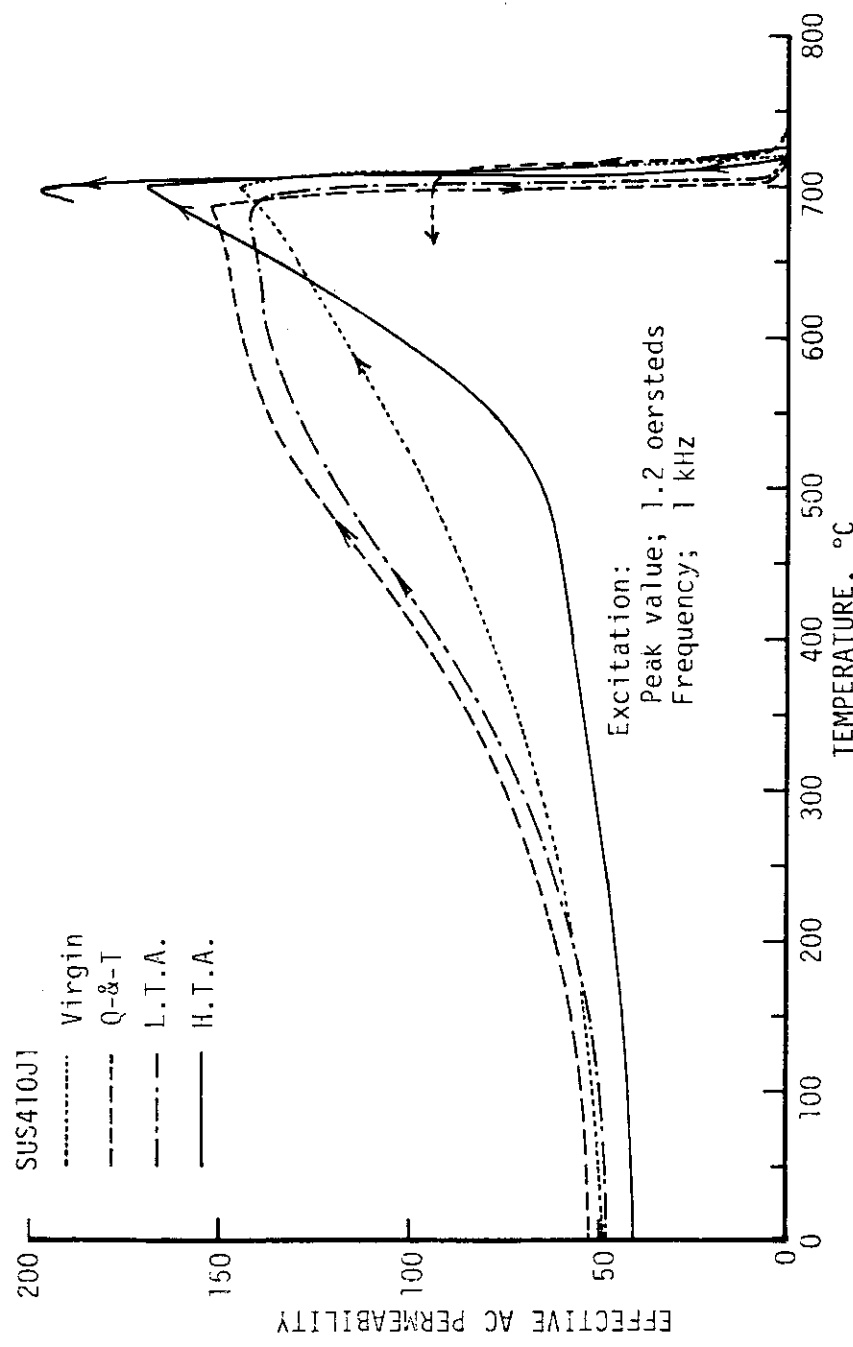


Fig. 4.2-7 Effective ac permeabilities of heat-treated SUS 410J1's and their changes with temperatures.

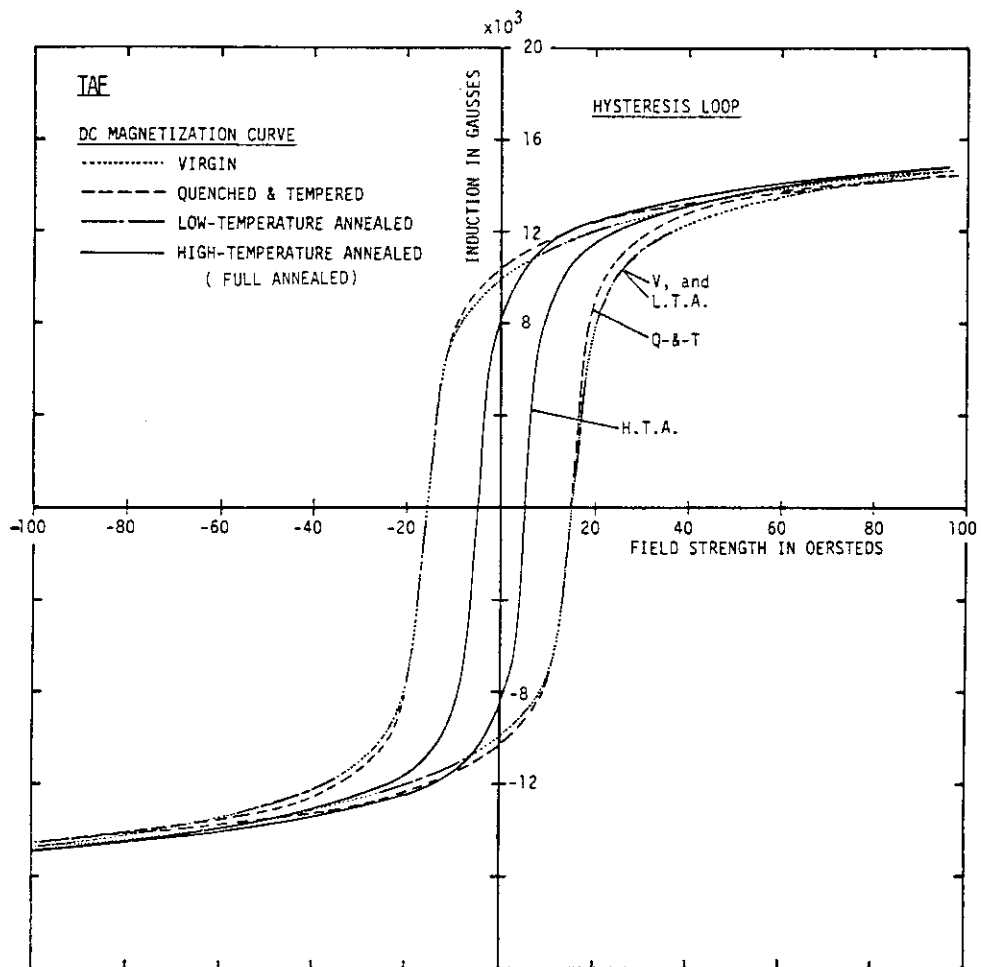


Fig. 4.3-1 Variations of dc hysteresis magnetization curve of TAF with heat treatments.

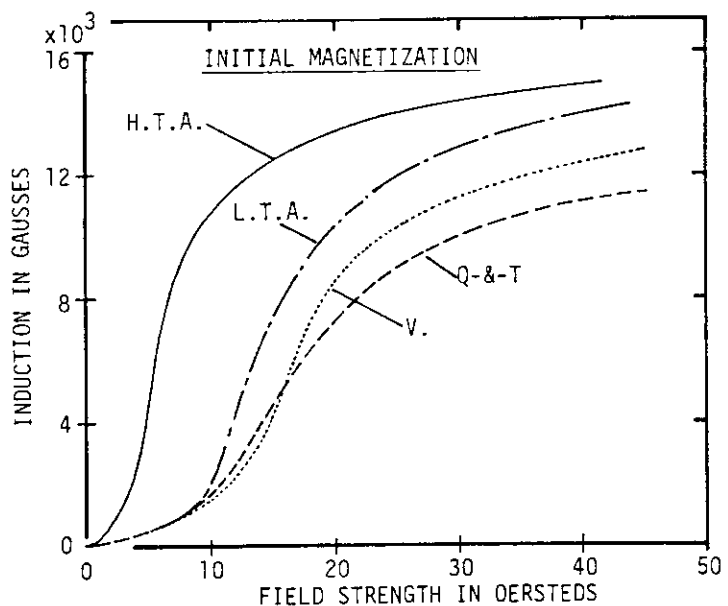


Fig. 4.3-2 Variations of dc initial magnetization curve of TAF with heat treatments.

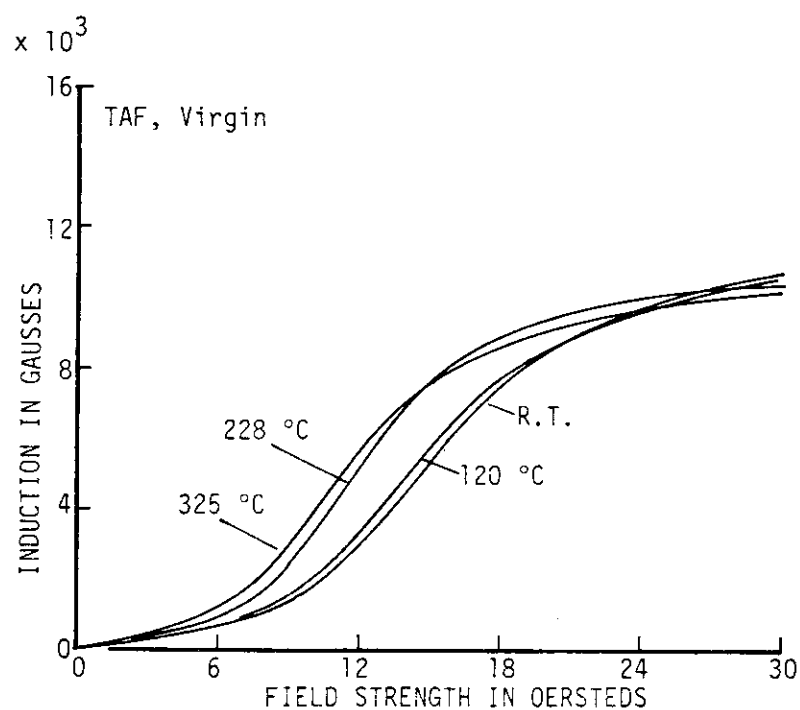


Fig. 4.3-3 Changes of dc initial magnetization curve of TAF virgin-piece with temperatures.

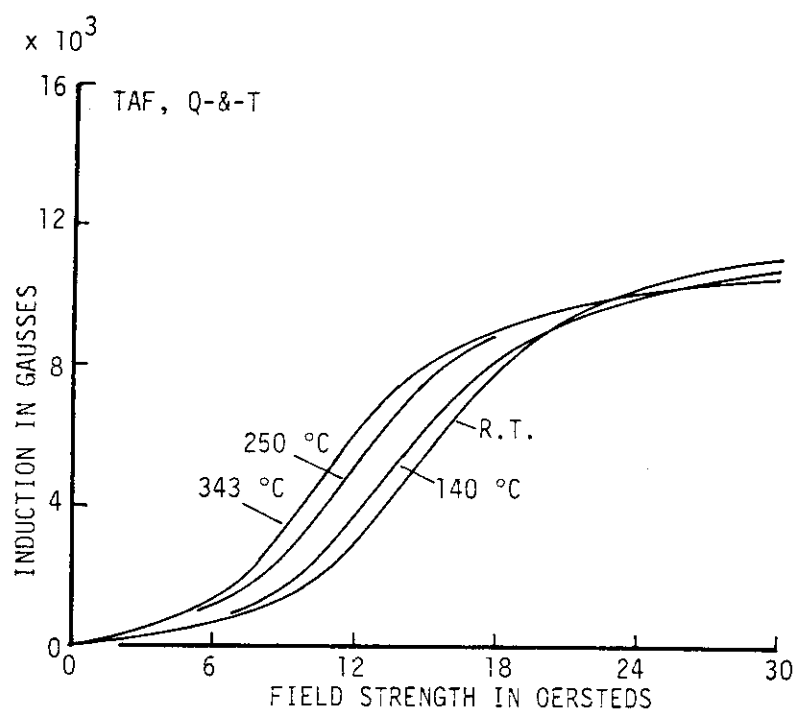


Fig. 4.3-4 Changes of dc initial magnetization curve of quenched-and-tempered TAF with temperatures.

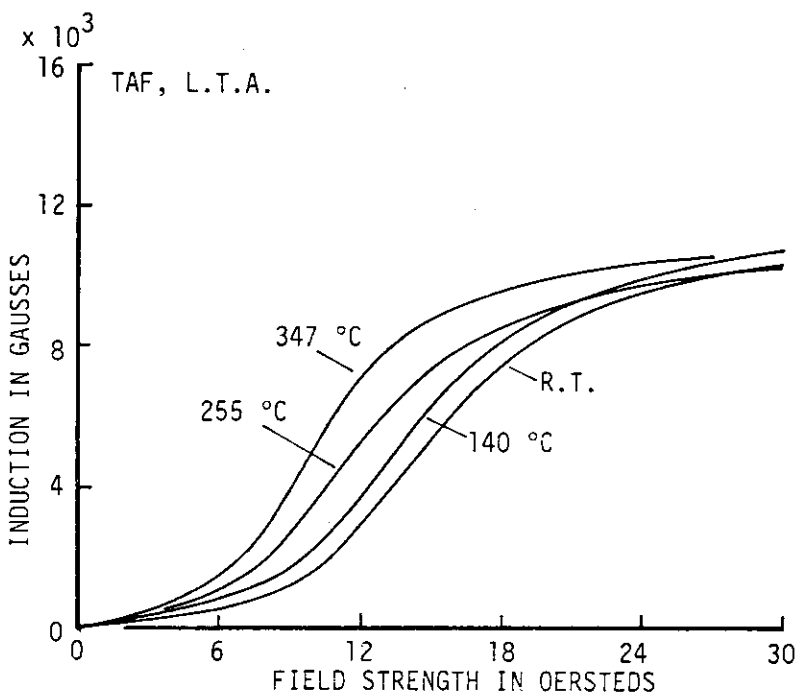


Fig. 4.3-5 Changes of dc initial magnetization curve of low-temperature annealed TAF with temperatures.

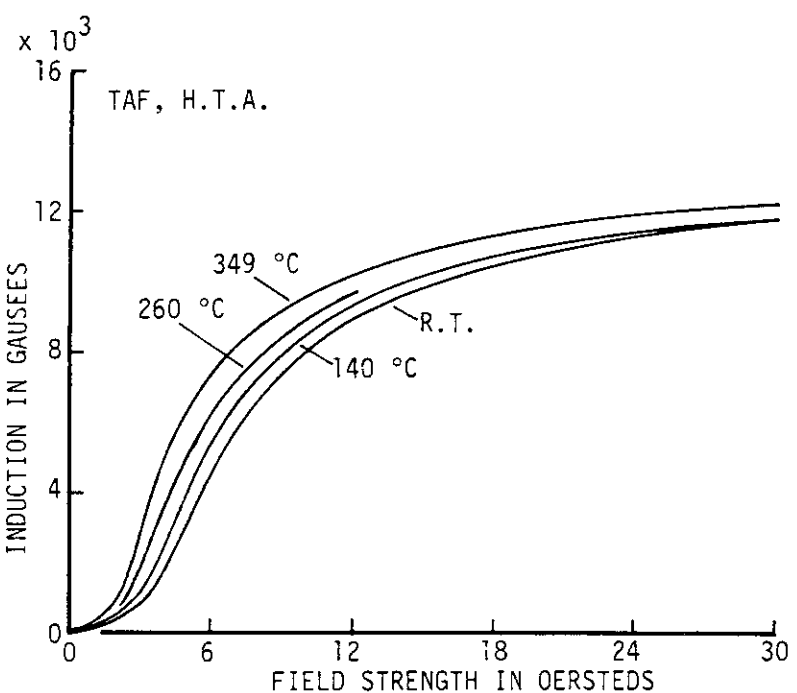


Fig. 4.3-6 Changes of dc initial magnetization curve of full (high-temperature) annealed TAF with temperatures.

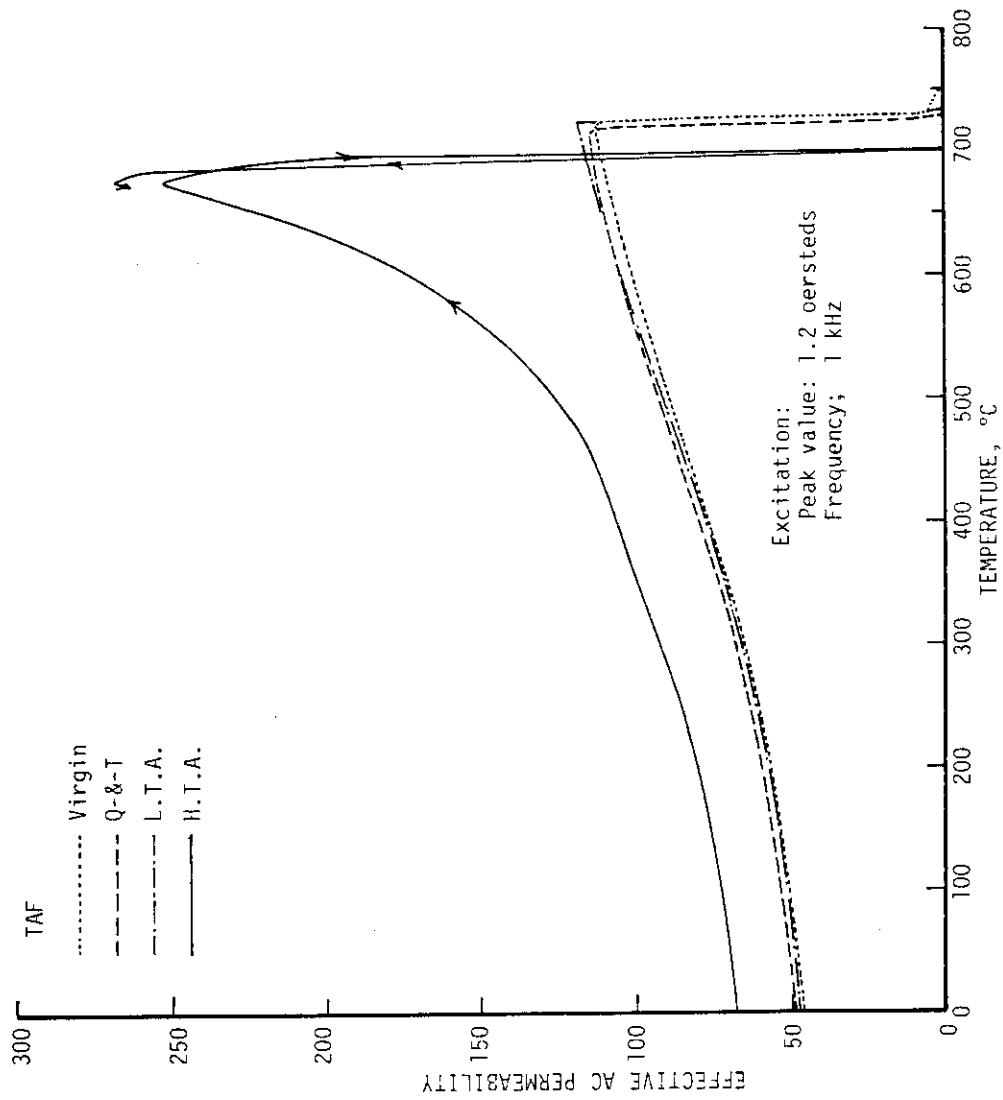


Fig. 4.3-7 Effective ac permeabilities of heat-treated TAF's and their changes with temperatures.

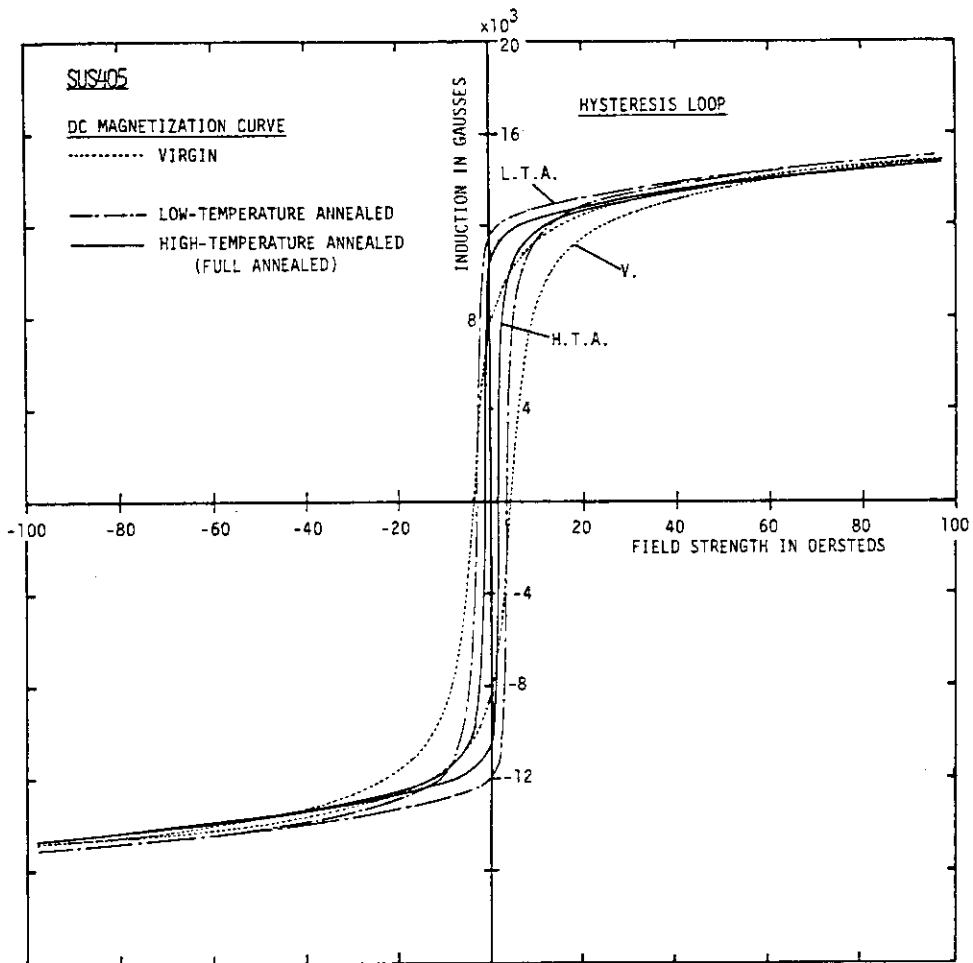


Fig. 4.4-1 Variations of dc hysteresis magnetization curve of SUS 405 with heat treatments.

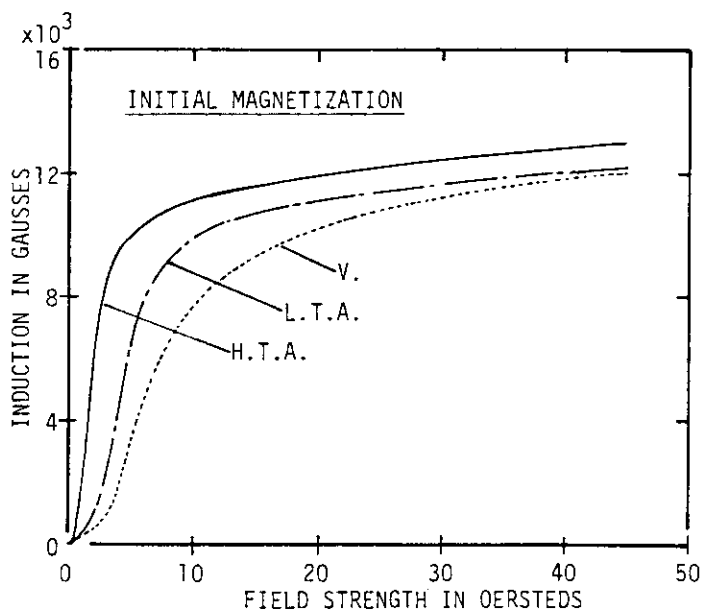


Fig. 4.4-2 Variations of dc initial magnetization curve of SUS 405 with heat treatments.

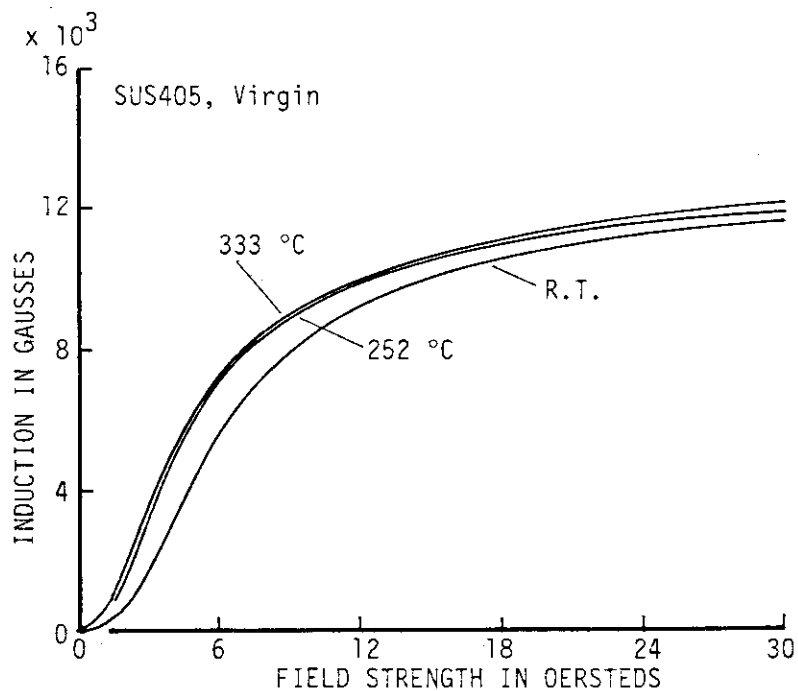


Fig. 4.4-3 Changes of dc initial magnetization curve of SUS-405 virgin-piece with temperatures.

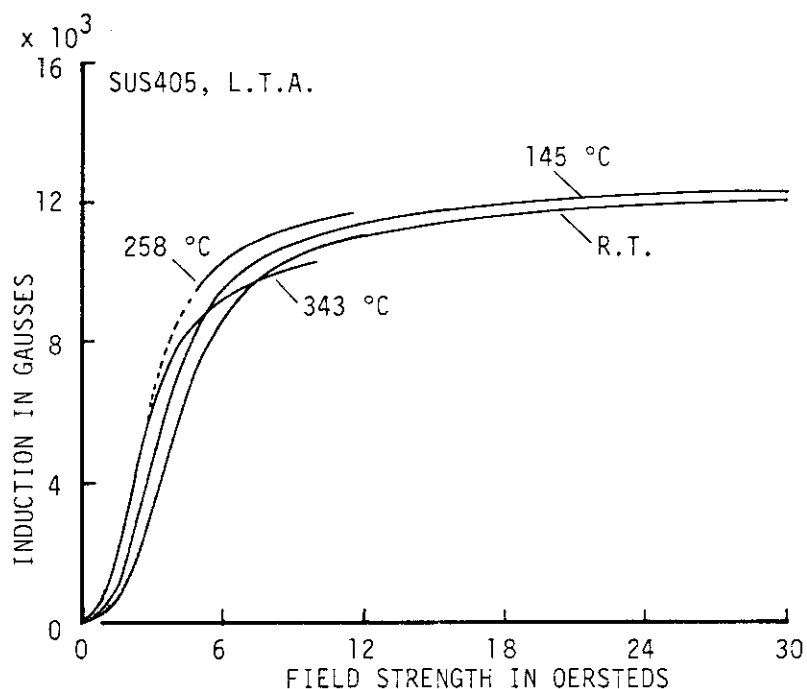


Fig. 4.4-4 Changes of dc initial magnetization curve of low-temperature annealed SUS 405 with temperatures.

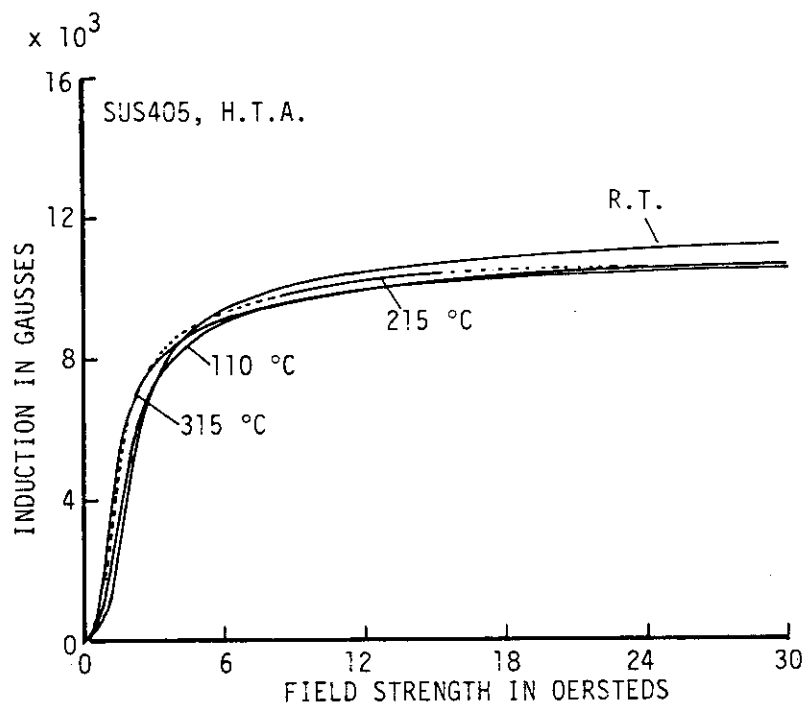


Fig. 4.4-5 Changes of dc initial magnetization curve of full (high-temperature) annealed SUS 405 with temperatures.

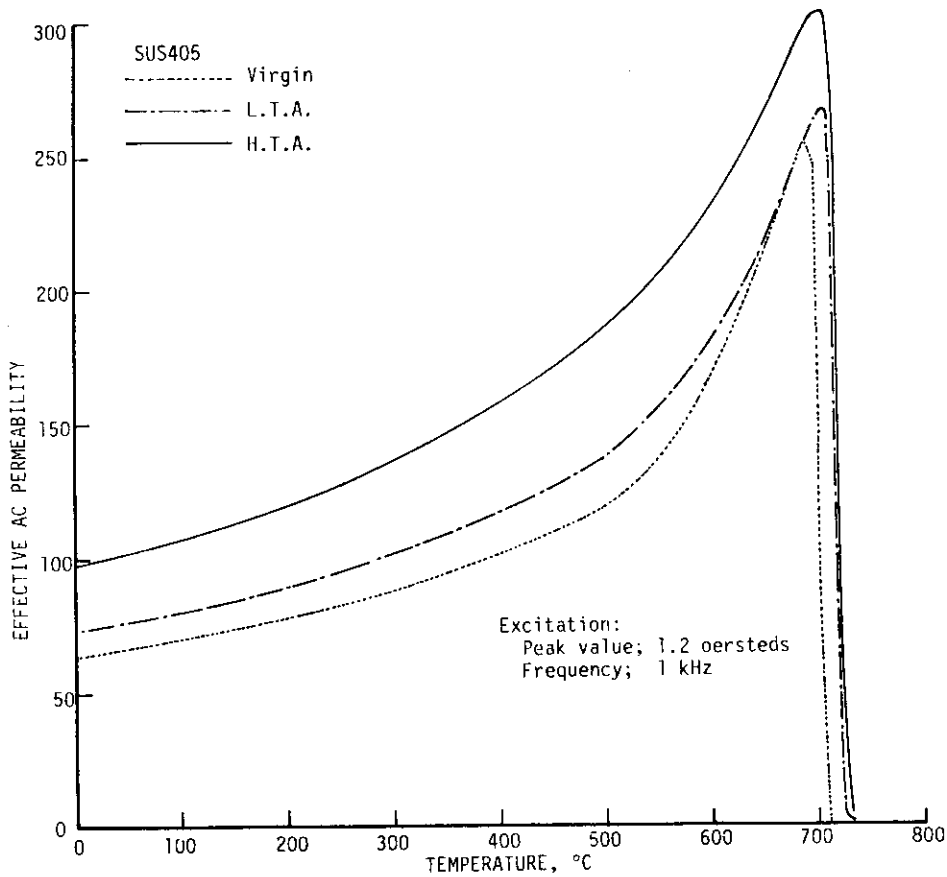


Fig. 4.4-6 Effective ac permeabilities of heat-treated SUS 405's and their changes with temperatures.

Table 4.5-1 Vickers hardnesses and coercive forces of heat-treated SUS 403's.

Sample	Heat Treatment	Vickers Hardness	Coercive Force, Oe.
1	V	144	5.8
2	Q-&-T	228	10.4
3	H.T.A	147	6.2
4	H.T.A/H _{ac}	135	5.0

V: Virgin
 Q-&-T: Quenched and Tempered
 H.T.A: High-temperature (Full)
 Annealed
 H.T.A/H_{ac}: H.T.A with AC Magnetic Field

Table 4.5-2 Variations of effective ac permeabilities of SUS 410J1's, TAF's and SUS 405 with heat cycle.

Material	Heat Treatment	Effective AC Permeability $\mu_1(14^\circ\text{C}) \rightarrow 750^\circ\text{C} \rightarrow \mu_2(18^\circ\text{C})$	Variation, %
SUS410J1	Q-&-T	73.15	+7.3
	L.T.A.	64.01	+5.4
	V	67.60	+7.1
TAF	Q-&-T	63.63	+3.6
	H.T.A.	69.34	+7.3
	V	75.70	+4.7
SUS405	V	83.82	+5.0

Table 4.5-3 Variations of effective ac permeabilities of SUS 410J1's, TAF's and SUS 405's with heat cycles.

T.H.	Material and Heat Treatment											
	SUS410J1				TAF				SUS405			
	V	Q-&-T	L.T.A	H.T.A	V	Q-&-T	L.T.A	H.T.A	V	L.T.A	H.T.A	
1 R.T	45.3	44.2	45.3	28.5	44.5	46.1	44.2	72.8	68.6	101.7	148.3	
2 350												
3 R.T	45.3	45.0	46.1	29.3	44.2	46.5	44.2	70.1	63.1	97.5	153.2	
4 450												
5 R.T	47.6	48.4	48.8	30.5	45.0	47.6	54.0	69.3	67.4	94.1	139.8	
6 R.T	50.7	51.8	51.4	53.7	45.3	48.4	45.3	70.1	78.5	95.6	138.3	
7 600												
8 R.T	51.4	53.0	52.6	54.5	46.1	48.8	45.3	71.6	81.9	98.7	139.5	

T.H.: Temperature History, °C; between 5 and 6, specimens were at R.T. (10 - 17 °C) for about 30 minutes.

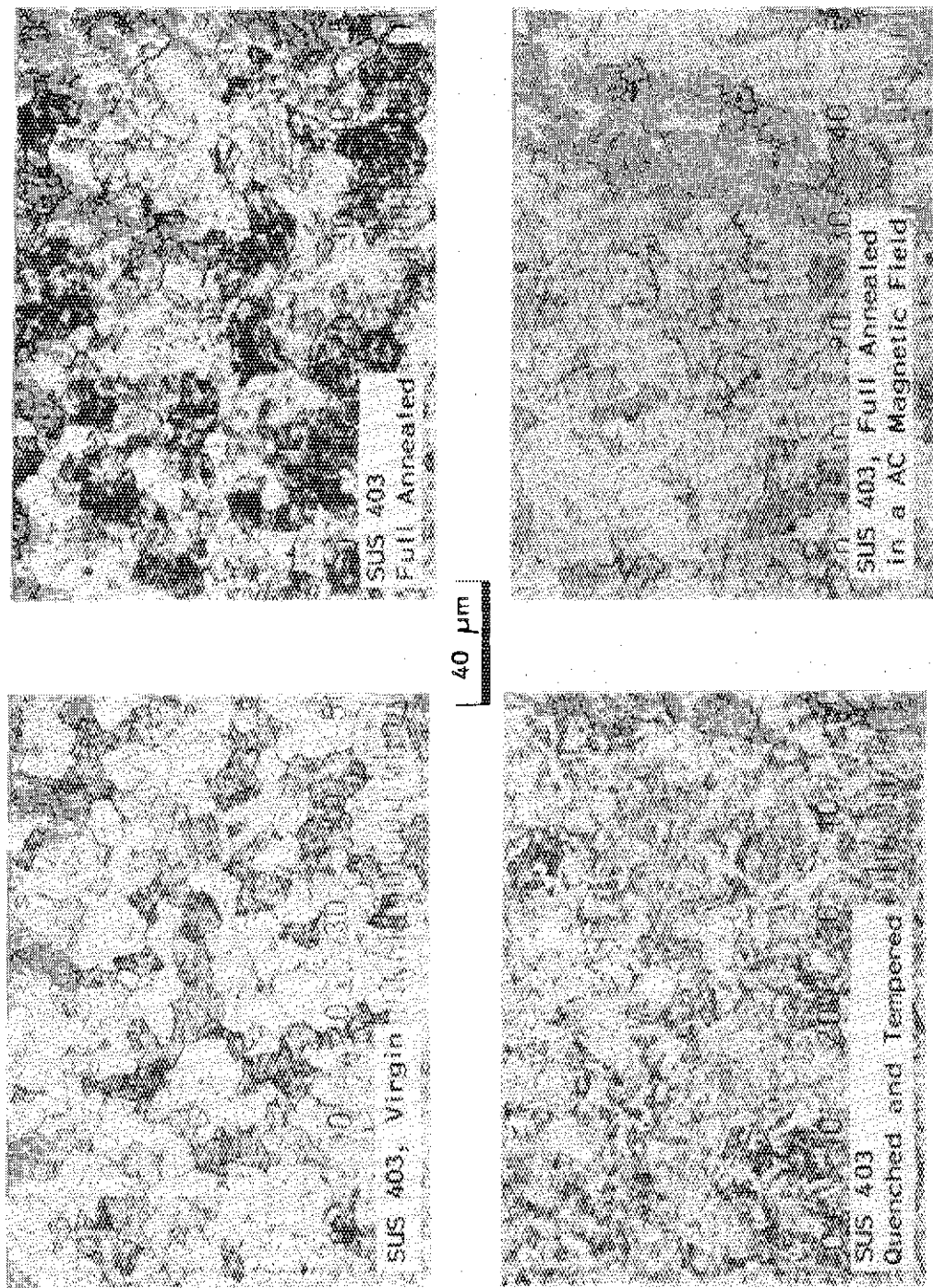


Photo. 4.5-1(1) Microstructures of virgin and heat-treated SUS 403 test pieces (I):
magnification, $\times 300$.

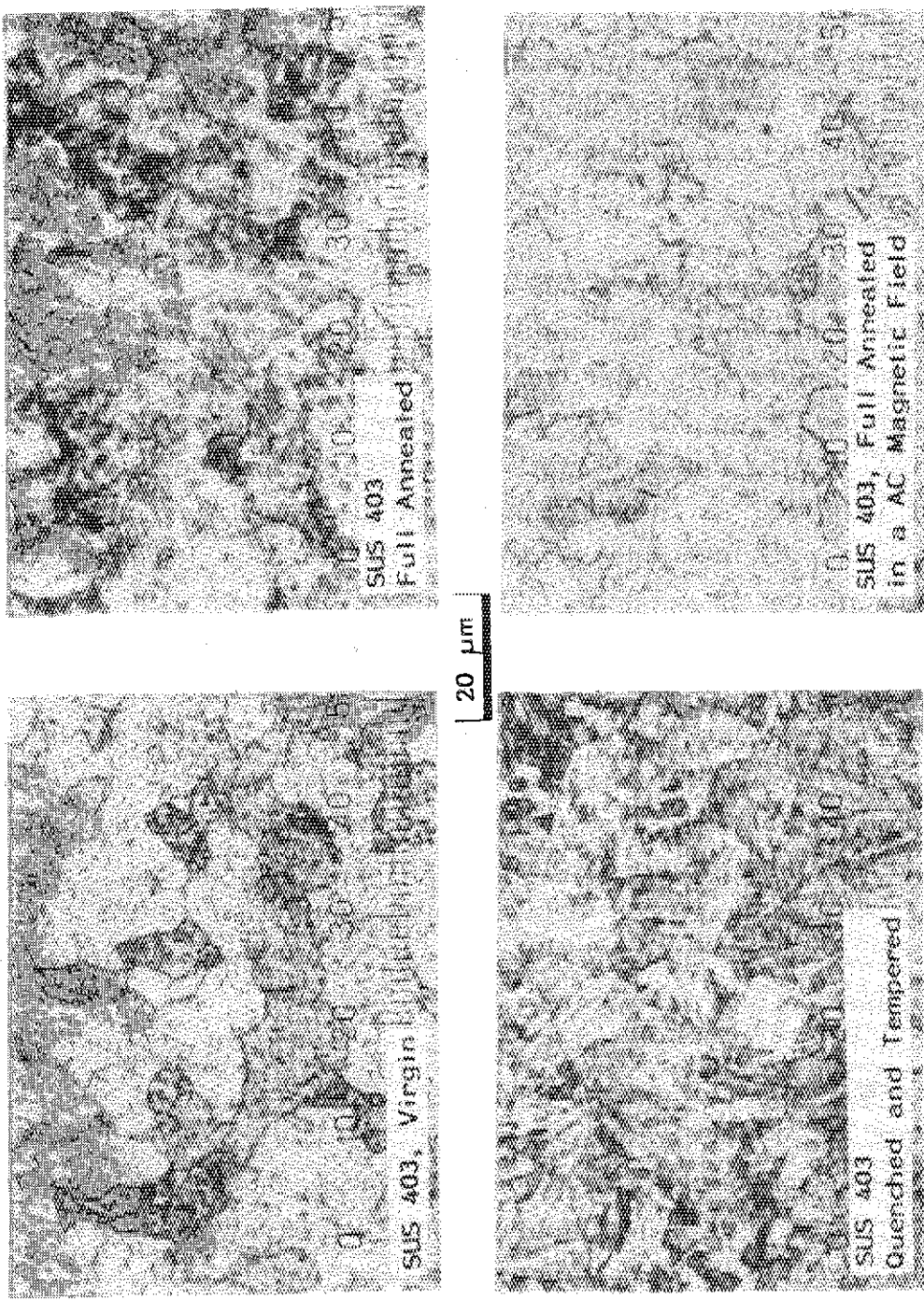


Photo. 4.5-1(2) Microstructures of virgin and heat-treated SUS 403 test pieces (II):
magnification, $\times 600$.

V. RESULTS OF MEASUREMENTS: INVERSE MAGNETOSTRICTION

The measurements were performed at room temperature and 300 °C for six different excitation conditions. All data are presented in Appendices. In the following, the data for the excitation of (10 mA, 2.22 Oe)/(400 Hz) and (100 mA, 22.2 Oe)/(400 Hz) are summarized and discussed.

1. Inverse Magnetostriiction of SUS 403

Figure 5.1-1 shows the results; the inverse magnetostriiction of SUS 403 and its changes with heat treatments and ambient temperatures (room temperature (R.T.) to 300 °C). Here, the term "INDUCTION" means the peak value of induced alternative magnetic flux density by an ac excitation with 400 Hz. The effective ac permeabilities can be, therefore, obtained with dividing the values of induction in gausses by the value of excitation in oersteds. The results obtained with an excitation field of 2.22 Oe represent the inverse magnetostrictions in the range of "initial permeability", and those with 22.2 Oe are about in the range of "maximum permeability". The gradients of the curves shown in the figure give the inverse-magnetostriuctive sensitivities: the quenched-and-tempered piece is least sensitive and the full-annealed (high-temperature annealed) piece is most sensitive.

Since the material SUS 403 is almost equivalent to the AISI 410, the results for the virgin piece agree well with those presented in the previous paper⁽⁶⁾.

2. Inverse Magnetostriiction of SUS 410J1

Figure 5.2-1 shows the results for SUS 410J1. The quenched-and-tempered and low-temperature annealed pieces showed their interesting behaviors: their inverse magnetostrictions for tension are negative for the excitation field of 2.22 Oe but positive for 22.2 Oe. This means that there exist a proper excitation where the inverse magnetostriiction is about zero.

3. Inverse Magnetostriiction of TAF

Figure 5.3-1 shows the results for TAF. The inverse magnetostrictive sensitivity of TAF is relatively small as compared with those of the former two. It is almost zero in the rage of initial permeability.

4. Inverse Magnetostriiction of SUS 405

Figure 5.4-1 shows the results for SUS 405. The inverse magnetostriictive sensitivity is relatively large for compression but nearly zero for tension. Since the coercive force of SUS 405 is small as shown in Fig. 4.4-1, the excitation field of 2.22 Oe exceeded a little over the range of the initial permeability. This resulted in that the obtained inverse magnetostriictions with 2.22 Oe, as shown in the figure-left, are relatively high-sensitive to the stress.

5. Annexes: Metallographical Observation

After the measurements of inverse magnetostriiction, metallographical observations of all tested pieces were carried out. The results are shown in Photo's. 5.5-1 to 5.5-4. They show that SUS 403 was austenitic in virgin state, and that SUS 410J1 and TAF were martensitic.

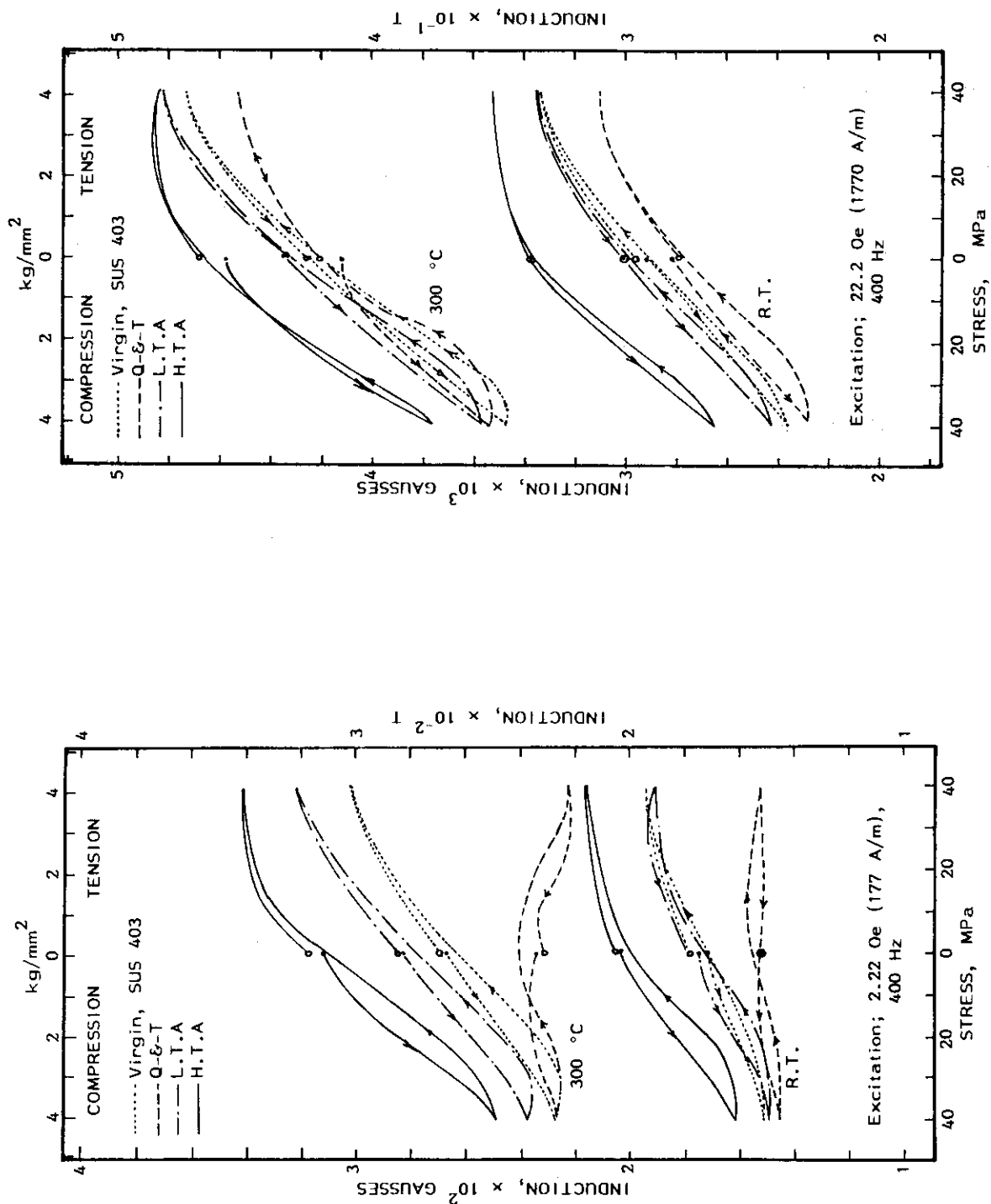


Fig. 5.1-1 Inverse magnetostrictions of virgin and heat-treated SUS 403's
at room temperature and 300 °C.

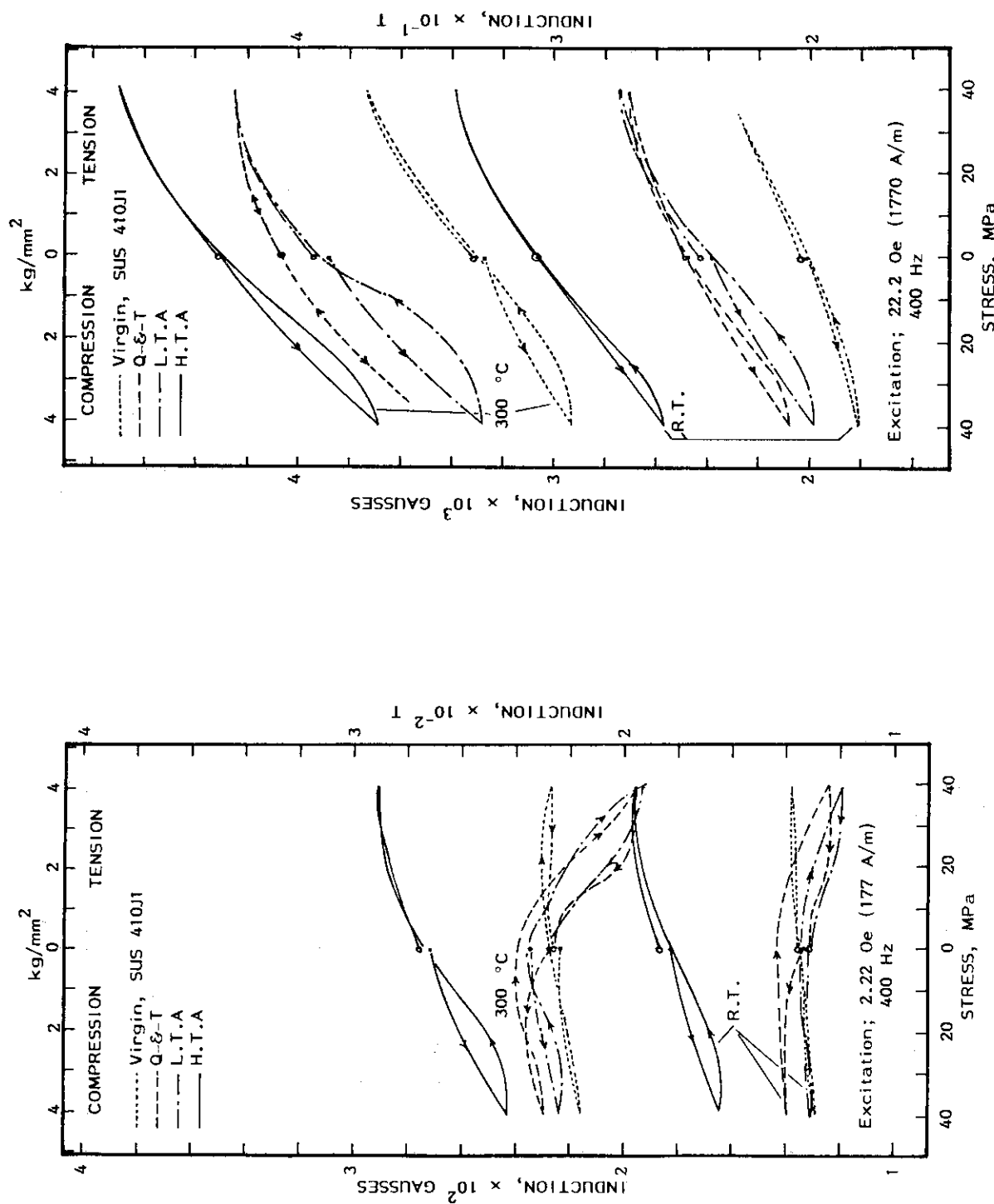


Fig. 5.2-1 Inverse magnetostrictions of virgin and heat-treated SUS 410J1's at room temperature and 300 °C.

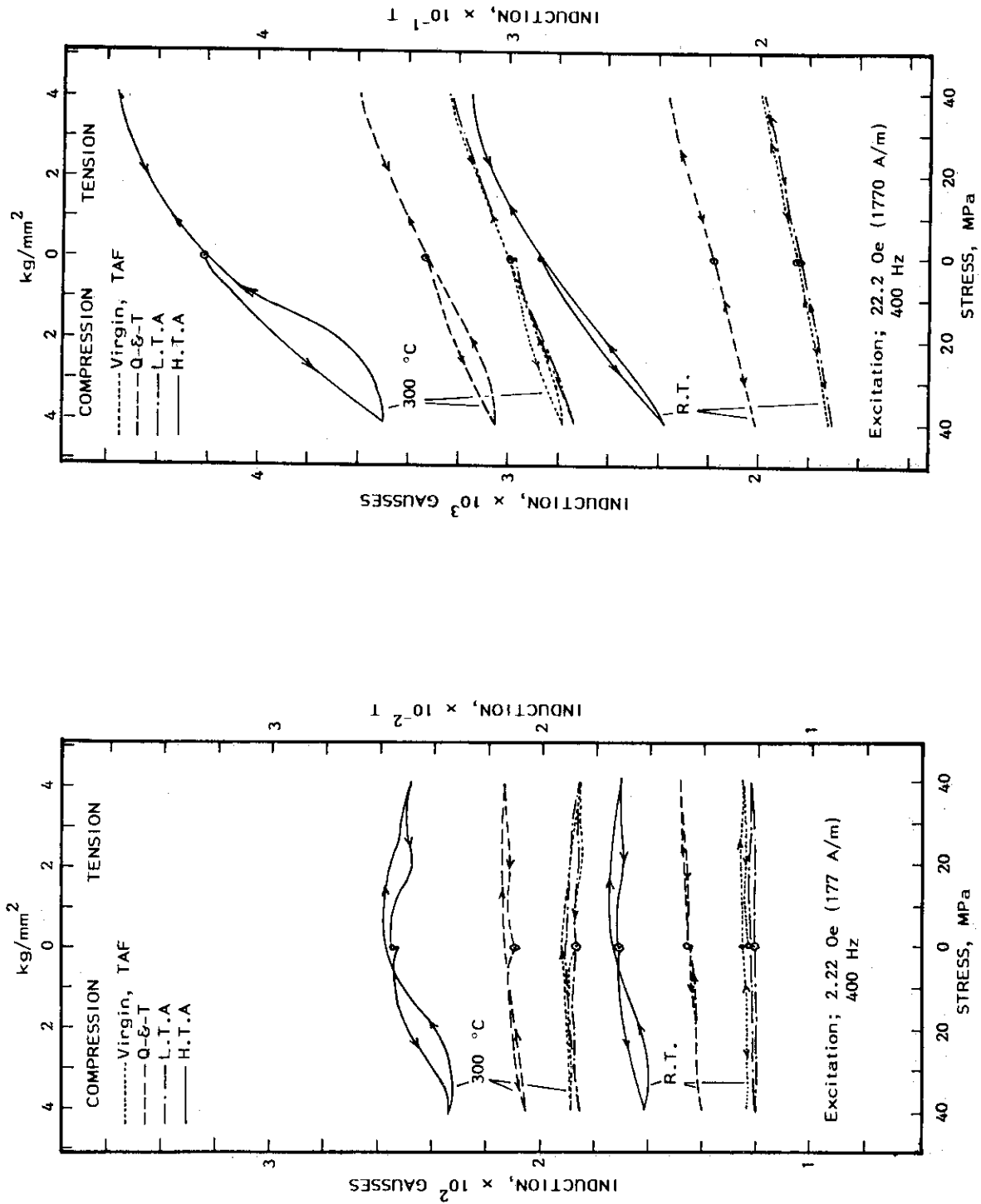


Fig. 5.3-1 Inverse magnetostrictions of virgin and heat-treated TAF's at room temperature and 300 °C.

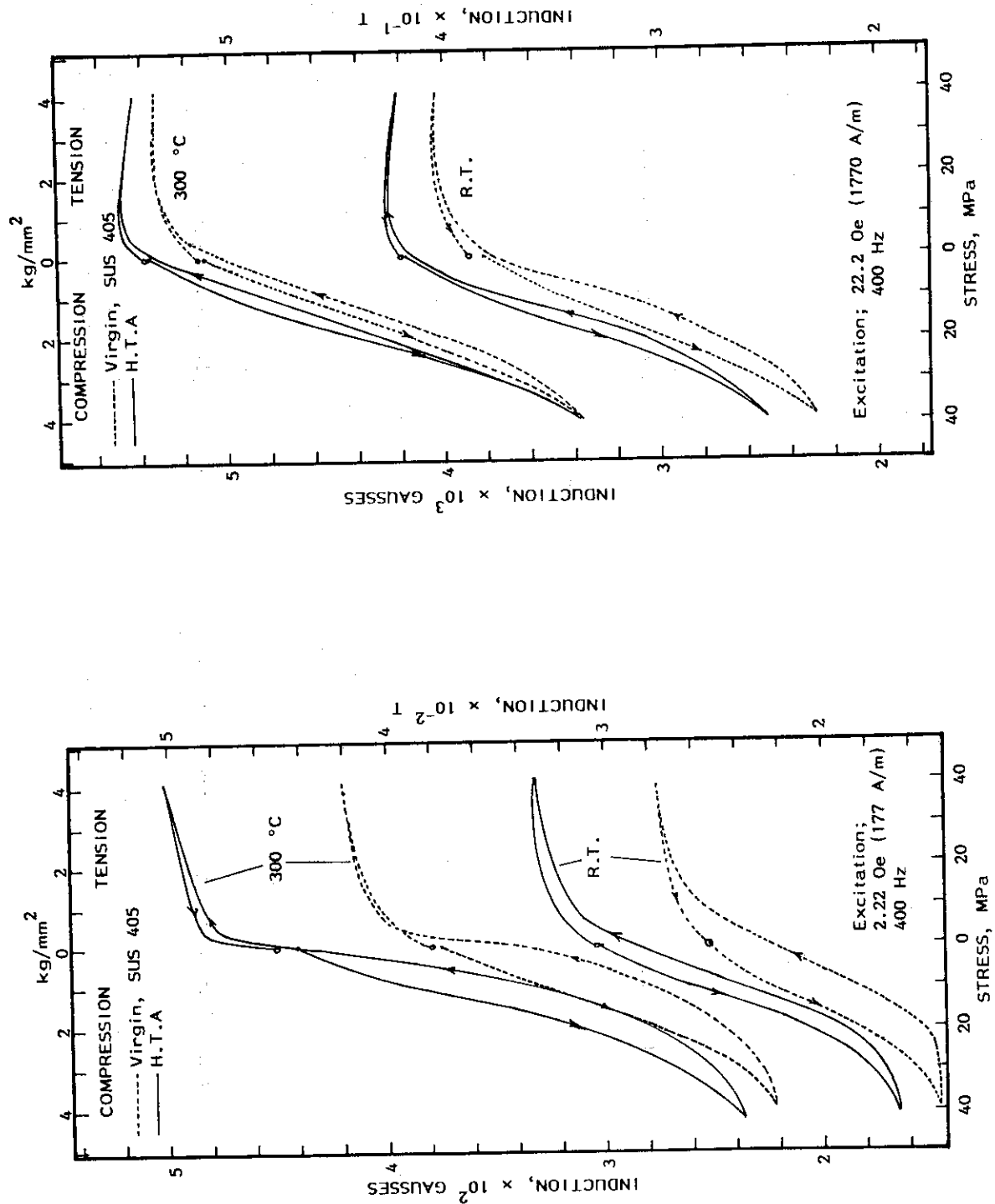


Fig. 5.4-1 Inverse magnetostrictions of virgin and full-annealed SUS 405's
at room temperature and 300 °C.

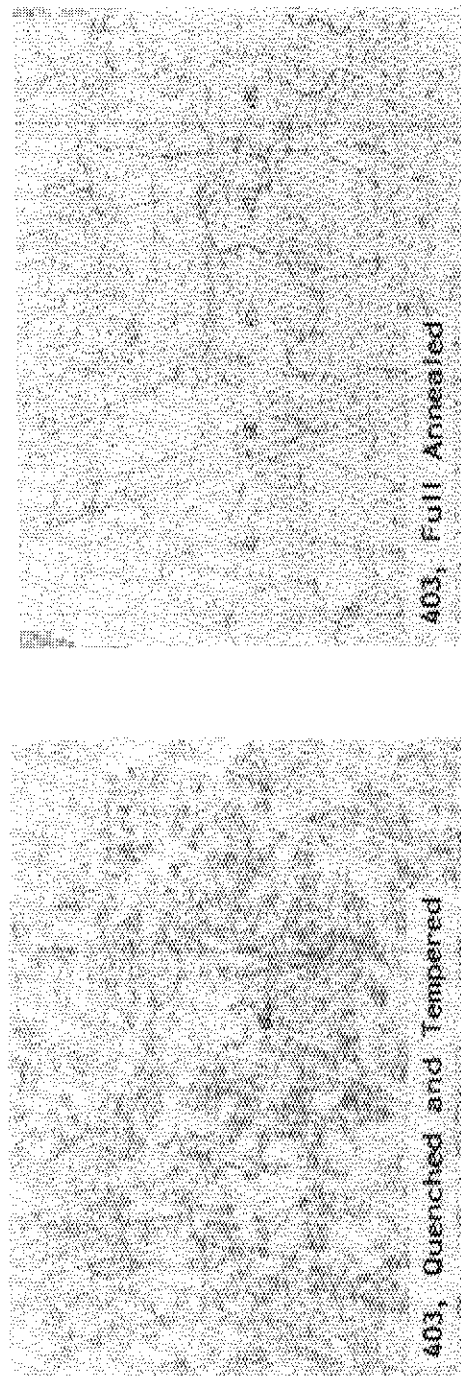
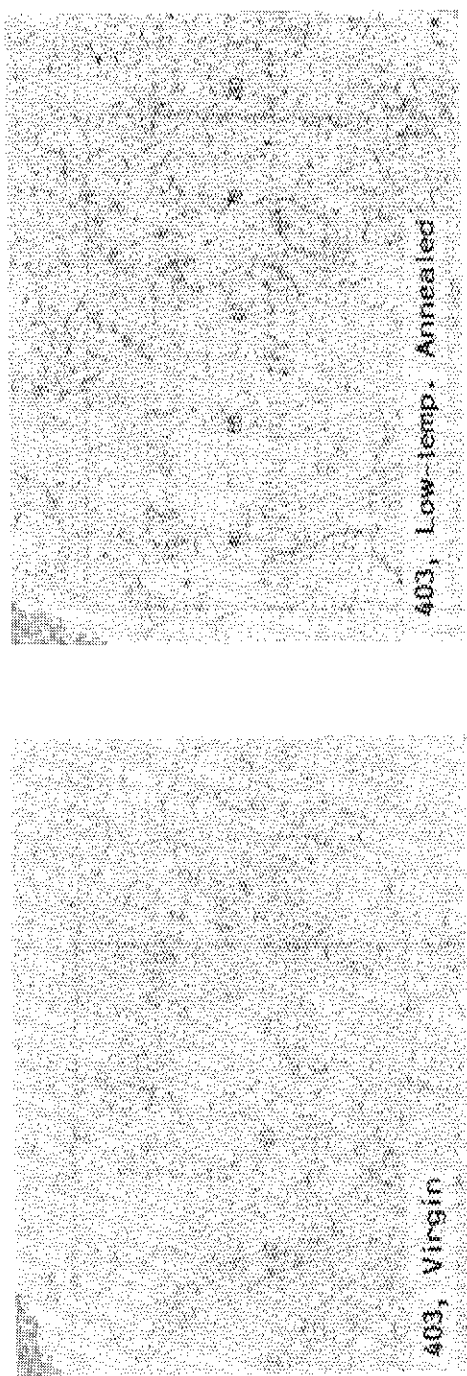
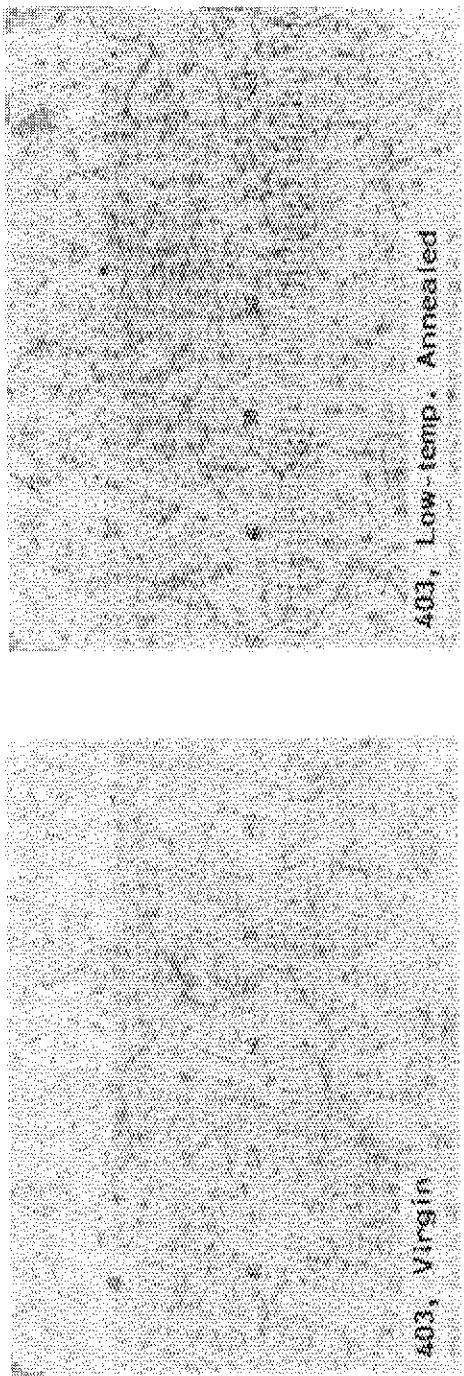
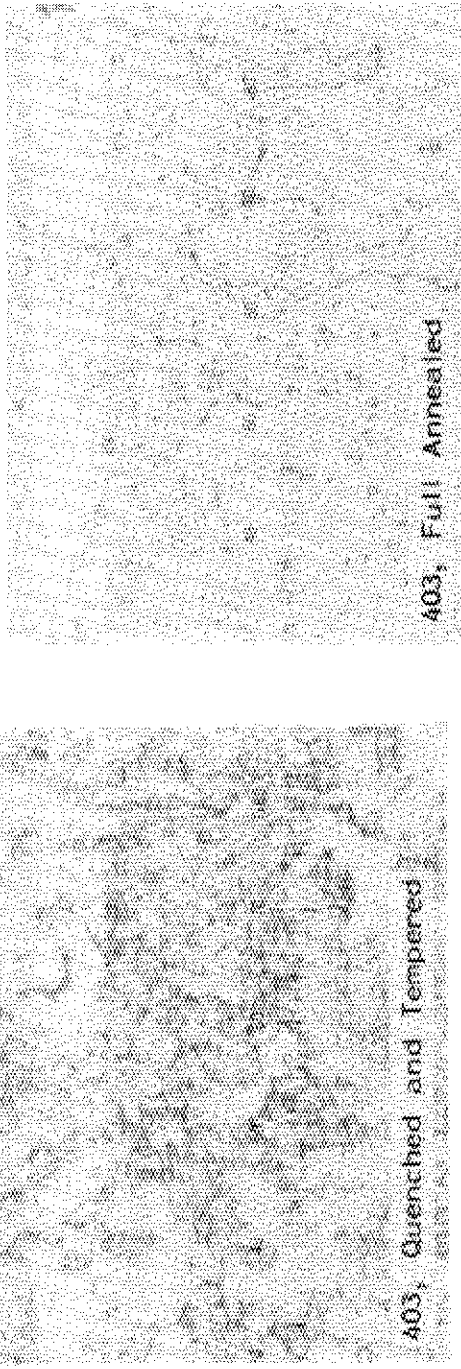


Photo. 5.5-1(1) Microstructures of virgin and heat-treated SUS 403 pieces for inverse magnetostriction tests (I); magnification, X 300.



403, Virgin

20 μm



403, Quenched and Tempered

403, Full Annealed

Photo. 5.5-1(2) Microstructures of virgin and heat-treated SUS 403 pieces for inverse magnetostriiction tests (II): magnification, X 600.

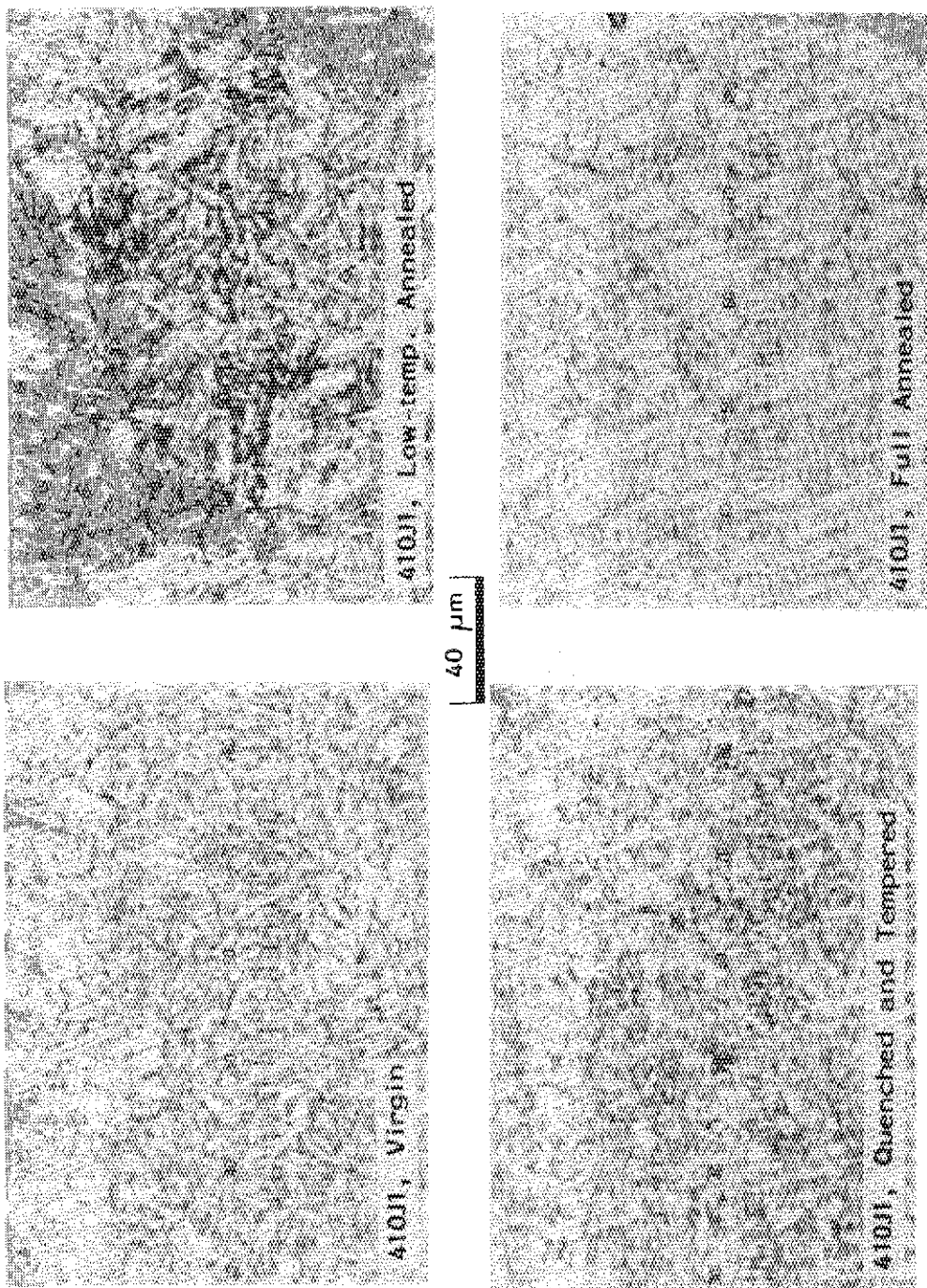


Photo. 5.5-2(1) Microstructures of virgin and heat-treated SUS 410J1 pieces for inverse magnetostriiction tests (I): magnification, X 300.

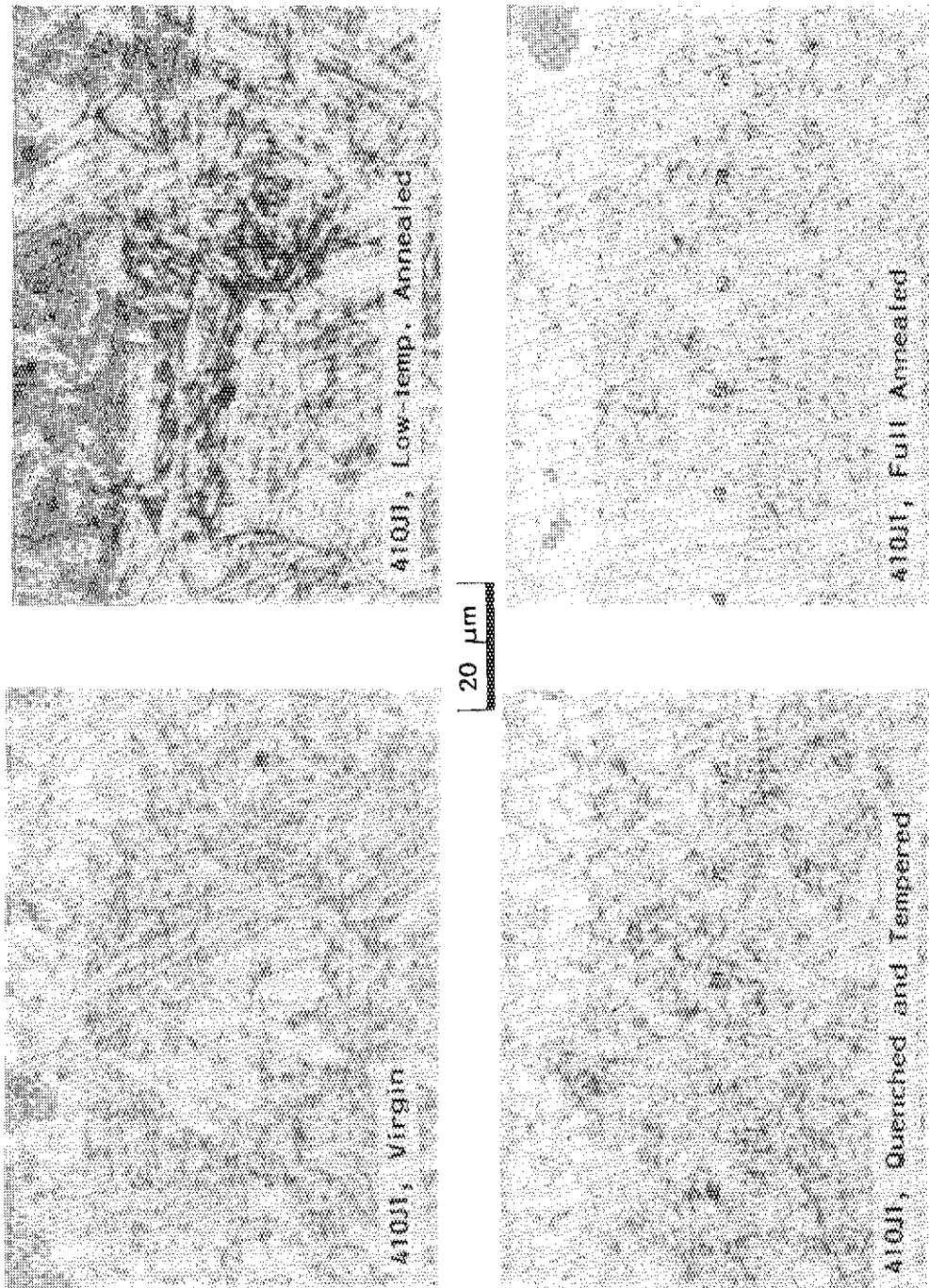


Photo. 5.5-2(2) Microstructures of virgin and heat-treated SUS 410J1 pieces for inverse magnetostriiction tests (II): magnification, $\times 600$.

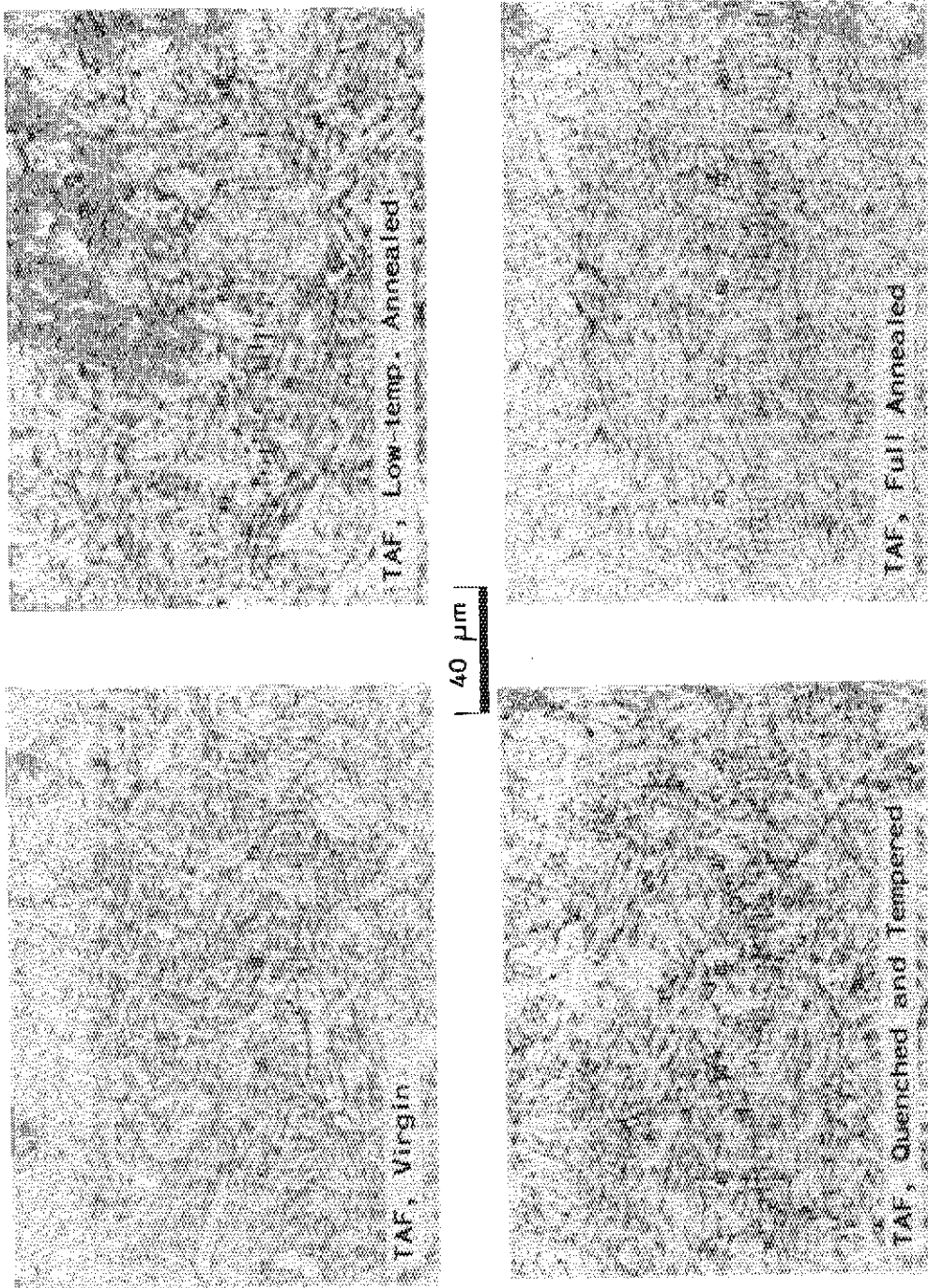


Photo. 5.5-3(1) Microstructures of virgin and heat-treated TAF pieces for inverse magnetostriction tests (I): magnification, X 300.

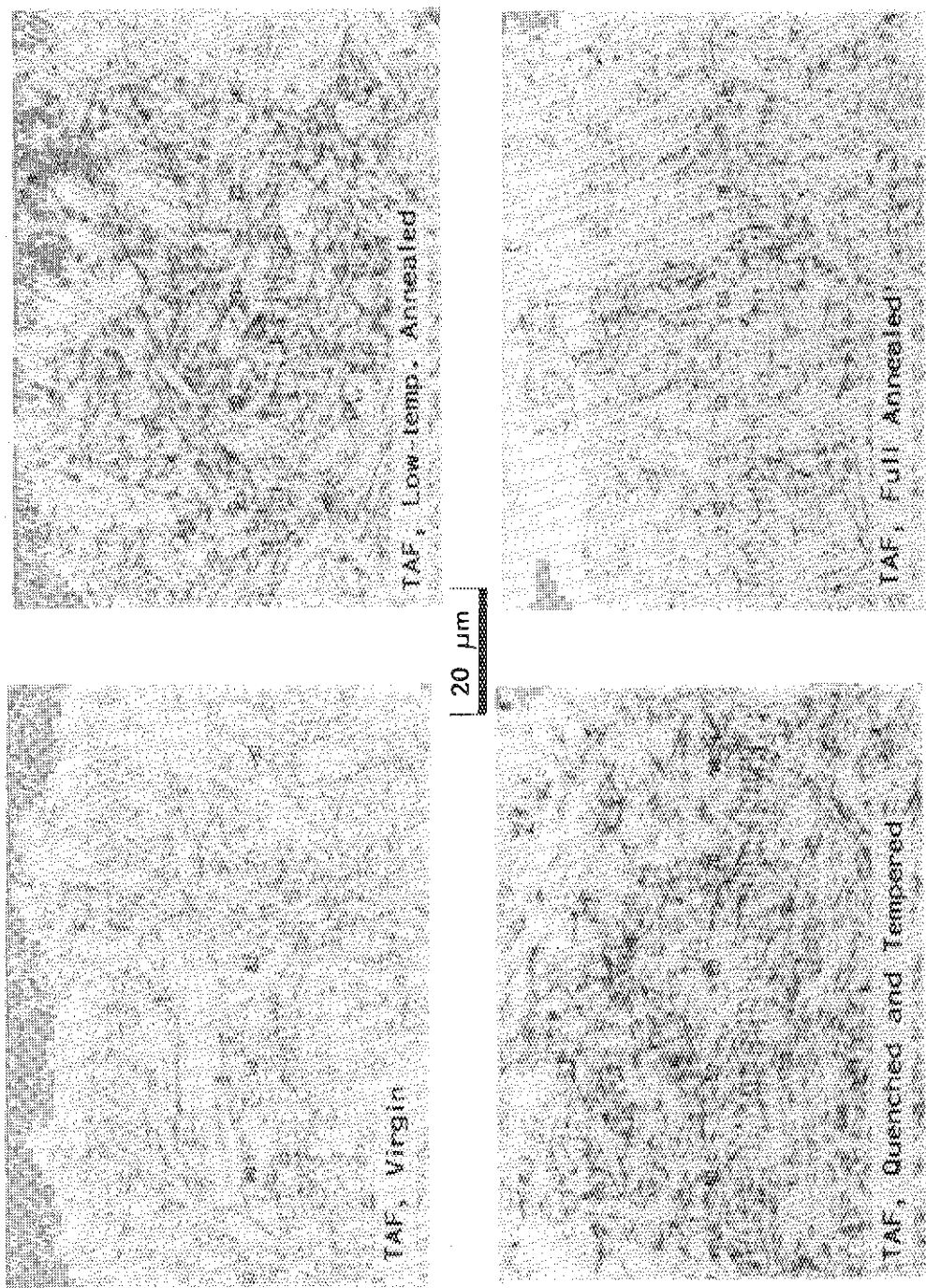
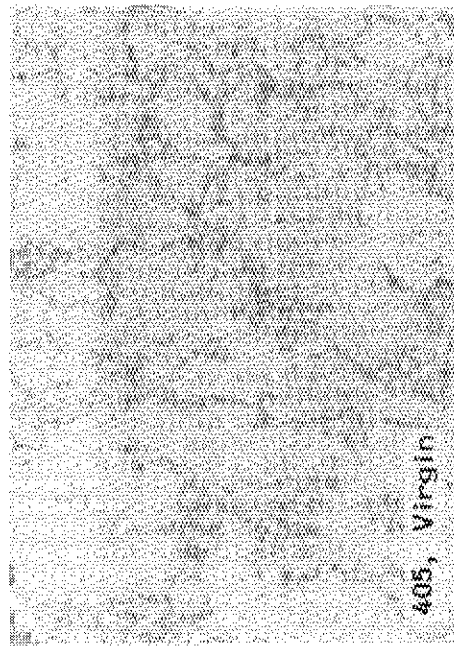
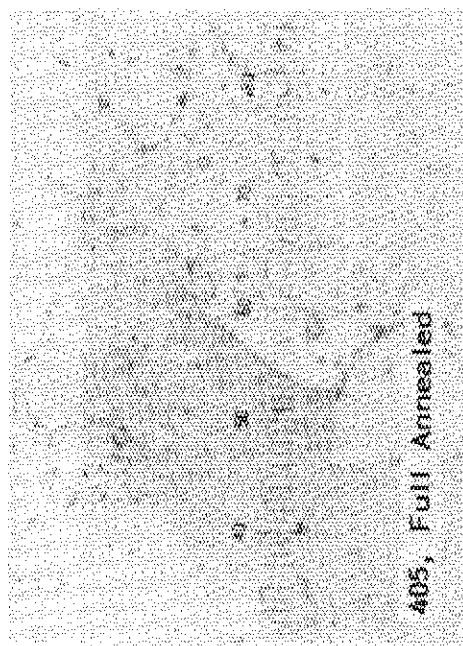


Photo. 5.5-3(2) Microstructures of virgin and heat-treated TAF pieces for inverse magnetostriction tests (II): magnification, $\times 600$.

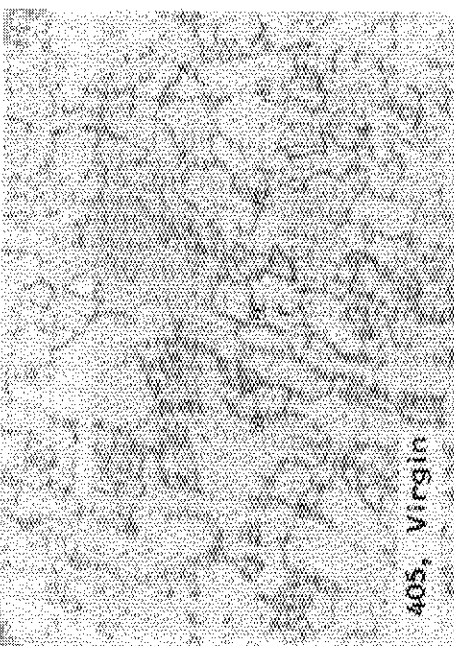


405, Virgin

20 μm

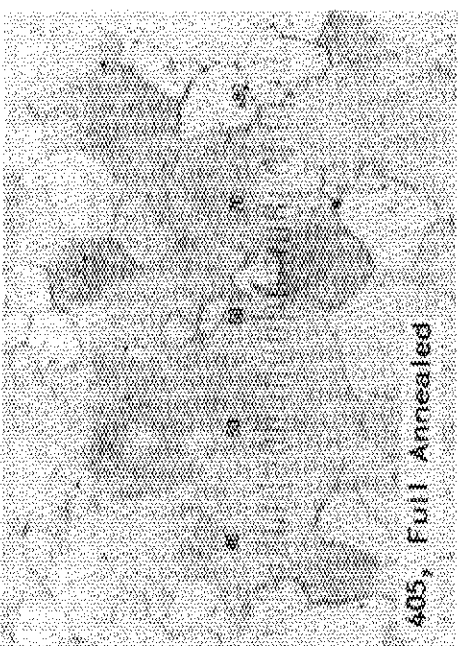


405, Full Annealed



405, Virgin

40 μm



405, Full Annealed

Photo. 5.5-4 Microstructures of virgin and full-annealed SUS 405 pieces for inverse magnetostriiction tests: magnification, X 300 (left) and X 600 (right).

VI. SUMMARY

The magnetic characteristics of ferromagnetic stainless steels, SUS 403, SUS 410J1, TAF and SUS 405, can be summarized from an applicative point of view as follows:

- (1) They are magnetically harder than the ordinary soft magnetic materials but softer than the semi-hard materials.
- (2) They have been originally produced as structure materials so that their magnetic characteristics are somewhat irregular from piece to piece.
- (3) Except the full-annealed SUS 410J1, their saturation inductions are about 15000 gauss; and the coercive forces of martensitic steels (SUS 403, SUS 410J1, TAF) are about 6 to 15 oersteds and the ferritic one (SUS 405) about 2 to 5 oersteds. The Curie points are 710 to 730 °C.
- (4) The magnetic characteristics vary with heat treatments. The quenching and tempering increases the coercive force and the rectangularity. The full annealing decreases the saturation induction and the permeability, slightly. The full annealing for SUS 410J1 brings about a different effect: it causes a large decrease of the saturation induction and a large increase of the coercive force.
- (5) The magnetic characteristics are slightly varied with temperature cycles, mostly between 1st and 2nd cycles. In an actual application, therefore, the aging with several temperature cyclings in the temperature range of actual use is very effective to stabilize the characteristics.
- (6) Their inverse magnetostrictions are relatively large for compression but small for tension.
- (7) They seem to be an excellent magnetic material for the application at the environment where high-temperature and corrosion resistivities are required.

ACKNOWLEDGEMENT

The authors are deeply indebted to Prof., Dr. K. Murakami of Tohoku University and his staffs for their help to the initial stage of this work in the measurement of magnetic characteristics of virgin SUS 403 pieces, and wish to thank Mr. J. Miyao for his assistance in this work and to Dr. Y. Kazumata for his valuable advices in preparation of this report.

REFERENCES

- (1) R. M. Bozorth: "Ferromagnetism", D. Van Nostrand Co. Inc., p. 14 (1951)
- (2) M. Hansen: "Constitution of Binary Alloys", Mc-Graw Hill, p. 527 (1958)
- (3) Ref. (1), p.229
- (4) ibid., p. 228
- (5) ibid., p. 375
- (6) K. Ara and M. J. Brakas: IEEE Trans. Magnetics, Mag-11(5), p. 1352 (1975)

ACKNOWLEDGEMENT

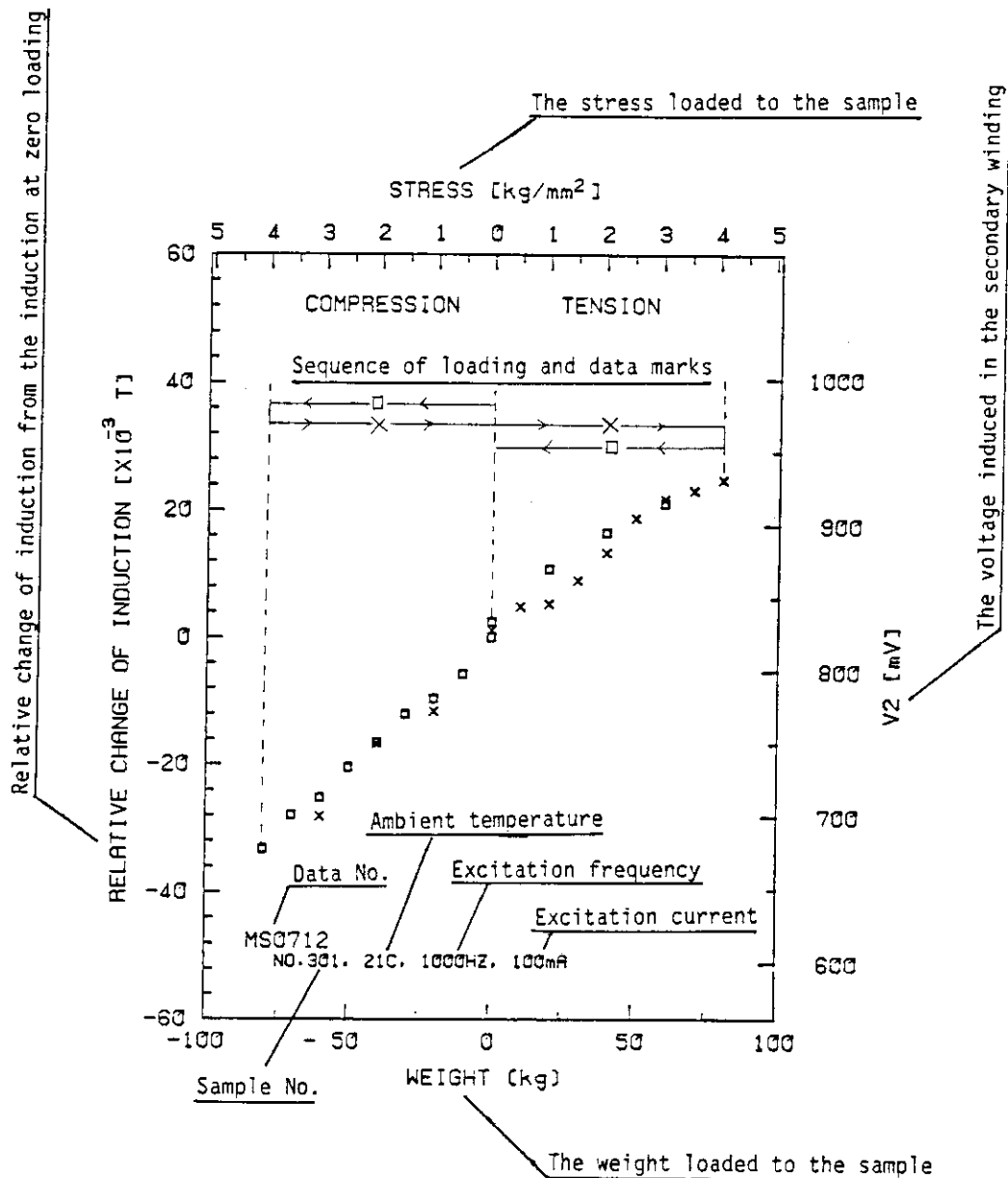
The authors are deeply indebted to Prof., Dr. K. Murakami of Tohoku University and his staffs for their help to the initial stage of this work in the measurement of magnetic characteristics of virgin SUS 403 pieces, and wish to thank Mr. J. Miyao for his assistance in this work and to Dr. Y. Kazumata for his valuable advices in preparation of this report.

REFERENCES

- (1) R. M. Bozorth: "Ferromagnetism", D. Van Nostrand Co. Inc., p. 14 (1951)
- (2) M. Hansen: "Constitution of Binary Alloys", Mc-Graw Hill, p. 527 (1958)
- (3) Ref. (1), p.229
- (4) ibid., p. 228
- (5) ibid., p. 375
- (6) K. Ara and M. J. Brakas: IEEE Trans. Magnetics, Mag-11(5), p. 1352 (1975)

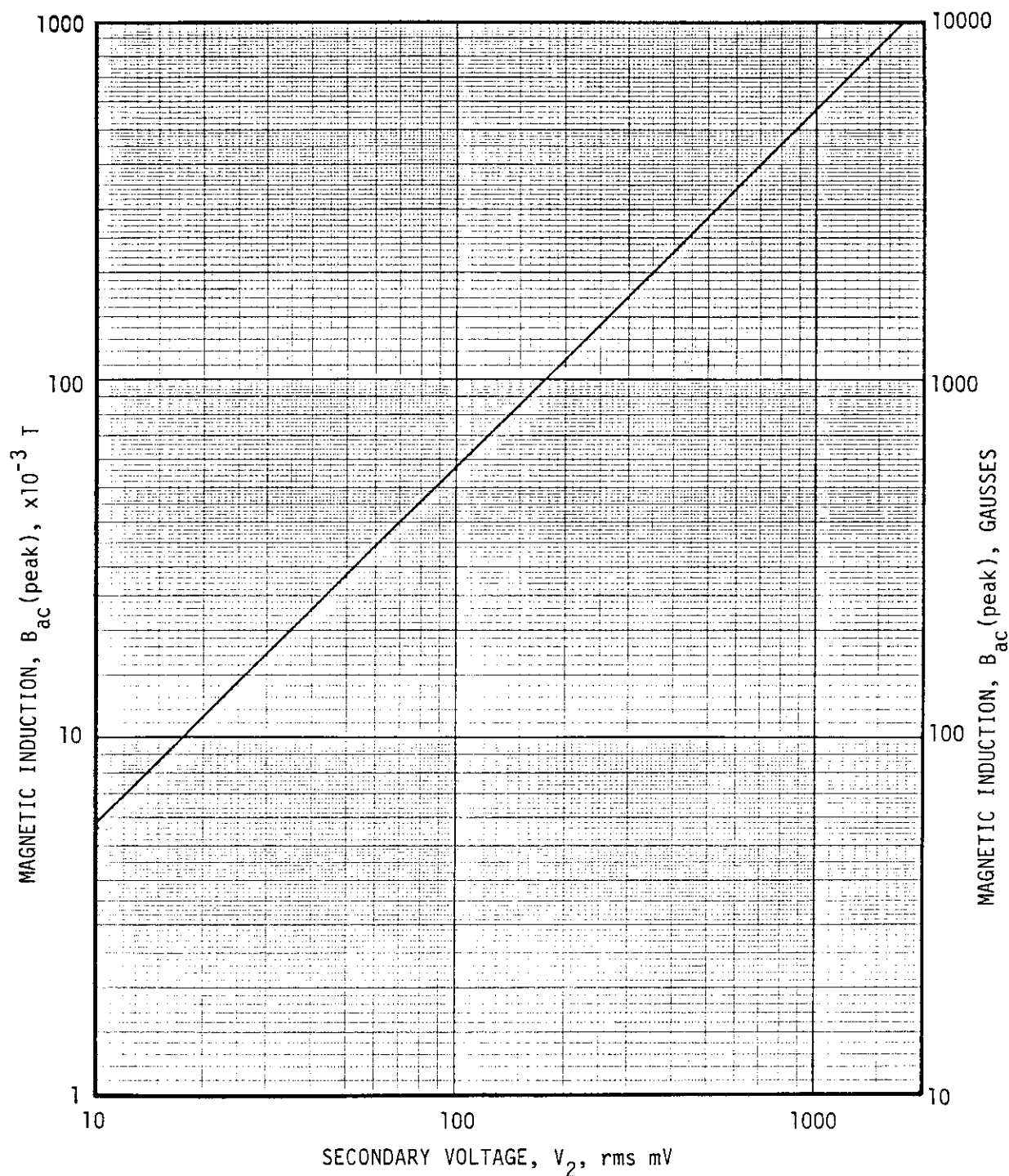
**APPENDICES: INVERSE MAGNETOSTRICTION DATA OF
FERROMAGNETIC STAINLESS STEELS**

Introduction for Understanding



Excitation-Current/Excitation-Strength Conversion

Excitation Current rms mA	Excitation Strength Oersteds	A/m
10	2.22	177
20	4.44	354
30	6.66	531
50	11.1	885
70	15.5	1239
100	22.2	1770



Magnetic-Induction/Secondary-Voltage Conversion

**Appendix I: Inverse magnetostriction data,
measured with 400 Hz-excitation
and at room temperature.**

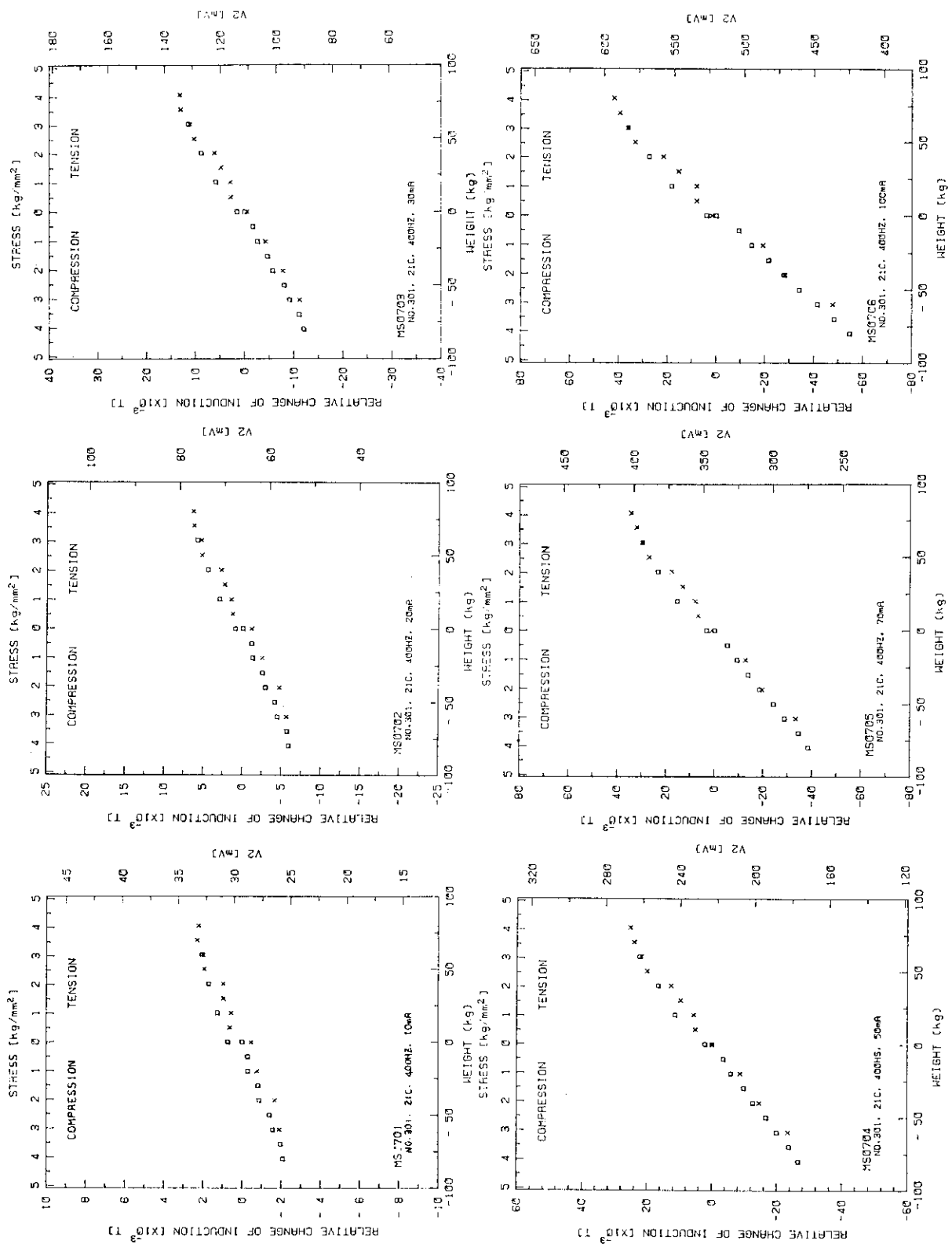


Fig. A1-1 Of SUS 403, virgin

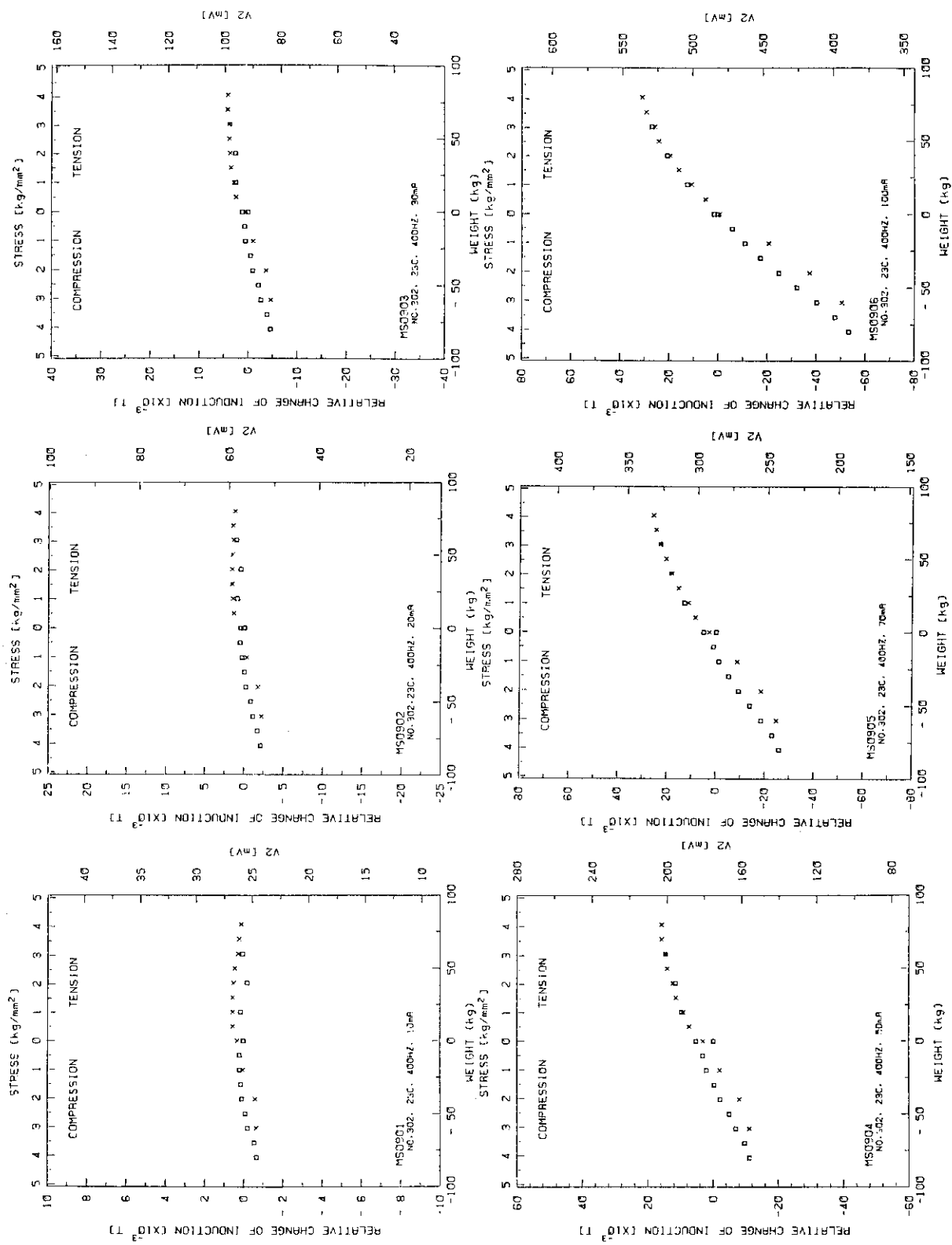


Fig. A1-2 Of SUS 403, as quenched and tempered

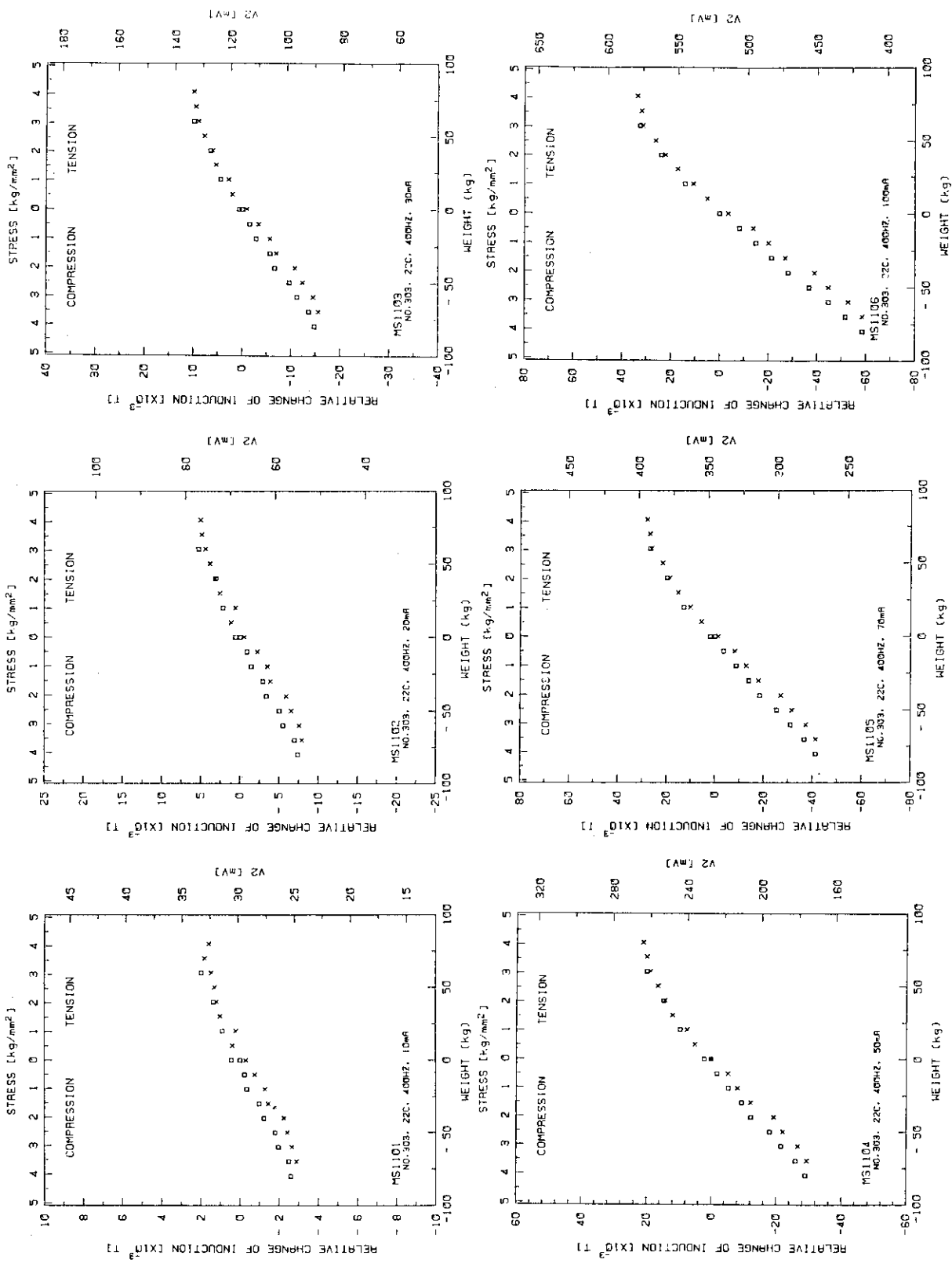


Fig. AI-3 Of SUS 403, as low-temperature annealed

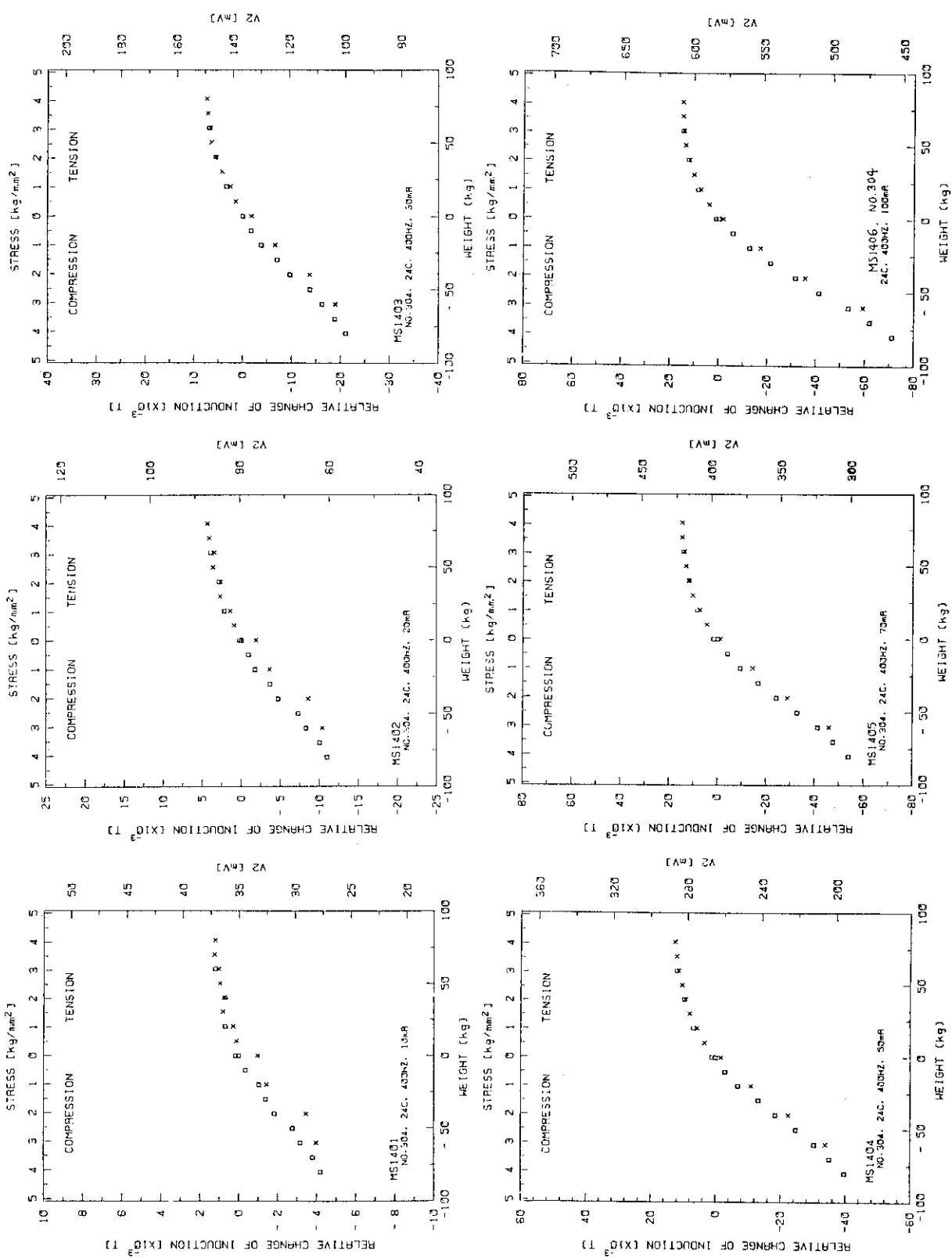


Fig. AI-4 Of SUS 403, as full annealed

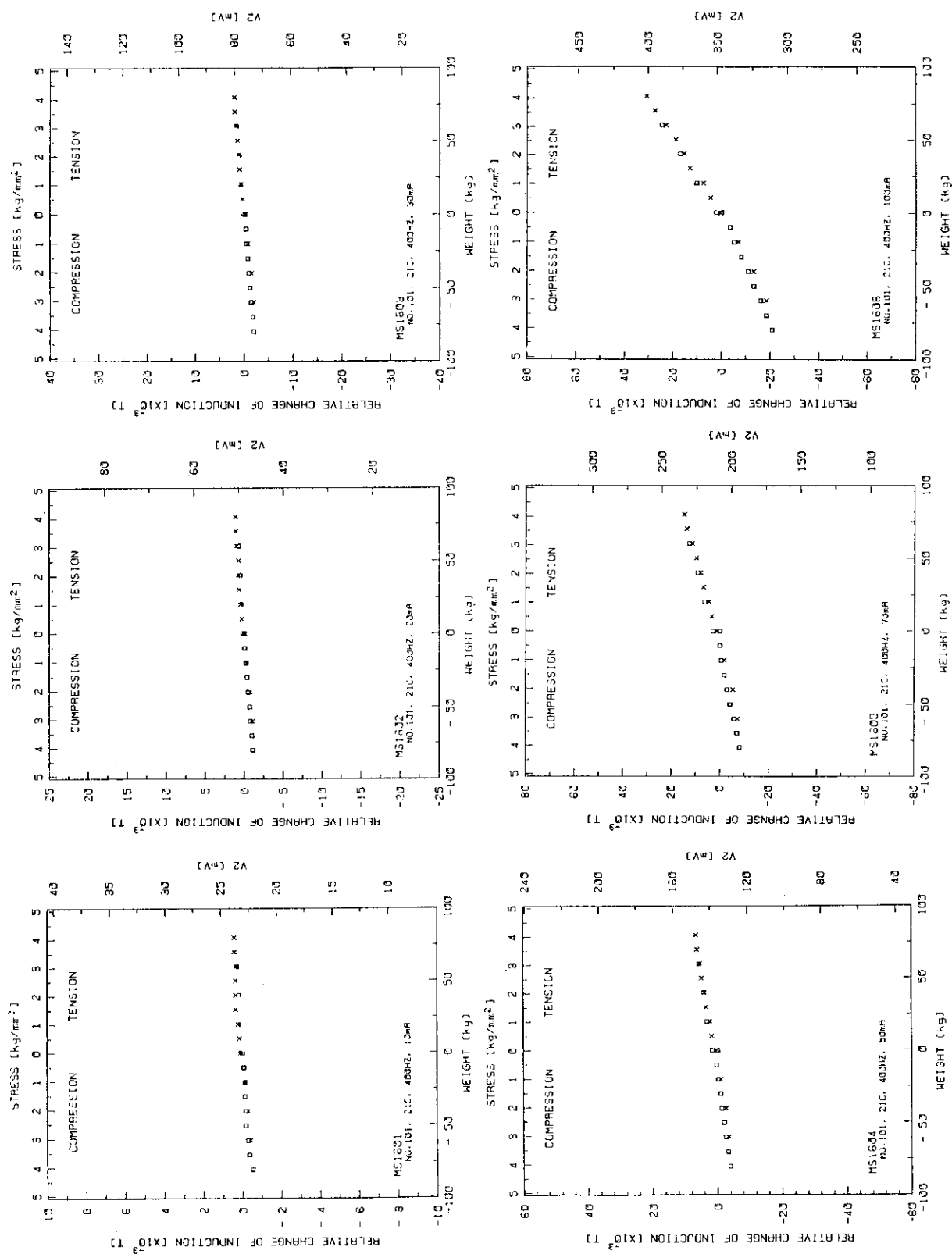


Fig. A1-5 Of SUS 410J1, virgin

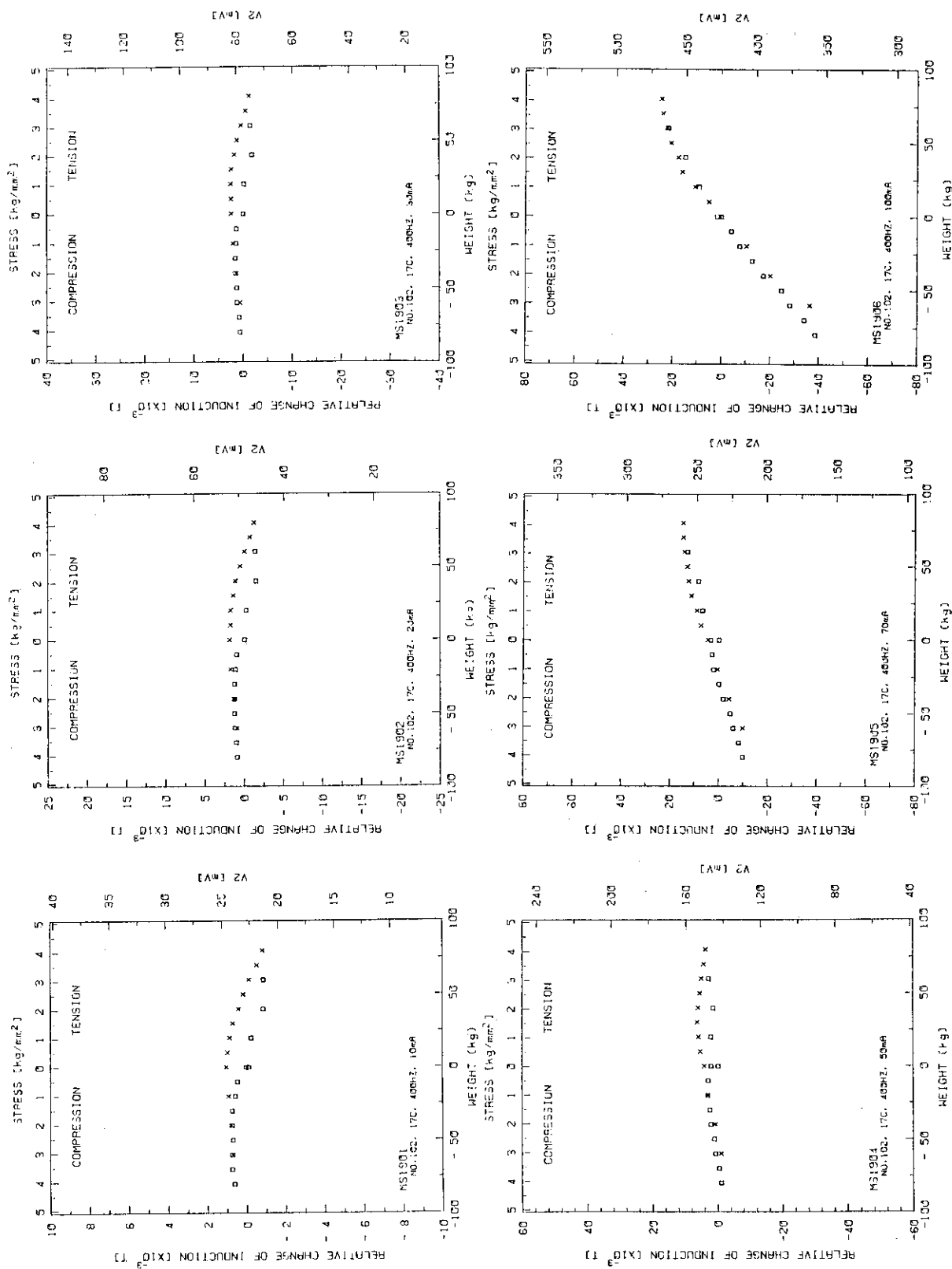


Fig. A1-6 Of SUS 410J1, as quenched and tempered

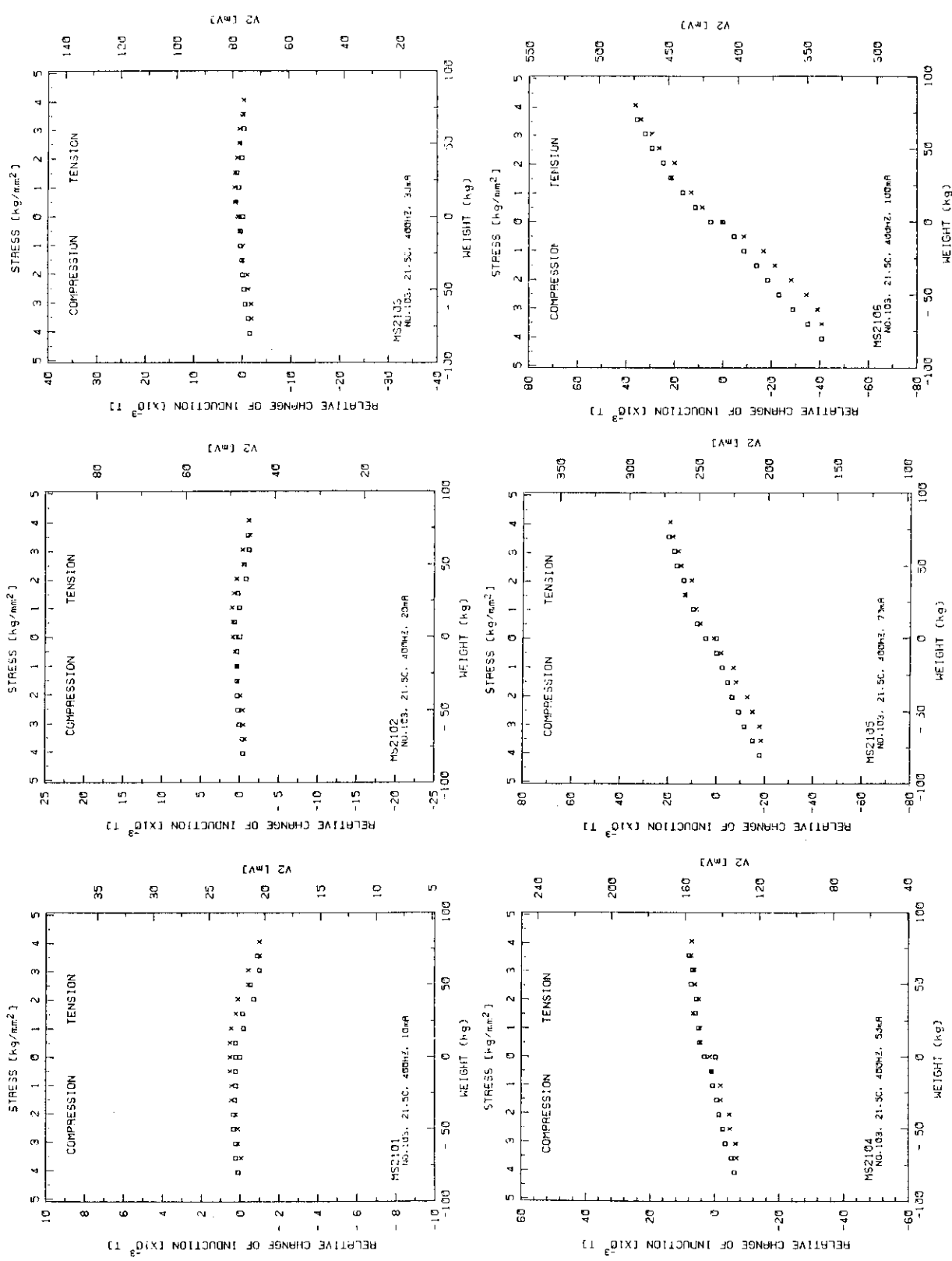


Fig. A1-7 of SUS 410JL, as low-temperature annealed

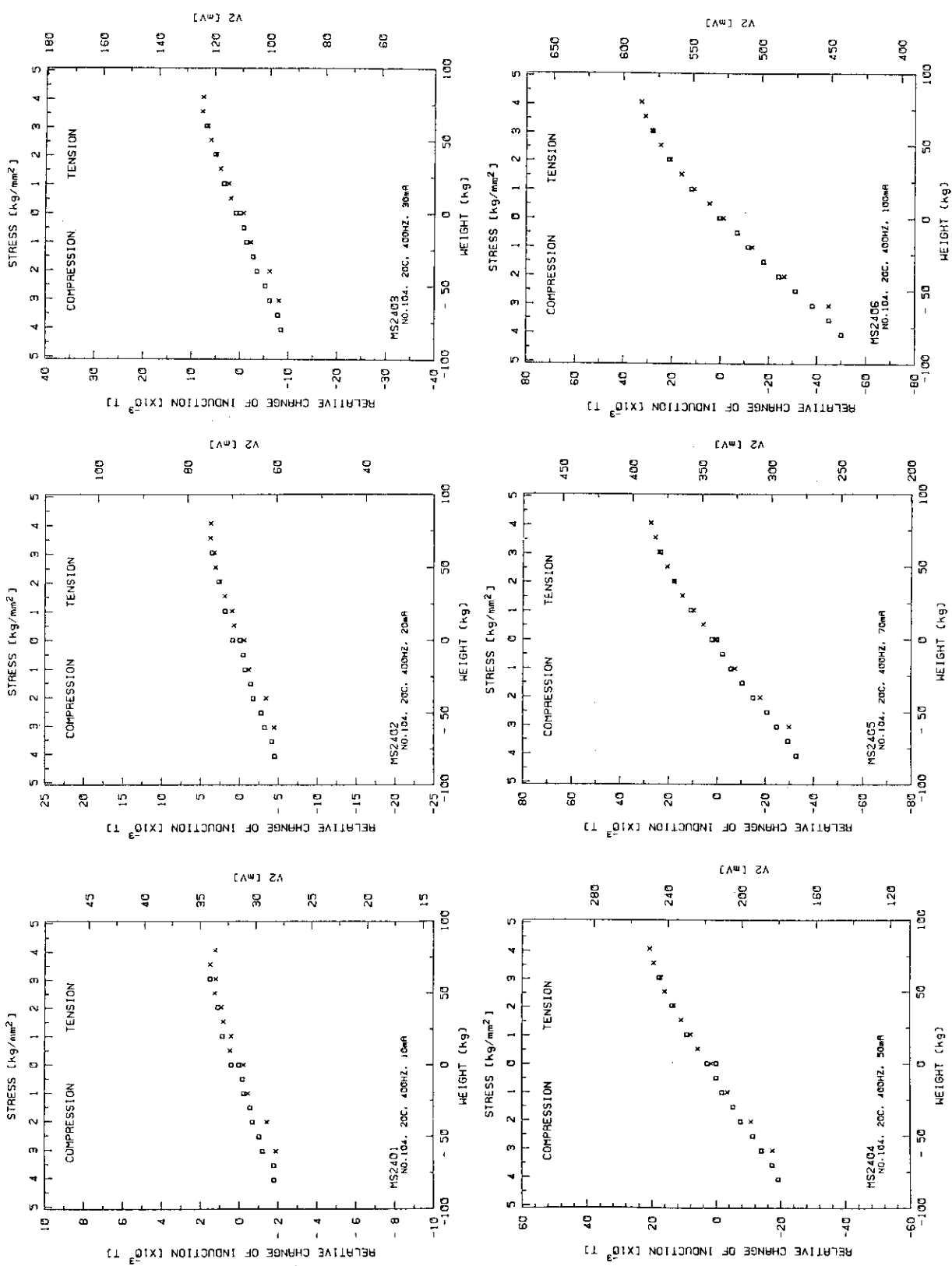


Fig. A1-8 OF SUS 410J1, AS FULL annealed

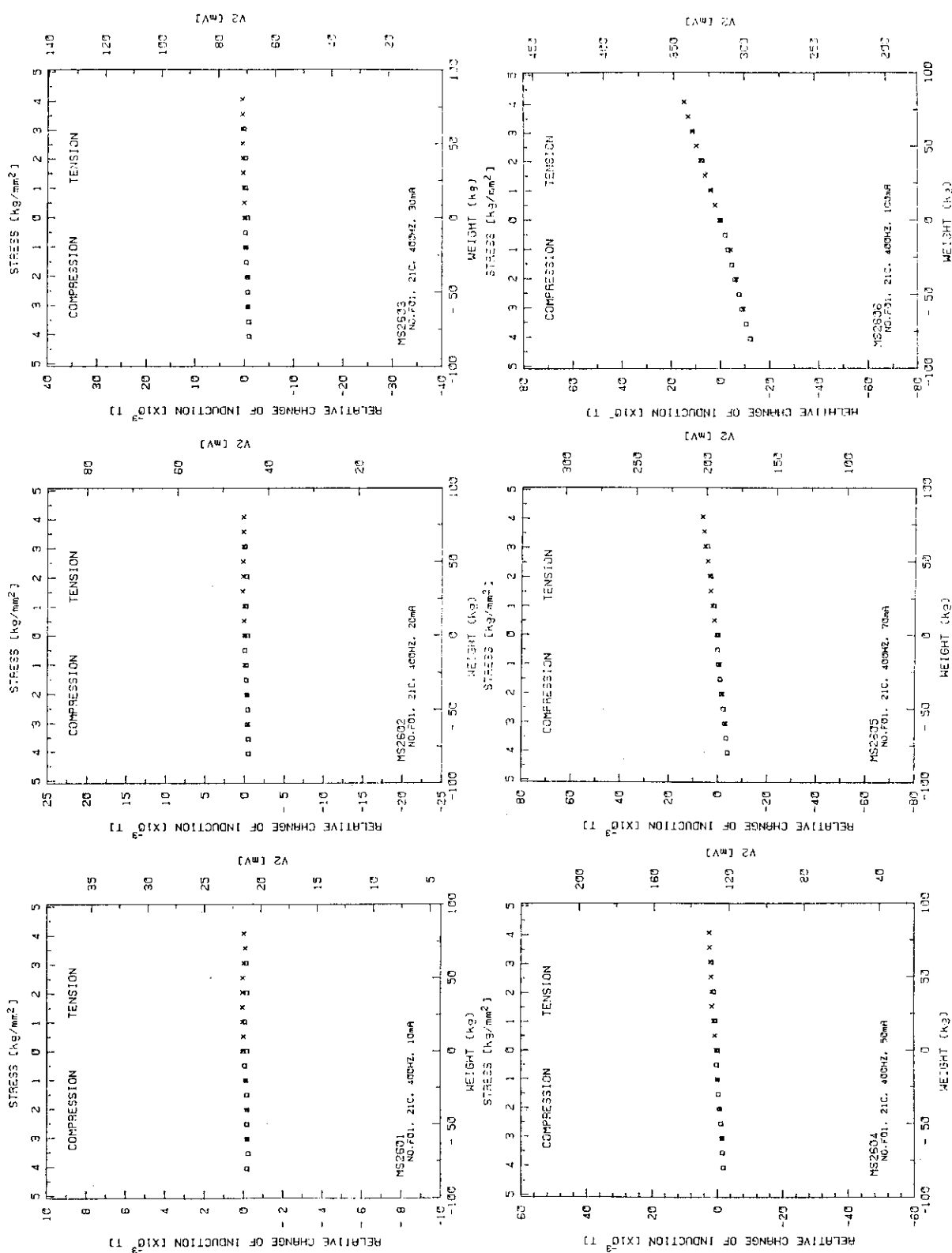


Fig. A1-9 Of TAF, virgin

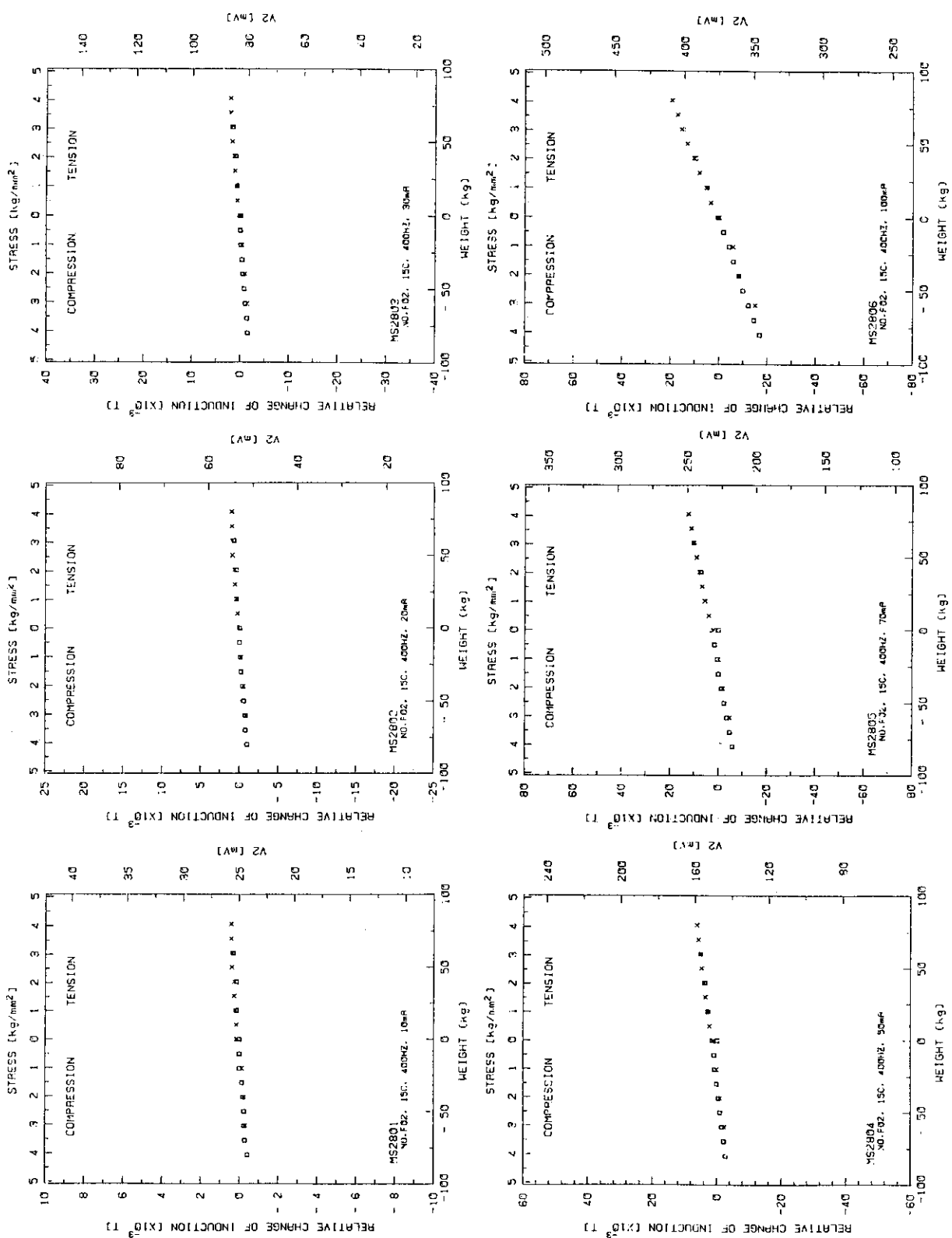


Fig. A1-10 of TAF, as quenched and tempered

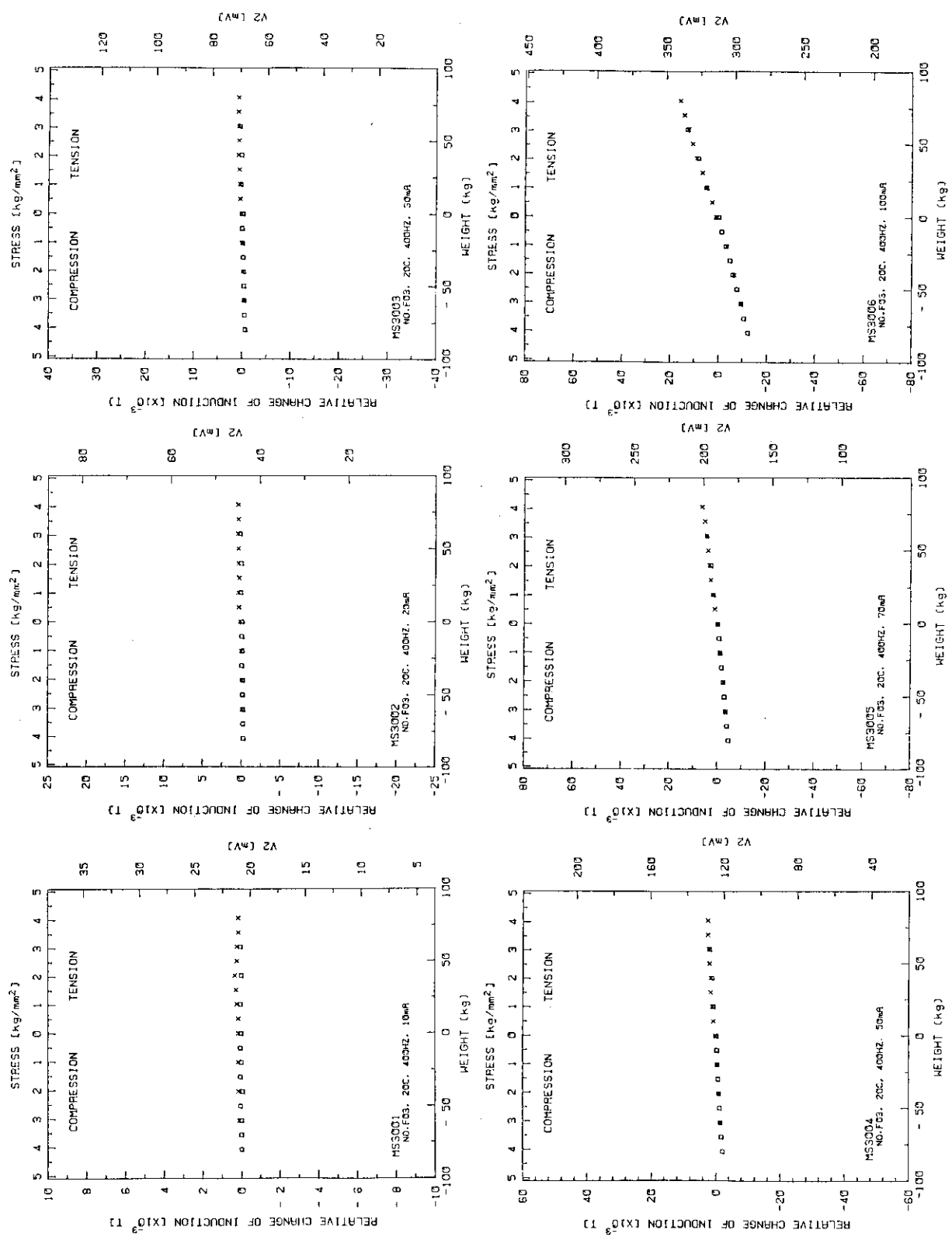


Fig. A1-11 Of TAF, as low-temperature annealed

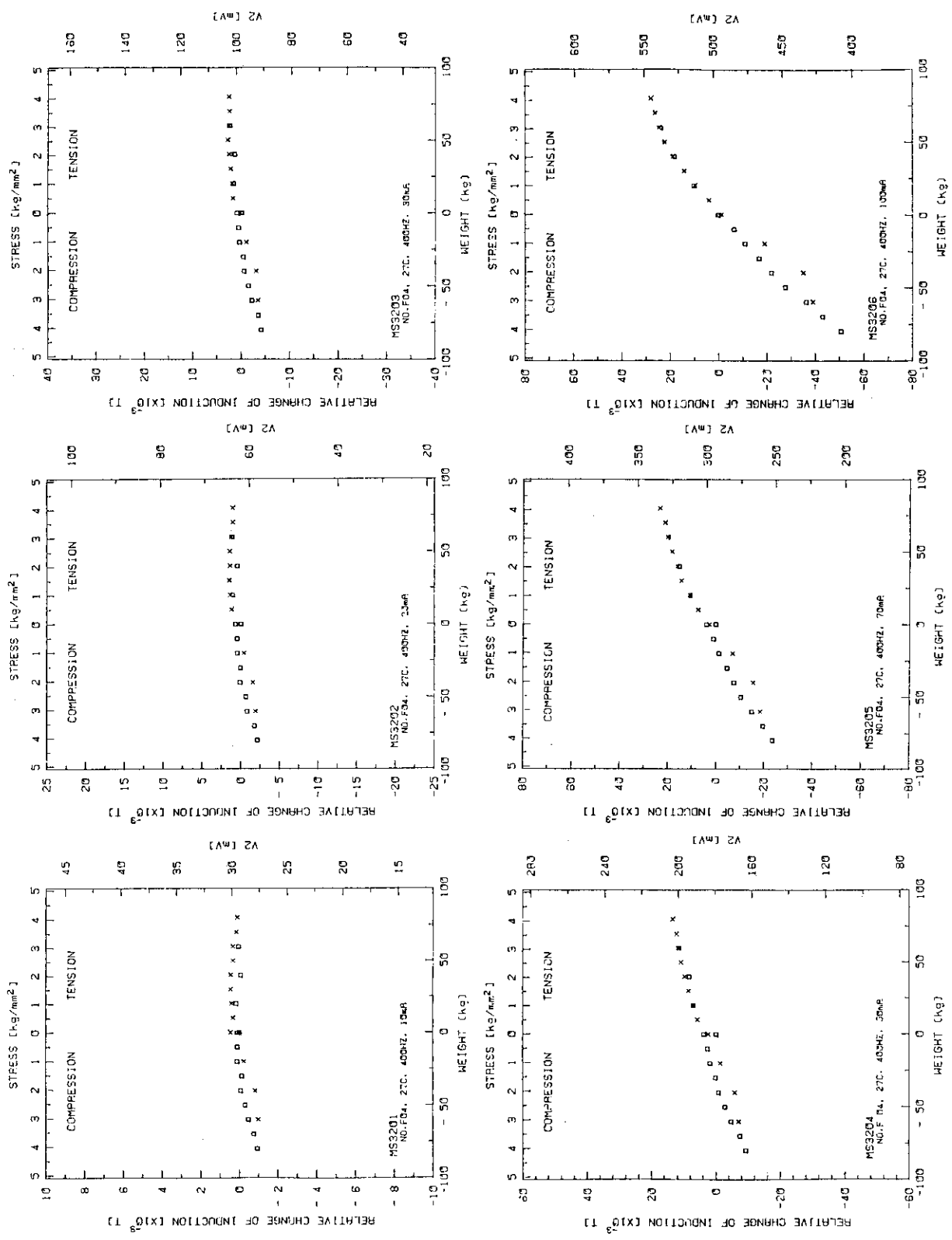


Fig. A1-12 Off TAF, as full annealed

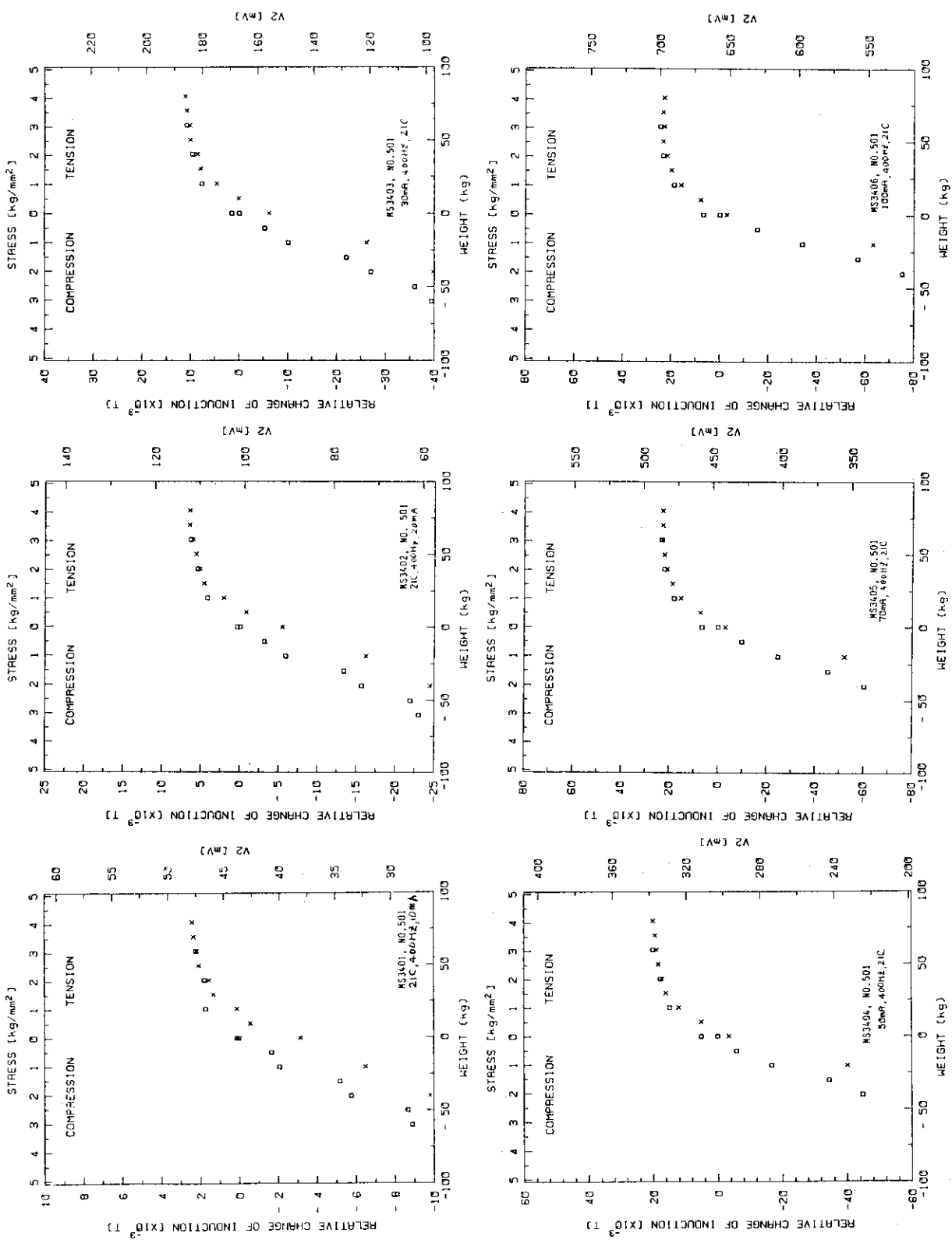


Fig. A1-13 of SUS 405, virgin

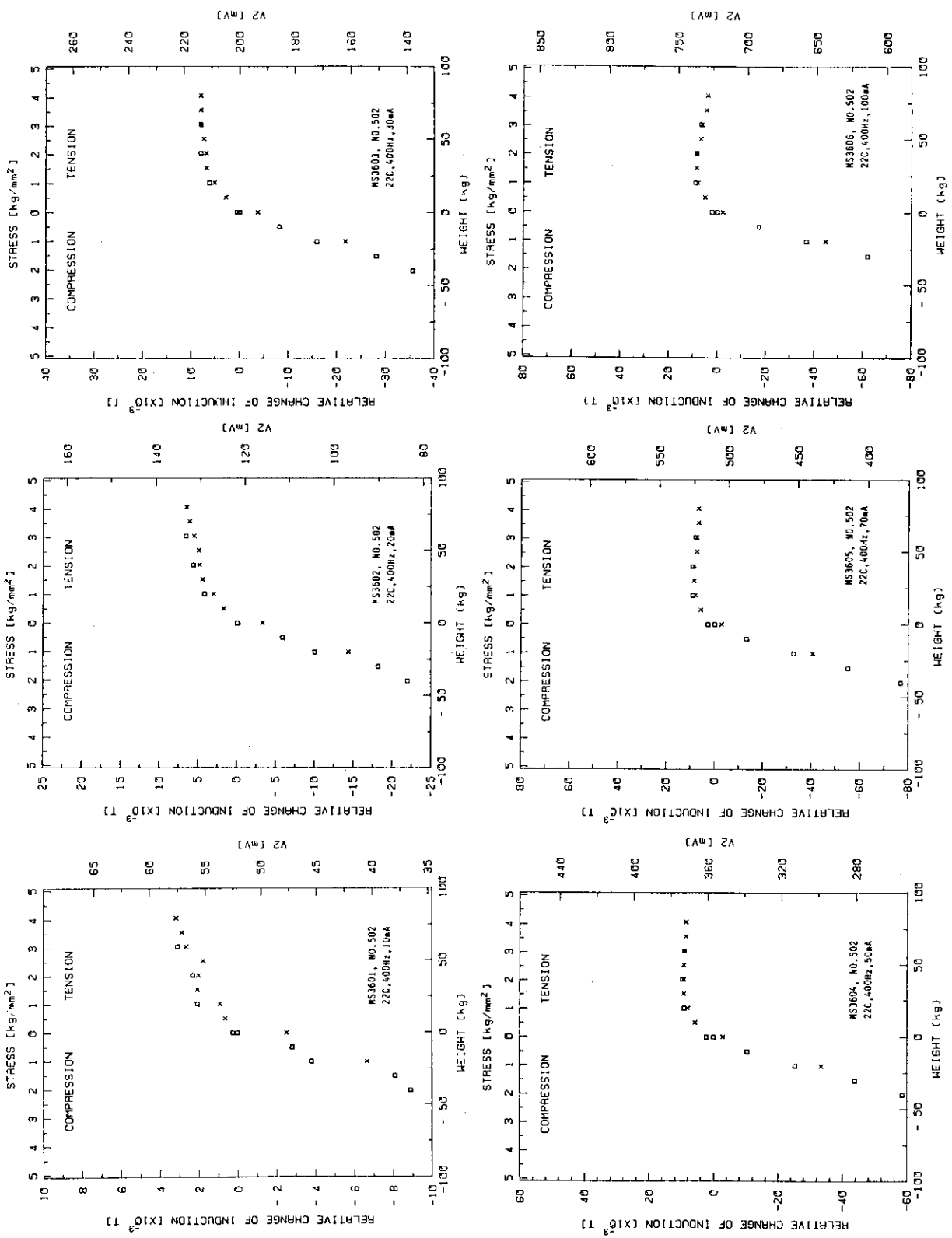


Fig. A1-14 Of SUS 405, as full annealed

**Appendix II: Inverse magnetostriction data,
measured with 400 Hz-excitation
and at 300 °C.**

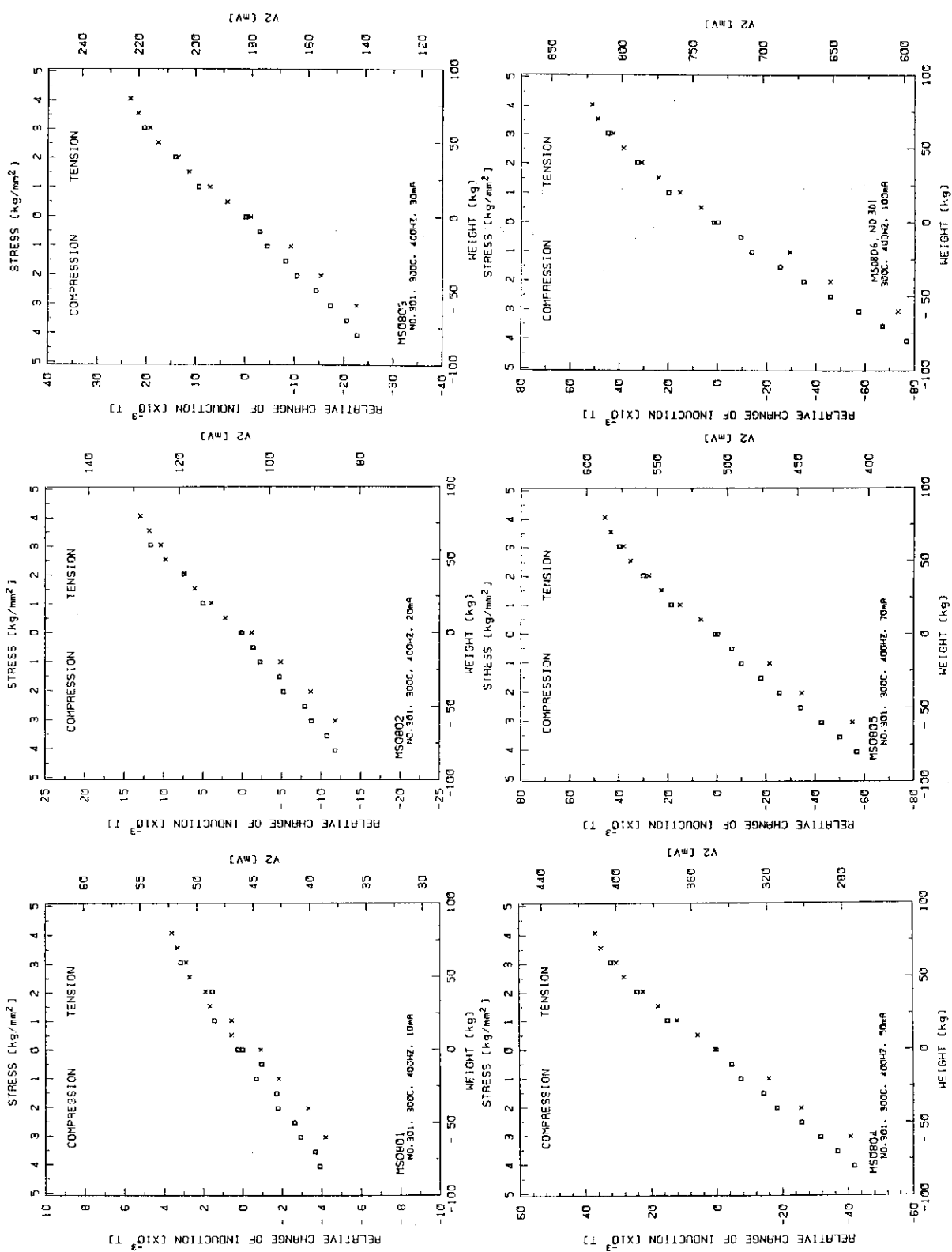


Fig. AII-1 of SUS 403, virgin

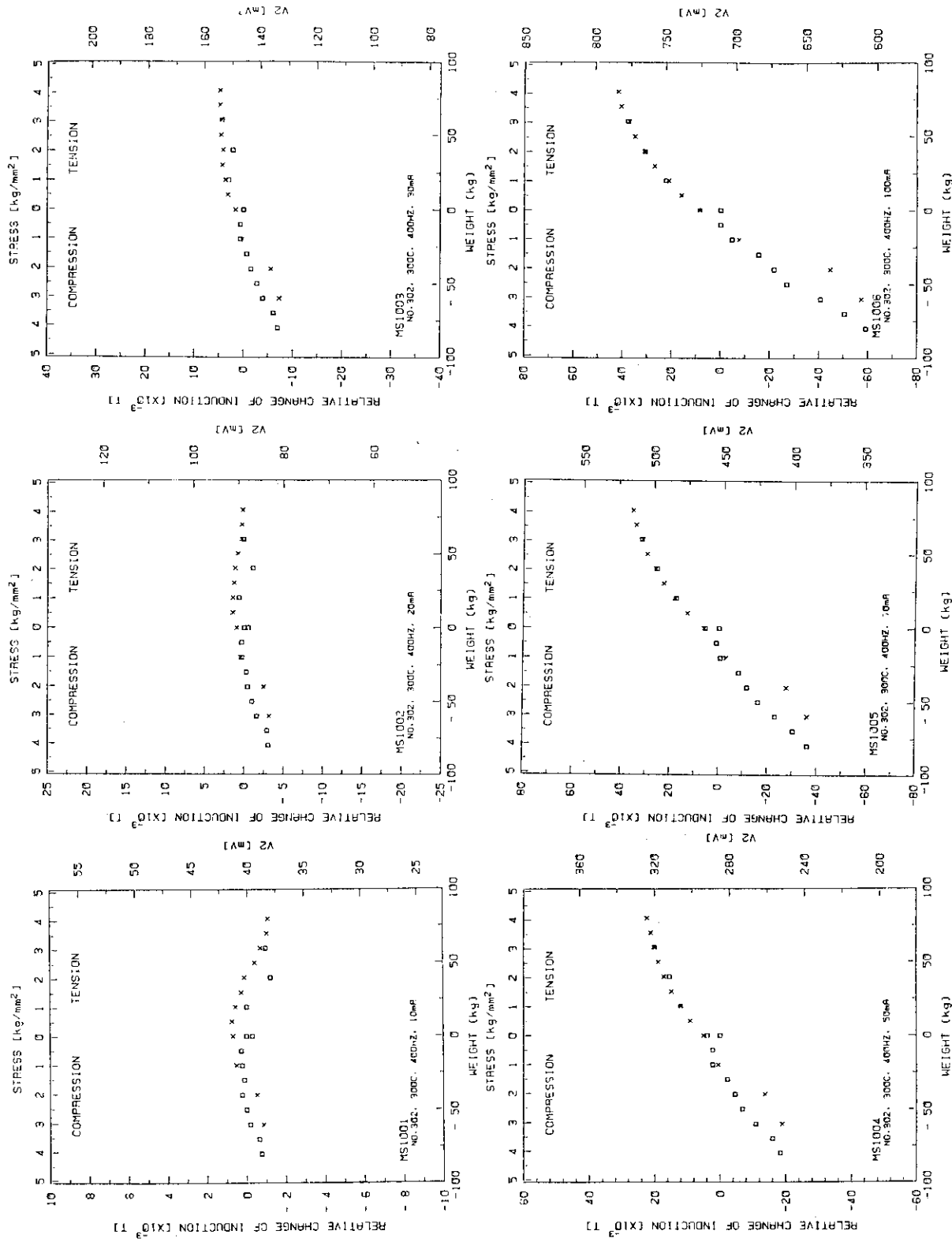


Fig. AII-2 of SUS 403, as quenched and tempered

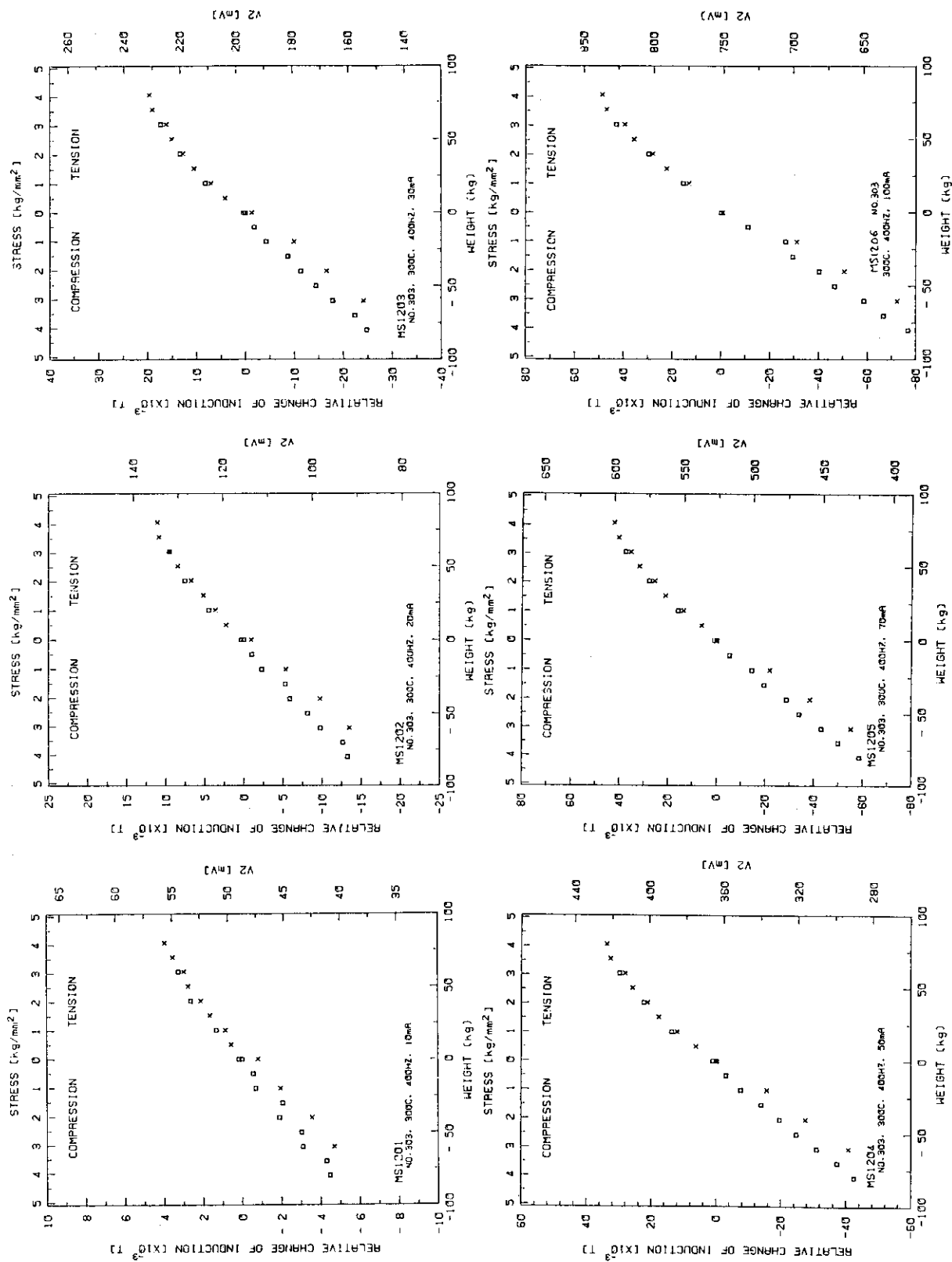


Fig. AII-3 Of SUS 403, as low-temperature annealed

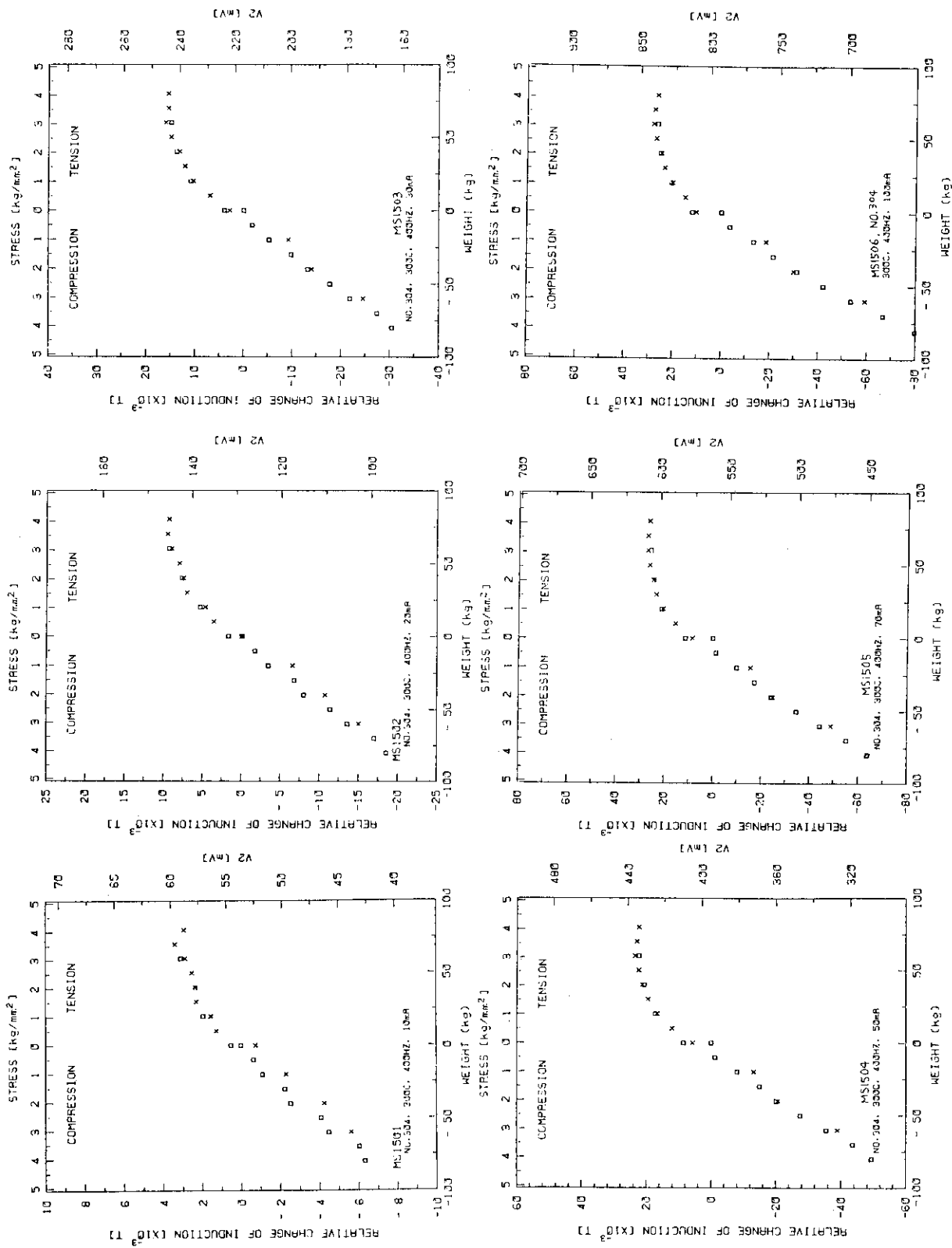


Fig. AII-4 OF SUS 403, AS FULL ANNEALED

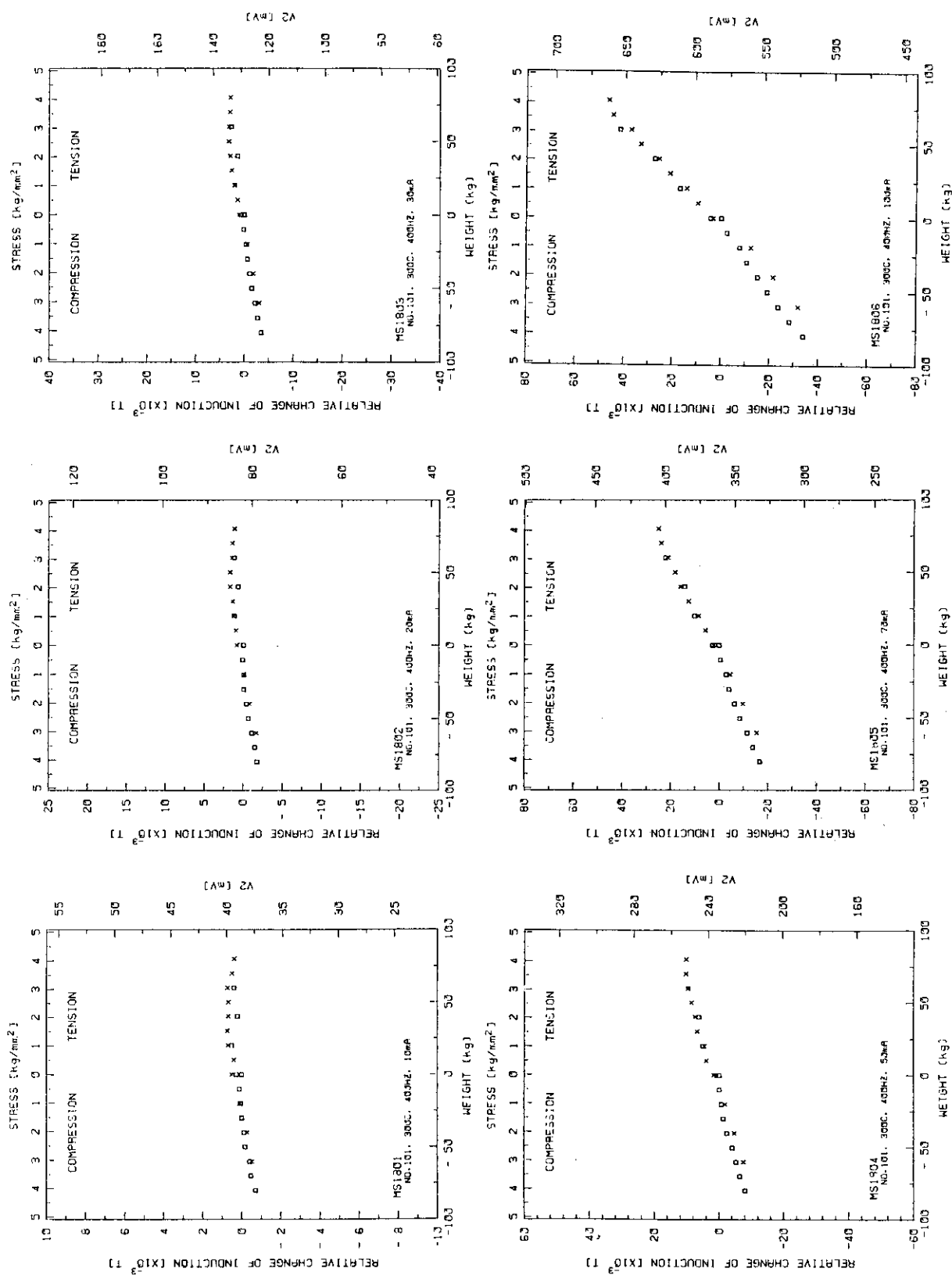


Fig. AII-5 Of SUS 410J1, virgin

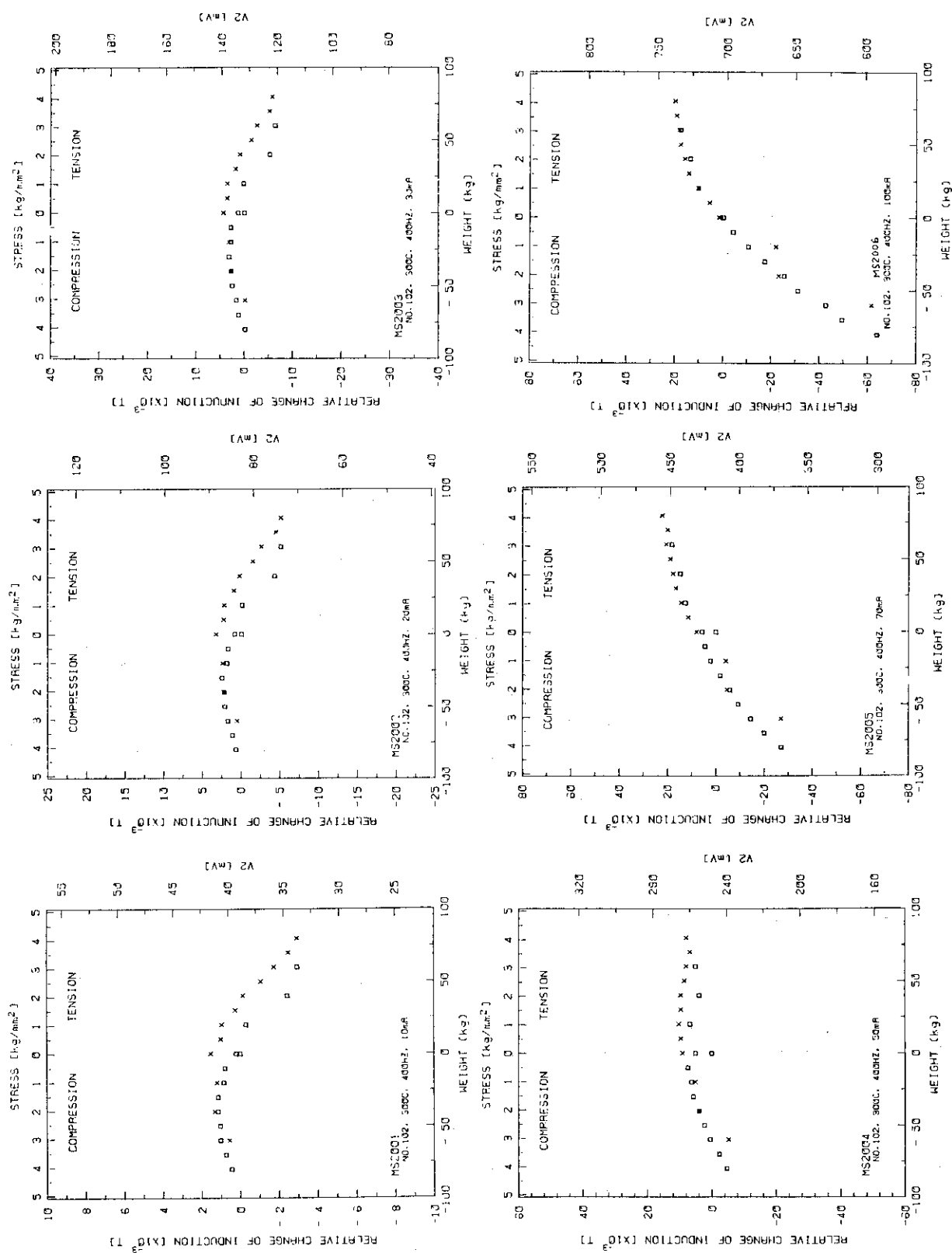


Fig. AII-6 Of SUS 410J1, as quenched and tempered

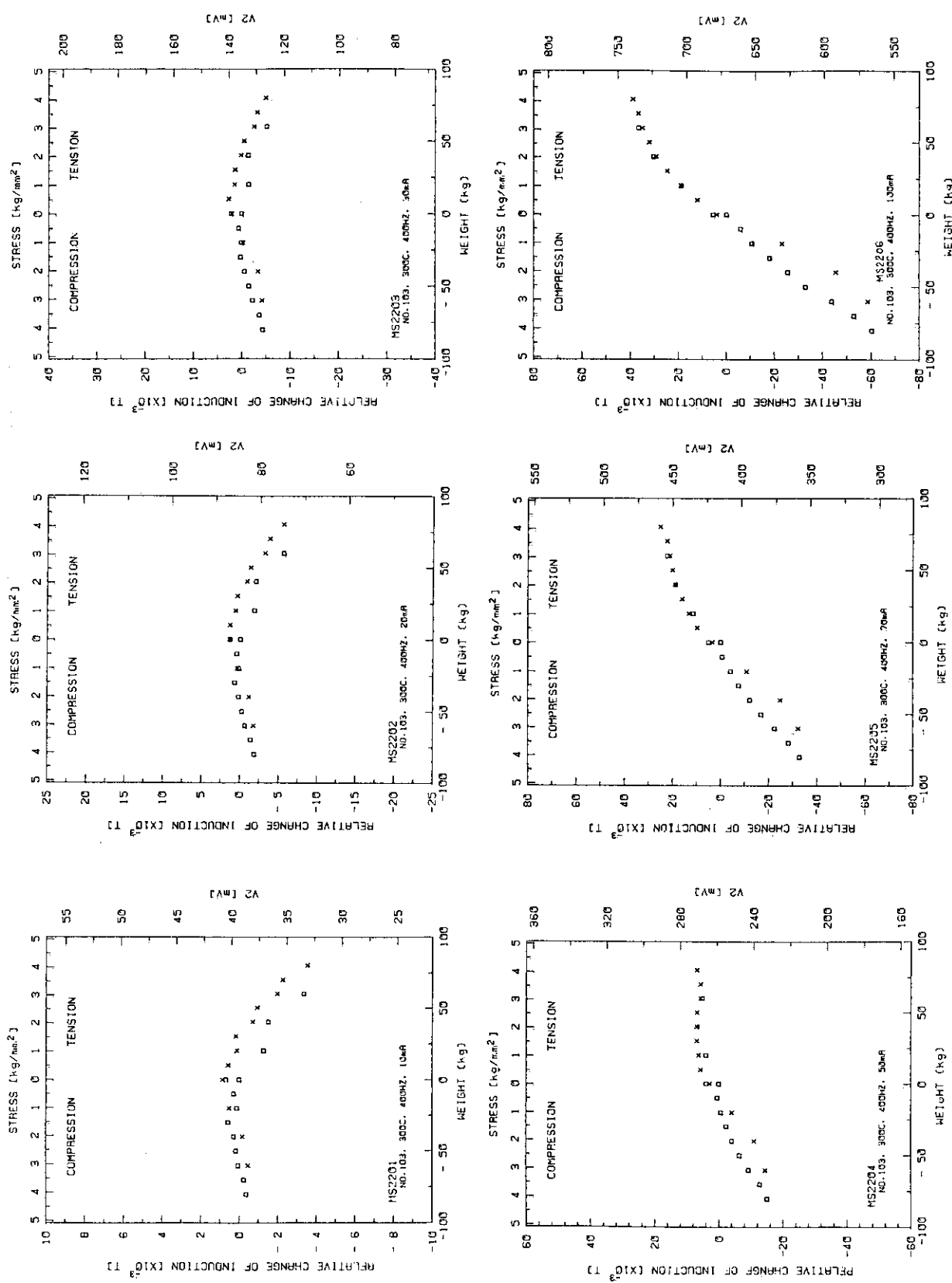


Fig. AII-7 Of SUS 410J1, as low-temperature annealed

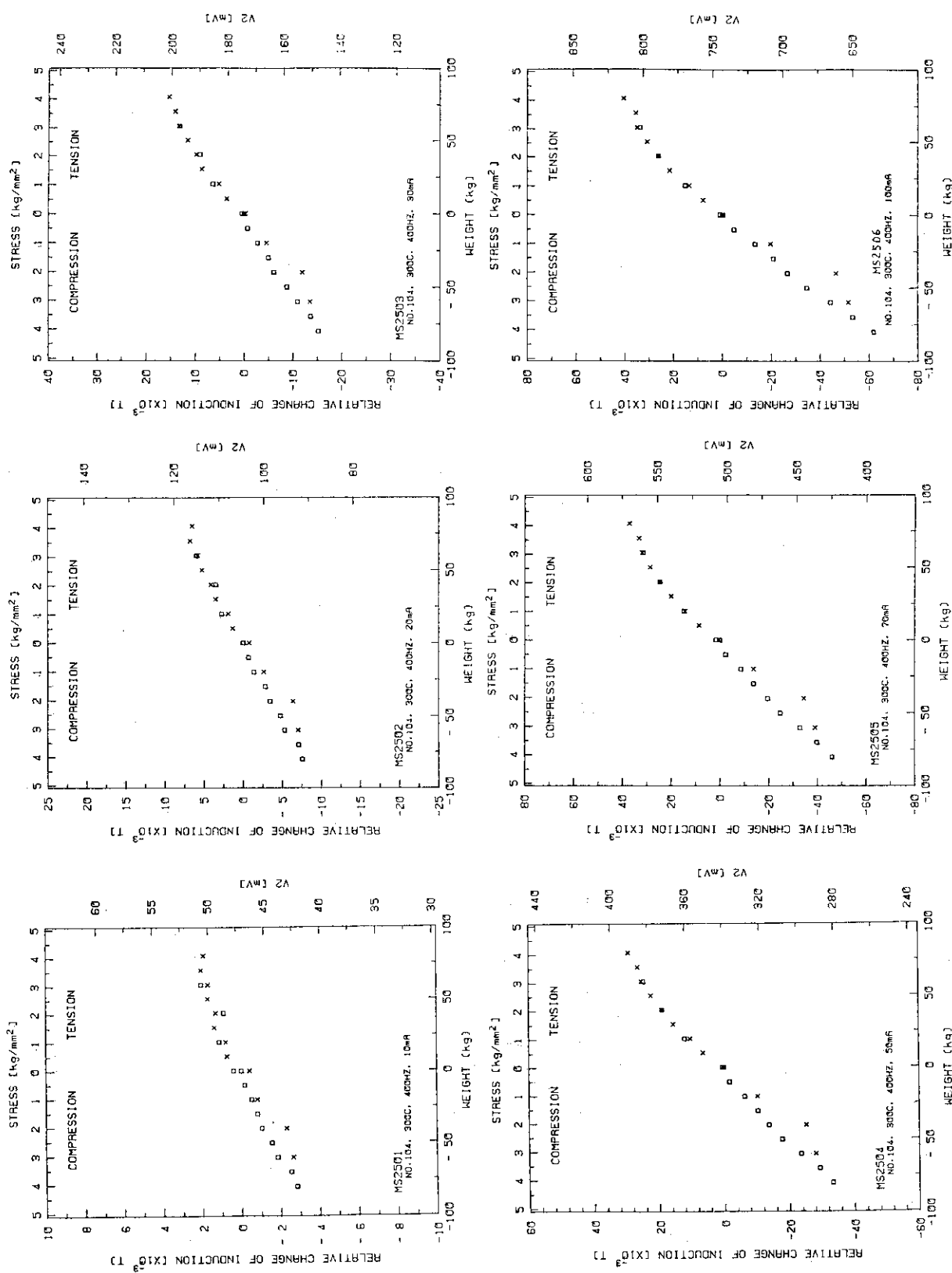


Fig. AII-8 Of SUS 410J1, as full annealed

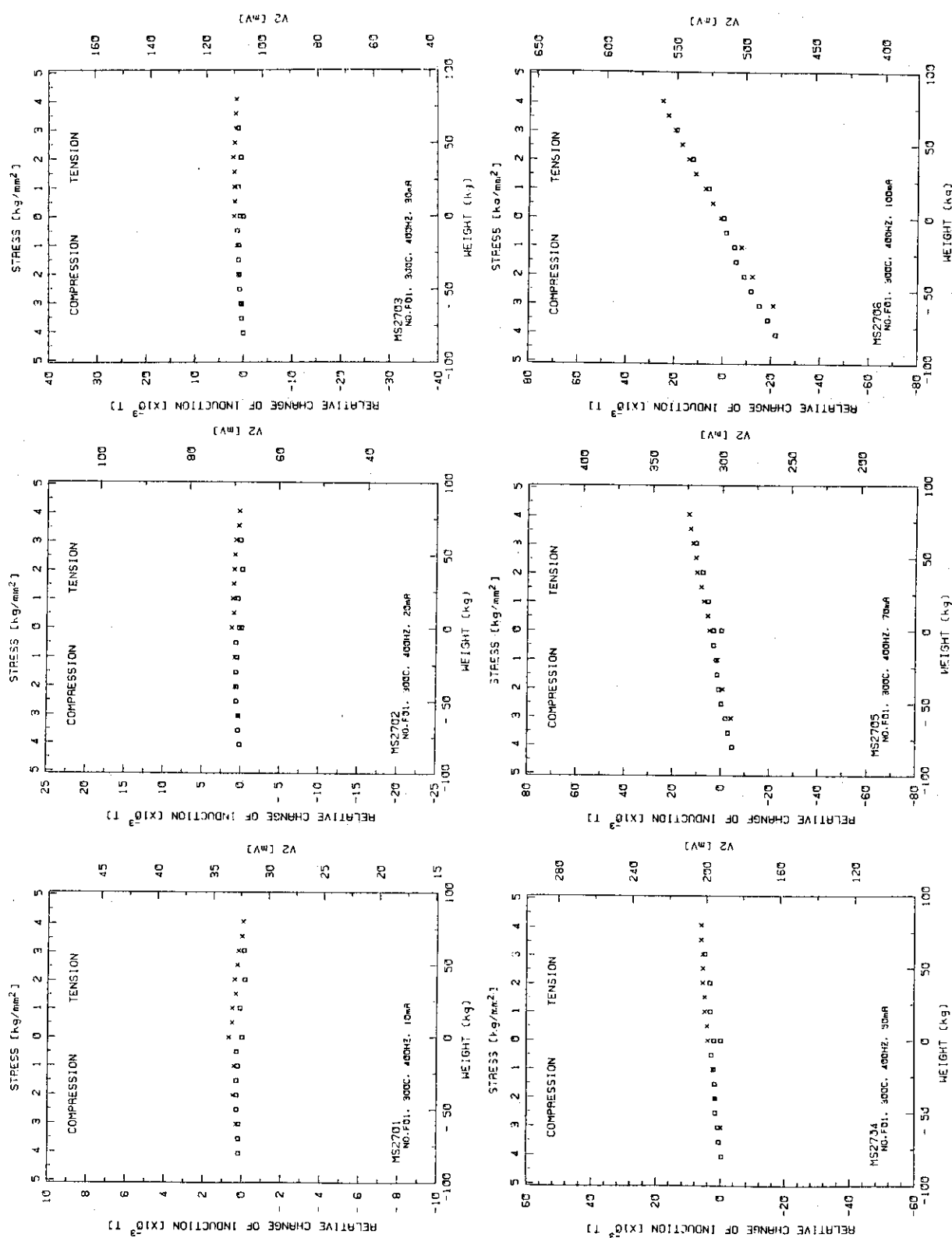


Fig. AII-9
of TAF, virgin

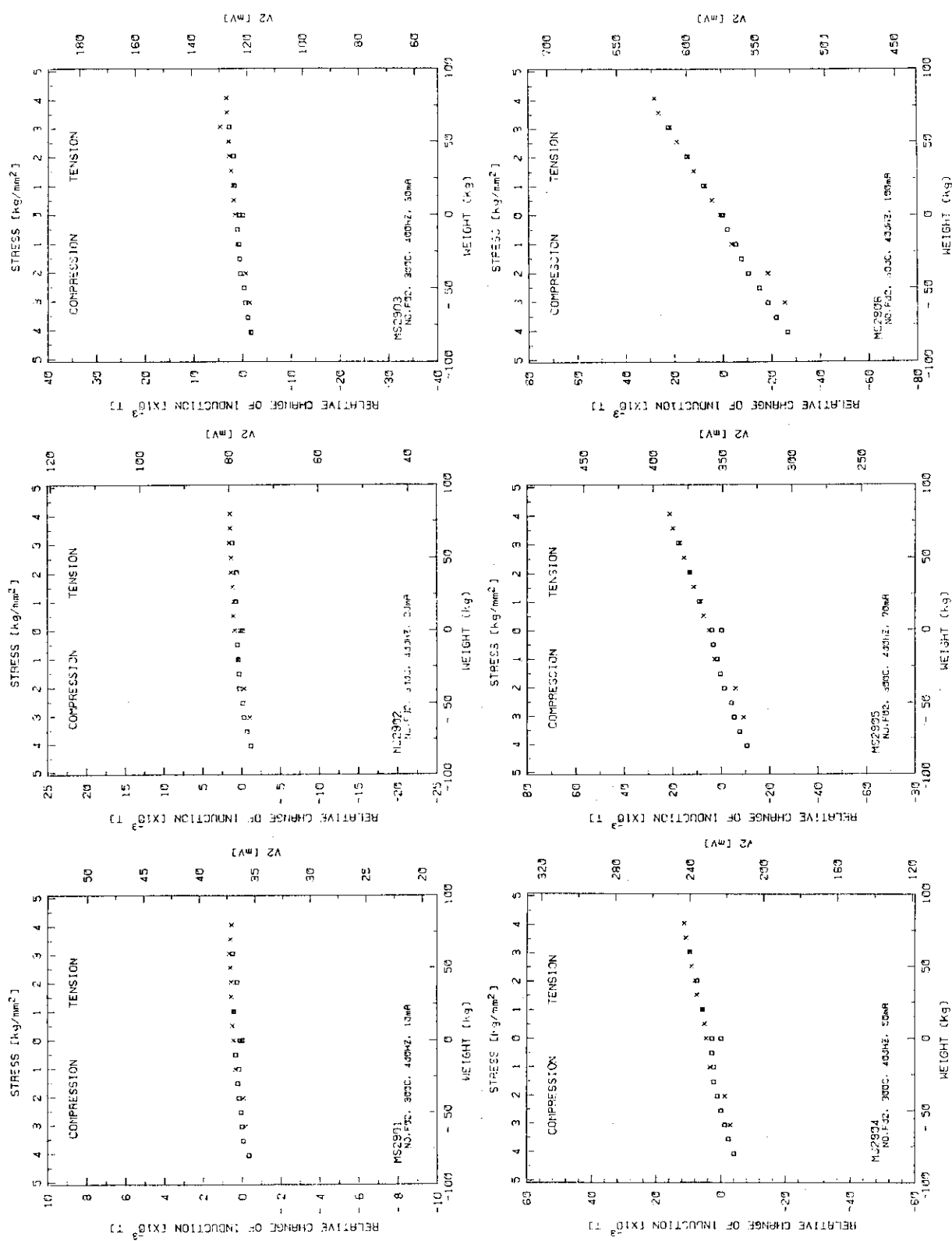


Fig. AII-10 OF TAF, as quenched and tempered

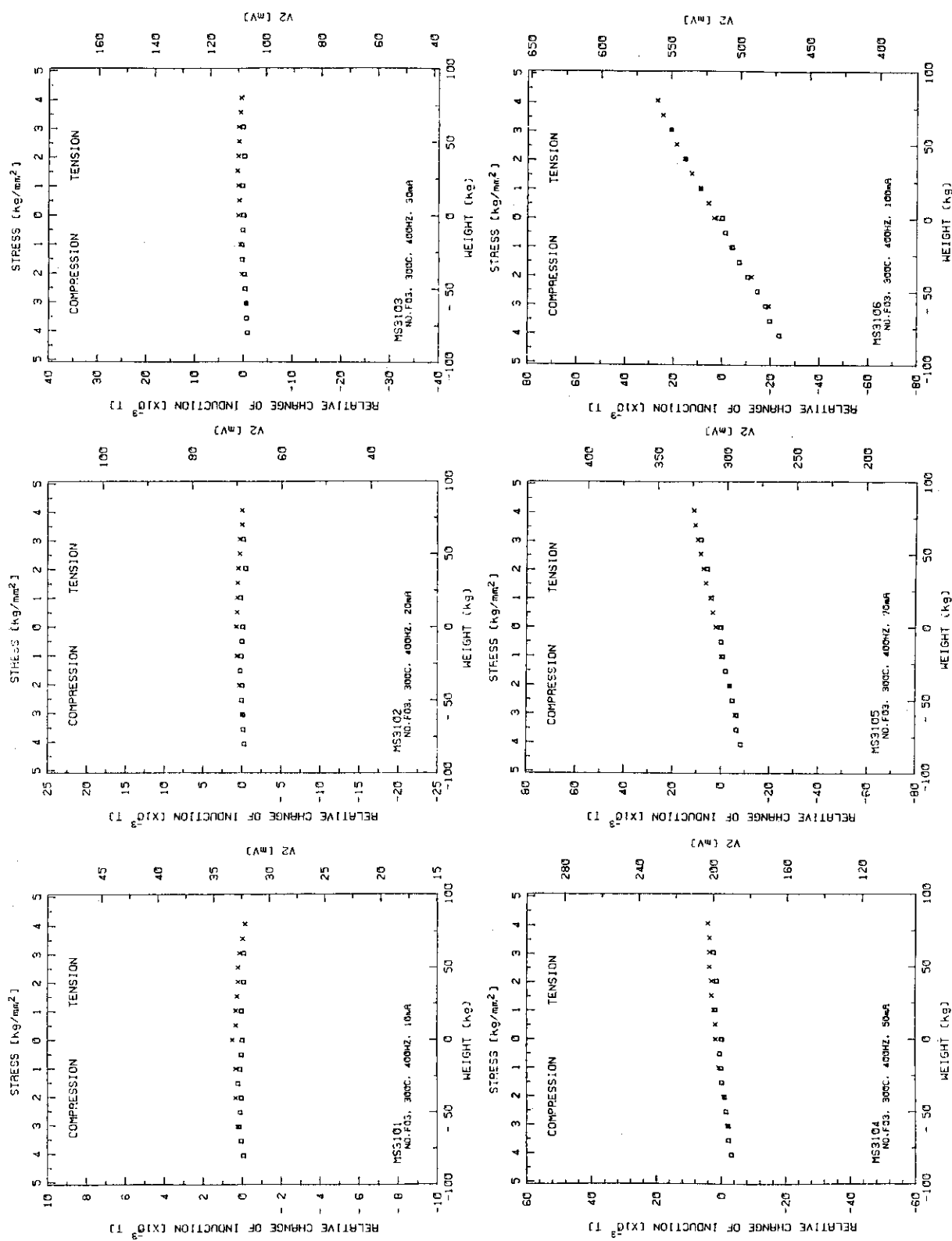


Fig. AII-11 Off TAF, as low-temperature annealed

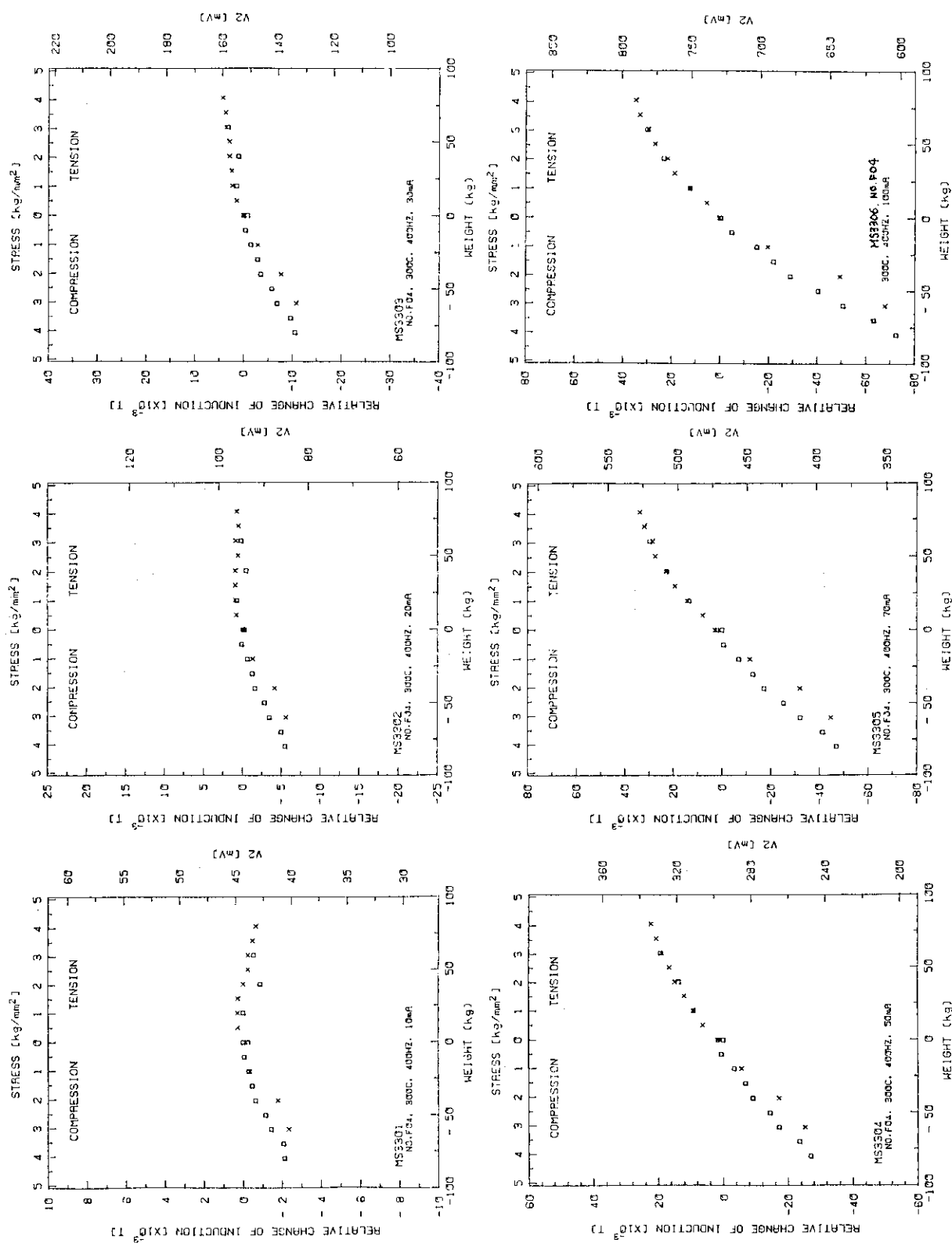


Fig. AII-12 Of TAF, as full annealed

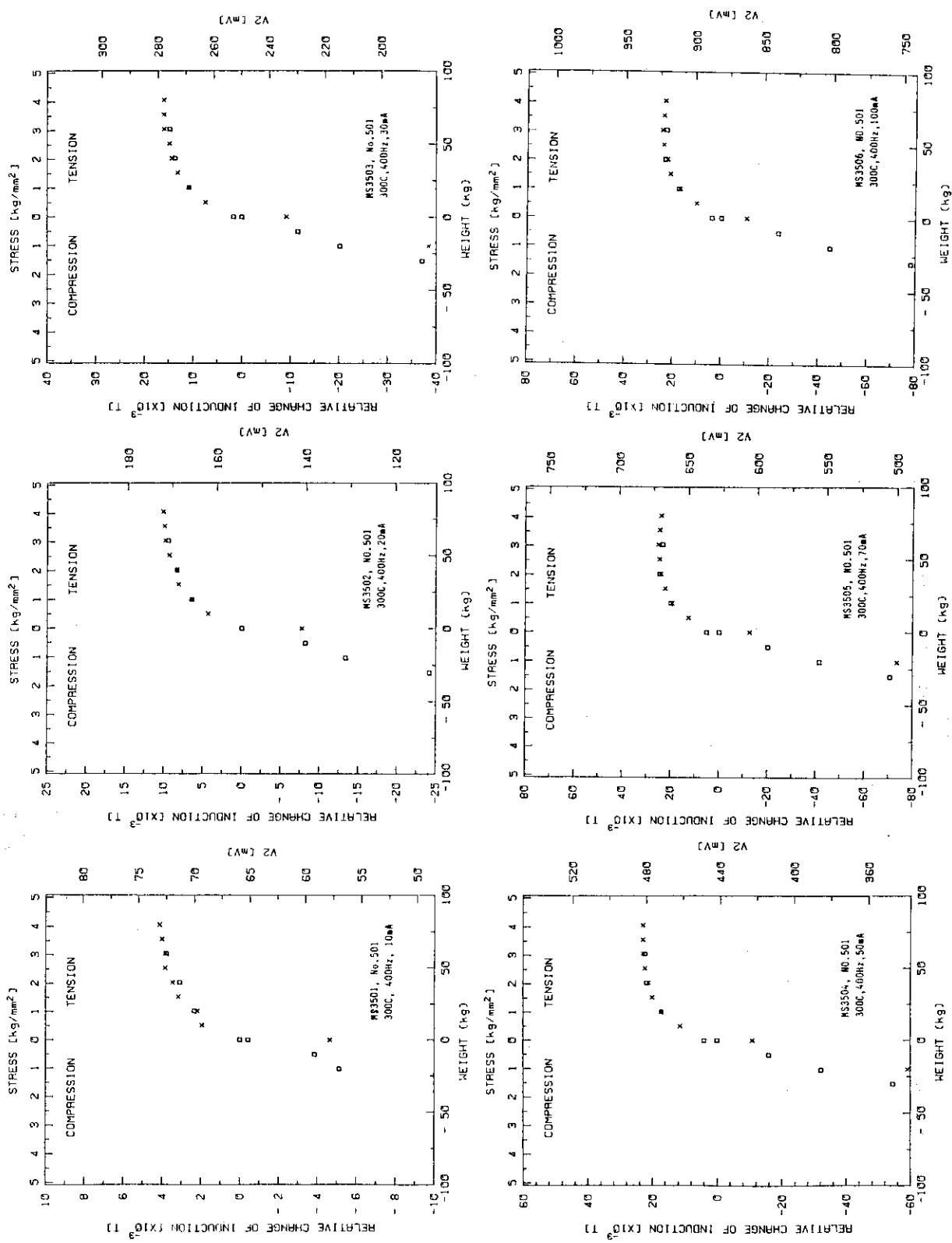


Fig. AII-13 of SUS 405, virgin

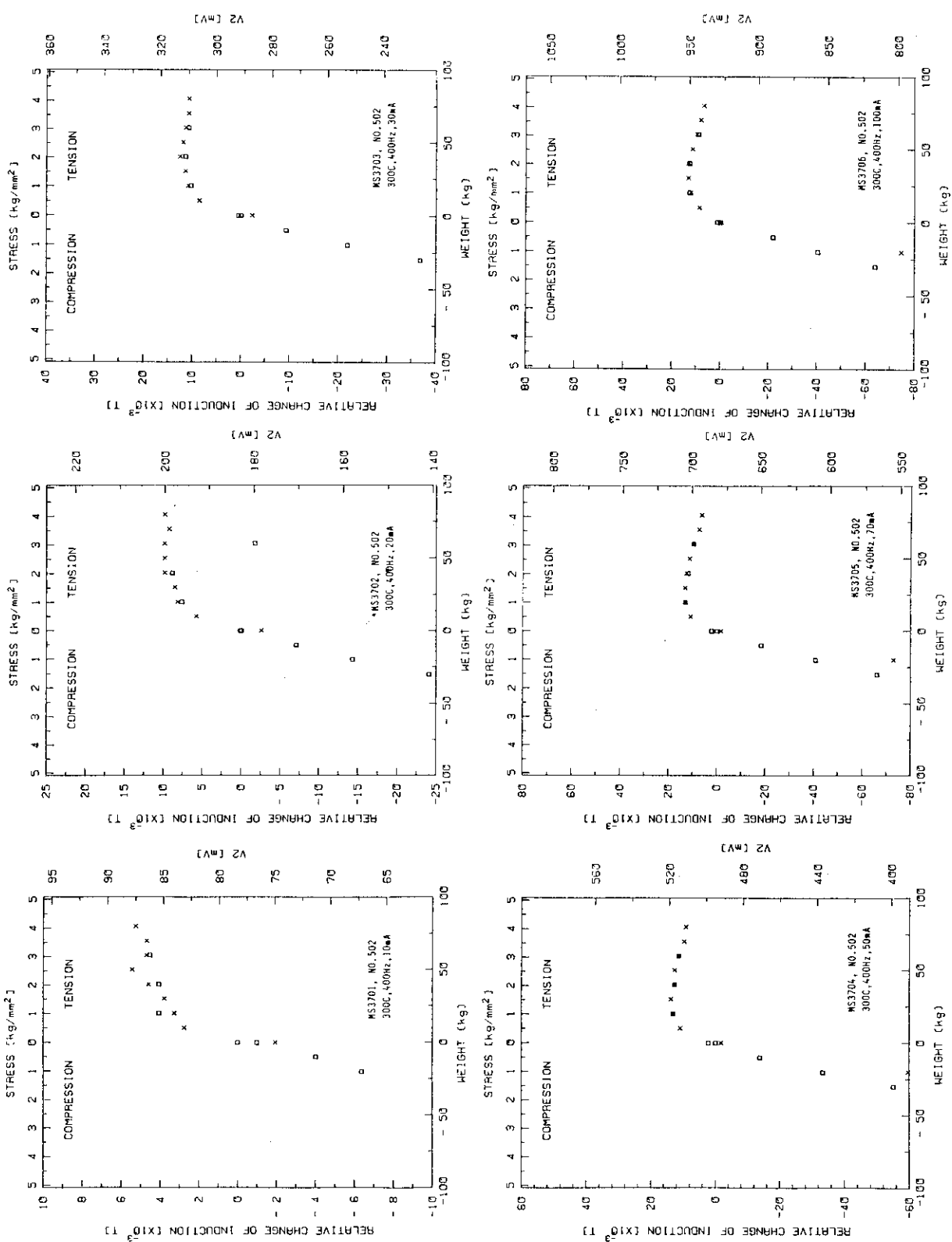


Fig. AII-14 Of SUS 405, as full annealed